STRUCTURAL STUDIES
BETWEEN USP7-NTD AND ITS SUBSTRATES

NIHARIKA LUTHRA

A THESIS SUBMITTED TO THE FACULTY OF GRADUATE STUDIES IN

PARTIAL FULFILLMENT OF THE REQUIREMENTS FOR THE DEGREE OF

MASTER OF SCIENCE

DEPARTMENT OF BIOLOGY

YORK UNIVERSITY

TORONTO, ONTARIO

APRIL 2014

ABSTRACT

USP7 is a deubiquitinase implicated in processes such as DNA damage and tumor suppression. The molecular basis of interaction of USP7 with substrates is still under examination. One mechanism for substrate recognition is a P/AXXS motif on the substrate, recognized by USP7-NTD. This study involves two substrates, checkpoint with forkhead and ring finger domains (CHFR) and minichromosome maintenance binding protein (MCM-BP) involved with mitotic checkpoint and DNA replication, respectively. To understand the basis for interaction, co-crystal structures of USP7-NTD with $CHFR^{PSTS}$ and $MCM\text{-}BP^{PSTS}$ peptides were determined, which revealed a mechanism previously established between USP7 and p53, HDM2, HDMX and EBNA1. The peptides interacted within a shallow groove on the surface of USP7-NTD lined by residues $^{164}DWGF^{167}$. Protein turnover assay was used to show the steady decrease of CHFR in the absence of USP7. This study has associated USP7 with DNA replication and confirmed its role at a cell cycle checkpoint.

ACKNOWLEDGEMENTS

My utmost gratitude goes towards my supervisor, Dr. Vivian Saridakis, for taking me under your wing and welcoming me into your lab. Thank you for always seeing the potential in me and encouraging me to strive for my best. Your constant support and patience has meant the world to me and I would not be here without it. You were there to guide me whenever I needed it and have been a constant positive force that has helped me achieve my goals. Thank you for being a true inspiration, for everything that you are, and for everything you've helped me to be.

I would like to thank my advisor, Dr. Terry Kubiseski, for sharing your valuable time and expertise for helping me on my project. I would also like to thank Dr. Chun Peng and Dr. Anthony Scime for taking time out from your tight schedules to be a part of my committee. Dr. Yi Sheng, I'd like to take this opportunity to thank you for all the times you allowed me to benefit from your knowledge and experience to better my project.

To Ira and Sara, I could not have asked for better mentors than you. I'm so grateful that I had the fortune to be a part of a wonderful lab, where each lab member, past and present, has been like family to me. Leila, Jay, Anna, Agnesa, Roland, Anthony, Neha, Sanja, Thaarshinee, Anuj, Tharanee, Mihai and members of the Sheng lab, I've had a great time working with all of you and in the process have formed memorable friendships with you.

To my Mom and Dad, whom I'd like to dedicate this achievement to. I have reached this stage in my life only because of the unconditional love and support I've always received from you. Last, and best, to my sister Nidhi for being my pillar of strength.

TABLE OF CONTENTS

LIST OF TABLES

LIST OF FIGRUES

LIST OF ABBREVIATIONS

AA Amino acid

A	Ala	Alanine
C	Cys	Cysteine
D	Asp	Aspartic acid/Aspartate
E	Glu	Glutamic acid/Gultamate
F	Phe	Phenylalanine
G	Gly	Glycine
H	His	Histidine
I	Ile	Isoleucine
K	Lys	Lysine
L	Leu	Leucine
M	Met	Methionine
N	Asn	Asparagine
P	Pro	Proline
Q	Gln	Glutamine
R	Arg	Arginine
S	Ser	Serine
T	Thr	Threonine
V	Val	Valine
W	Trp	Tryptophan
Y	Tyr	Tyrosine

ATP	Adenosine triphosphate
CCD	Charge-coupled device
Cdc25	Cell division cycle 25
Cdk1	Cyclin-dependent kinase 1
CHFR	Checkpoint with forkhead and ring finger domains
DUB	Deubiquitinating enzyme/Deubiquitinase
E1	Ubiquitin activating enzyme
E2	Ubiquitin conjugating enzyme
E3	Ubiquitin ligase
EBNA1	Epstein-Barr nuclear antigen 1
EBV	Epstein-Barr virus
FHA	Forkhead-associated domain
GMP	Guanosine monophosphate
GMPS	Guanosine monophosphate synthase
H2A	Histone protein 2A
H2B	Histone protein 2B
HDAC1	Histone deacetylase 1
HDM2	Human double minute 2
HDMX	Human double minute X
HECT	Homologous to the E6-AP carboxyl terminus
HEK293T	Human embryonic kidney 293 cells with SV40 Large T-antigen
HSV	Herpes simplex virus
ICP0	Infected cell protein 0
IKKγ	Inhibitor of nuclear factor kappa-B kinase subunit gamma
JAMM	Jab1/Mov34/Mpr1 Pad1 N-terminal+

JNK	c-Jun N-terminal kinases
kDa	Killodalton
Kiff22	Kinesin family member 22
MAD2	Mitotic arrest deficient 2
MCM	Minichromosome maintenance complex
MCM-BP	Minichromosome maintenance complex binding protein
MDM2	Murine double minute 2
MDMX	Murine double minute X
NF-κB	Nuclear factor kappa-light-chain-enhancer of activated B cells
OTU	Ovarian tumor protease
PAR	Poly[ADP-ribose]
PARP1	Poly[ADP-ribose] polymerase 1
PLK-1	Polo-like kinase 1
Pre-RC	Pre-replicative complex
RING	Really interesting new gene
RNF8	Ring finger protein 8
RPS27A	Ribosomal protein S27A
TLR	Toll-like receptor
TRAF	Tumor necrosis factor receptor-associated factor
Ub	Ubiquitin
UBA52	Ubiquitin A-52 residue ribosomal protein fusion gene
UBB	Ubiquitin B gene
UBC	Ubiquitin C gene
UbE2E1	Ubiquitin conjugating enzyme E2E 1
UbE2D1	Ubiquitin conjugating enzyme E2D 1

UbE2D2	Ubiquitin conjugating enzyme E2D 2
UbE2D3	Ubiquitin conjugating enzyme E2D 3
UBIP	Ubiquitous immunopoietic polypeptide
UBL	Ubiquitin-like domain
UCH	Ubiquitin C-terminal hydrolase
USP	Ubiquitin specific protease
USP7	Ubiquitin specific protease 7
USP7-CTD	USP7 C-terminal domain
USP7-NTD	USP7 N-terminal domain
XMP	Xanthosine monophosphate

CHAPTER 1: INTRODUCTION

Proteins are an essential part of a healthy functional cell. A vast amount of research is undertaken to study the pathways affected by mutations in a protein and defects in its regulation. Cells devote a large part of their resources to ensure appropriate synthesis and maintenance of these proteins, mainly through post-translational modifications. An important part of maintenance is the destruction or degradation of proteins, and most of this work is attributed to one system – the ubiquitin-proteasome system whereby a protein tagged with ubiquitin is targeted for proteolysis.

1.1 Ubiquitin

Ubiquitin is a small 8.5 kDa regulatory protein (Haglund and Dikic 2005) that gets conjugated to target proteins as a post translational modification. It is structurally and functionally highly conserved in mammals and plants, and when first discovered, it was observed to be expressed ubiquitously in almost all living cells including bacteria and yeast (Goldstein et al. 1975). When it was discovered, it was seen to be able to induce the differentiation of T and B cells of the immune system. Based on this and its universal presence in living cells, it was initially termed UBIP, or ubiquitous immunopoietic polypeptide (Goldstein et al. 1975). However, it was later renamed ubiquitin when it was discovered that UBIP does not have immunopoietic function, and it is not present in bacterial cells (Ciechanover 2005).

The function of ubiquitin remained unknown until the ATP-dependent proteolytic activity of the cell was being studied, and the conjugation of a protein of about 8.5 kDa was found to be essential for recognition of the target protein by a downstream protease in the

presence of ATP (Ciechanover 2005). Through various tests, this factor was later found to be ubiquitin and its importance was established when it was found to be able to conjugate to H2A and H2B histone proteins in a manner that was reflective of the proteolytic activity studied earlier (Ciechanover 2005). The ubiquitin-proteasome system has since been an area with intense research dedicated to understanding it better.

There are four genes in mammals that encode for ubiquitin, and it is synthesized bound to precursors, not as monomeric ubiquitin. UBB and UBC encode for polyubiquitin chains, whereas UBA52 and RPS27A encode for ubiquitin fused to ribosomal proteins (Kimura and Tanaka 2010). Upon further processing, a pool of monomeric ubiquitin becomes available for use in the ubiquitination process.

The ubiquitin protein is the most conserved eukaryotic protein. One of its most important features is two glycine residues at its C-terminal tail, which are required for conjugation to target proteins. The glycine in ubiquitin forms an isopeptide bond with either the ε-NH_2 groups of the lysine residues on target proteins, or with their amino-terminal α-NH_2 group (Vijay-Kumar et al. 1987). Ubiquitin also contains seven lysine residues, which are important for forming polyubiquitin chains by linking the glycine of one ubiquitin to the lysine of another ubiquitin that is already bound to a substrate. The seven lysines are K6, K11, K27, K29, K33, K48 and K63; the signal provided by ubiquitination is characterized based on which of these lysine residues forms the ub-ub linkage.

1.2 Ubiquitination

Ubiquitin is conjugated to target proteins through a cascade of reactions. It is activated by E1, a ubiquitin-activating enzyme through adenylation and thioesterification of its carboxy-terminal carboxylate (Jin et al. 2007). It is then transferred to a cysteine residue in the active site of E2, a ubiquitin-conjugating enzyme, through a transthiolation reaction, following which an E3 ligase catalyzes its final transfer to the substrate protein (Ye and Rape 2009). The final transfer can occur in two ways, based on which class of E3 ligase is being employed. E3 with a HECT domain (homologous to E6-Ap carboxyl terminus) (You and Pickart 2001) gets charged with the ubiquitin from E2 in order to ligate it to the substrate. E3 with a RING domain (Really Interesting New Gene) (Deshaies and Joazeiro 2009) on the other hand, functions to bring the E2~ub complex in close proximity to the substrate in order to facilitate ligation (Ye and Rape 2009). The substrate protein is commonly ubiquitinated on the amino group of their internal lysine residues (Ciechanover and Saadon 2004).

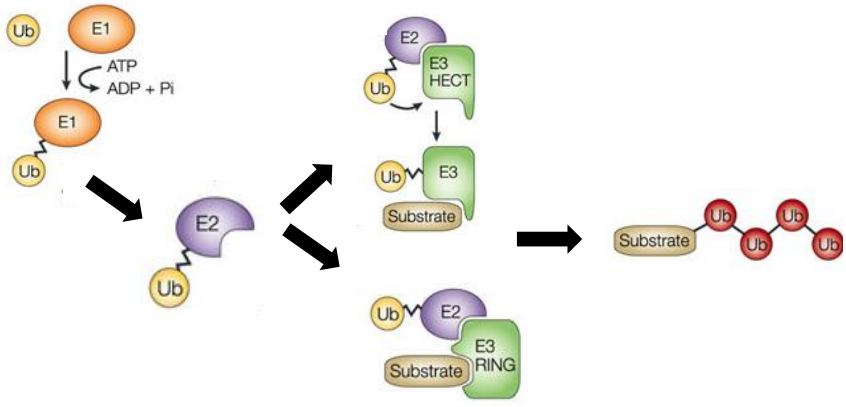

Figure 1.1: Ubiquitination pathway. E1 binds and activates ubiquitin (Ub). Ub is then transferred to E2, following which E3 ligase catalyzes transfer of Ub from E2~Ub to the substrate. E3 with a HECT domain charges itself with Ub prior to ligation onto substrate. E3 with RING domain facilitates transfer by bringing together E2~Ub and substrate.

A protein tagged with ubiquitin can have proteolytic or one of many non-proteolytic fates in the cell, depending on whether it is mono- or poly-ubiquitinated and the type of linkage within the chain (Hochstrasser 2009). Polyubiquitin chains are linked via one of seven lysine residues on ubiquitin. A chain with K48 linkage is targeted by the proteasome. Monoubiquitination and polyubiquitin linkages involving any of the other lysines allows the protein to be recognized by ubiquitin binding domains on target proteins to facilitate downstream cellular processes (Hochstrasser 2009). Ubiquitination has implications in various processes such as cell growth, DNA repair, immune function, regulation of the cell cycle, membrane trafficking and histone modification (Nath and Shadan 2009).

1.3 Deubiquitination

Ubiquitination is a reversible process, whereby one or more ubiquitin molecules get cleaved either from the substrate or as part of modification of a polyubiquitin chain. Deubiquitination is catalyzed by proteases called deubiquitinases or DUBs. An essential part of ubiquitination is the availability of monomeric ubiquitin molecules in the cell. However, ubiquitin can be translated as a chain of molecules instead of monomers, or have ribosomal proteins fused to it (Komander et al. 2009). DUBs play a role in processing these precursors to provide the cell with monomeric ubiquitin molecules (Komander et al. 2009). DUBs are also involved in cleaving mono- or poly-ubiquitin chains from substrate proteins to alter their fate. For a proteolytic signal, this would mean rescuing the substrate from degradation. However, for a non-proteolytic signal it would

either remove the signal (complete cleavage) or would alter the signal by editing the length of the ubiquitin chain (Komander et al. 2009).

The ubiquitinated state of a protein could differentiate between its inactive and active state and is involved in modulating protein-protein interactions. Malfunctioning DUBs have been linked to numerous diseases, including deficiencies in the immune system; mutations in DUBs have also been associated with cancer, thus making their normal functionality in the regulation of ubiquitin-dependent pathways essential for our healthy survival.

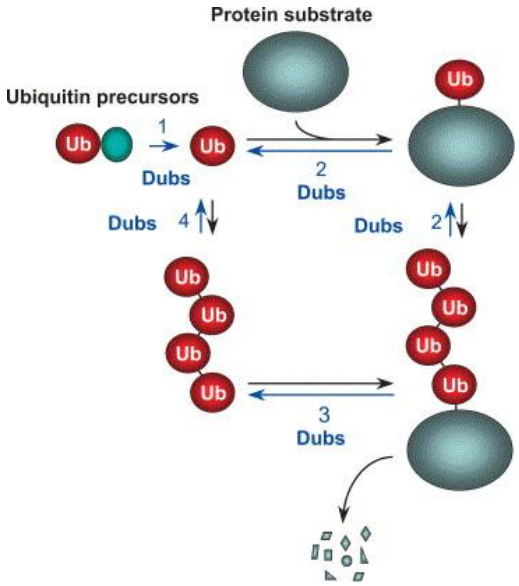

Figure 1.2. Functions of DUBs in the ubiquitin pathway. DUBs modify ubiquitin precursors to provide the cell with monomeric ubiquitin (1). By removing the ubiquitin signal or modifying the chain, DUBs can reverse or edit the ubiquitin-mediated fate of the substrate proteins (2). DUBs can also recycle ubiquitin from conjugates with proteins targeted for degradation (3). Finally, they also recycle unanchored ubiquitin chains by cleaving their linkage to produce monomeric ubiquitin molecules (4). (Amerik and Hochstrasser 2004)

1.4 Ubiquitin specific protease 7 (USP7)

In humans, DUBs can be classified into two classes – cysteine proteases and metalloproteases – based on the catalytic domain of the protein. The cysteine protease class includes four superfamilies, the ubiquitin specific proteases (USP), the ovarian tumours (OTU), the Machado-Josephin domains (MJD) and the ubiquitin C-terminal hydrolases (UCH). The metalloprotease class only consists of a zinc binding Jab1/Mov34/Mpr1 Pad1 N-terminal+ (MPN+) (JAMM) domain superfamily (Amerik and Hochstrasser 2004). The focus of this project is a DUB, from the cysteine protease class and ubiquitin specific protease superfamily, USP7.

1.4.1 Functional domains

Ubiquitin specific protease 7 (USP7) contains a classic cysteine protease catalytic domain, whose catalytic activity involves a nucleophilic attack to break the isopeptide bond between the C-terminal of ubiquitin and the lysine of the substrate protein, or between the C-terminal of ubiquitin and the lysine of the previous ubiquitin in a polyubiquitin chain (Chapman et al. 1997).

The catalytic domain of USP7 is flanked by accessory domains, with a TRAF homology domain on the N-terminus and five ubiquitin-like or UBL domains on the C-terminus. UBLs are structurally similar to ubiquitin but lack the terminal glycine residue required for conjugation to the lysine of the target protein (Faesen et al. 2012). The five UBLs together form the C-terminal domain of the protein. The N- terminal TRAF domain of USP7 has been found to be involved in substrate recognition and protein interaction,

whereas conformational changes in the UBLs in USP7-CTD have been shown to allow for ubiquitin binding and to enhance USP7's catalytic activity (Faesen et al. 2012).

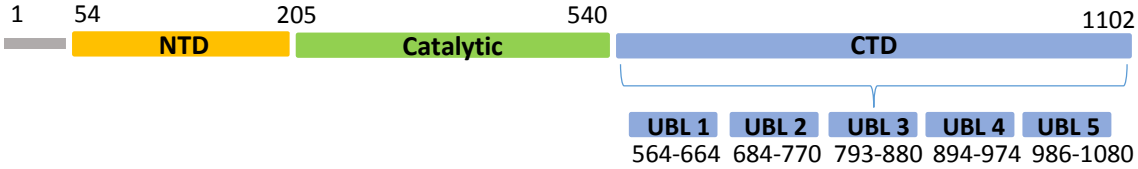

Figure 1.3. Schematic diagram of the domains of USP7. USP7 is a 128 kDa protein containing 1102 amino acid residues. Its N-terminal domain (NTD) consists of a TRAF-domain, from amino acid residues 54-205. The catalytic domain is a classic cysteine protease domain from residues 208-540. The longest domain of the protein is its C-terminal domain (CTD), from residues 564-1080. The CTD is formed from five UBLs (ubiquitin-like domains), each of which is structurally homologous to ubiquitin but lacks the terminal glycine required for linkage.

1.4.2 Interactions and cellular roles

USP7 is involved in various cellular processes including immune response, viral infections, DNA damage response, epigenetics and tumor suppression. Its function in these pathways is complimented by a vast number of substrates and interacting partners.

It is most popularly known for its role in the p53-MDM2-MDMX pathway. p53 is a tumor suppressor, with essential roles in cellular and genomic stability (Li et al. 2002) and binds to the N-terminal domain of USP7. Under normal conditions, cellular levels of p53 are regulated through monoubiquitination by MDM2 which is an E3 ligase (Moll and Petrenko 2003). However upon oncogenic stress, USP7 through its deubiquitinating activity rescues p53 from degradation, demonstrating a tumor suppressor function (Epping et al. 2011). MDM2 is also a known binding partner of USP7-NTD, and

interestingly, USP7 stabilizes MDM2 in addition to p53. This creates a feedback loop, which is a part of a regulatory mechanism to keep p53 at the required level.

Instead of suppressing USP7, guanine monophosphate synthase (GMPS) binds to USP7 to enhance its activity. It is a biosynthetic enzyme involved in the amidation of xanthosine-5'-monophosphate (XMP) to produce guanine monophosphate (GMP) (Nakamura and Lou 1995). It has been shown that defects in nucleotide metabolism result in immunodeficiency. GMPS is thus regarded as having potential for immunosuppressive therapy (Nakamura and Lou 1995). In 2004, research undertaken by van der Knaap and his colleagues revealed a role of GMPS in chromatin control. They discovered that it in order for histone H2B to be deubiquitinated by USP7, an association of GMPS with *Drosophila* USP7 is required, thus contributing to epigenetic silencing of homeotic genes. They also found this association to enhance USP7 deubiquitination of p53 (van der Knaap et al. 2004).

1.4.3 Exploitation of USP7 for viral propagation

Research has shown that a gene in breast cancer, TSPYL5, interacts with USP7 in order to block USP7 mediated upregulation of p53 (Epping et al. 2011). EBNA1, a protein from Epstein-Barr virus (EBV) is also involved in a similar mechanism to compete with p53 for binding to USP7, leading to downregulation of p53 mediated genes (Sheng et al. 2006).

Another viral protein, ICP0 is a protein from herpes simplex virus (HSV) and was the first protein found to bind with USP7 (Sheng et al.2006). While EBNA1 binds to the N-

terminus, ICP0 interacts with the C-terminal domain of USP7. It also functions in a manner opposite to EBNA1; whereas the latter binds to USP7 to prevent it from performing its deubiquitinase activity, ICP0 binds to USP7 to export it to the cytoplasm for it to perform its role in modulating the TLR-mediated innate immune response.

TLR or Toll-like receptors normally initiate an inflammatory response to invading pathogens as a part of the innate immune response. Through a cascade of reactions, the action of TLRs results in the activation of NF-κB which is a transcription factor involved in the production of proteins needed for the inflammatory response (van Lint et al. 2010), as well as mitogen-activated protein kinases JNK and p38.

Since this response is potent, the cell has various checks in place to avoid its hyper activation. One of the checks is USP7, which is responsible for regulating the TLR signalling using a negative feedback loop. Upon activation of the signalling pathway, USP7 exports to the cytoplasm and deubiquitinates K63-linked polyubiquitin chains on TRAF6 and IKKγ, which lead to inactivation of NF-κB/JNK and terminate the TLR-mediated response (Daubeuf et al. 2008). ICP0 exploits this negative feedback loop to inhibit the innate immune response and promote the survival and propagation of HSV.

Besides these proteins, USP7 partners up with a vast number of proteins in the cell for regulation and maintenance of normal cellular functions. The fact that numerous viruses and cancer cells have evolved to exploit the activity of USP7 as a part of their survival mechanism demonstrates the importance of its function as a tumor suppressor and cell regulator.

Numerous interaction studies of USP7 with its binding partners and substrates have shed light on the mechanisms of its interactions. However, the molecular basis of interaction of USP7 with its substrates is not yet fully understood. Using X-ray crystallography, this project focuses on structural studies of USP7 with two of its substrates/binding partners – CHFR and MCM-BP - to understand these interactions at a molecular level. Additionally, i*n vivo* studies assist in determining the relation between USP7 and CHFR in normal cellular conditions.

1.5 X-ray crystallography

X-ray crystallography is one of the methods used for determining protein structures. The method makes use of a protein crystal to diffract X-rays which produces a unique diffraction pattern. This pattern can be used to define the angles and intensities of the diffracted beams. These correspond to information about the electron density of the molecules which provide details on the average position of atoms in the crystal and chemical bonds. Refined models of atomic arrangement thus give rise to the protein's three dimensional structure (Smyth and Martin 2000).

Furthermore, co-crystal structures of a protein bound to its substrate (s) are used for various purposes such as drug design, to study specificity of ligands and the protein's enzymatic mechanisms, for site specific mutagenesis, or in general as a finer focus to further previously established research (Smyth and Martin 2000).

1.5.1 Interaction with USP7-NTD via substrate recognition motif

Crystal structures of the N-terminal (Saridakis et al. 2005), C-terminal (Faesen et al. 2011) and catalytic (Hu et al. 2002) domains of USP7 have been solved individually. Co-crystal structures of the NTD with peptides of some of its target proteins such as p53, HDM2, HDMX, UbE2E1 (Sarkari et al. 2010) and EBNA1 have also been established. Based on these structures as well as interaction assays, it is presently known that one mechanism for USP7 substrate recognition is by the presence of a P/AXXS motif on the substrate, which is recognized by a site on the N-terminal domain of USP7.

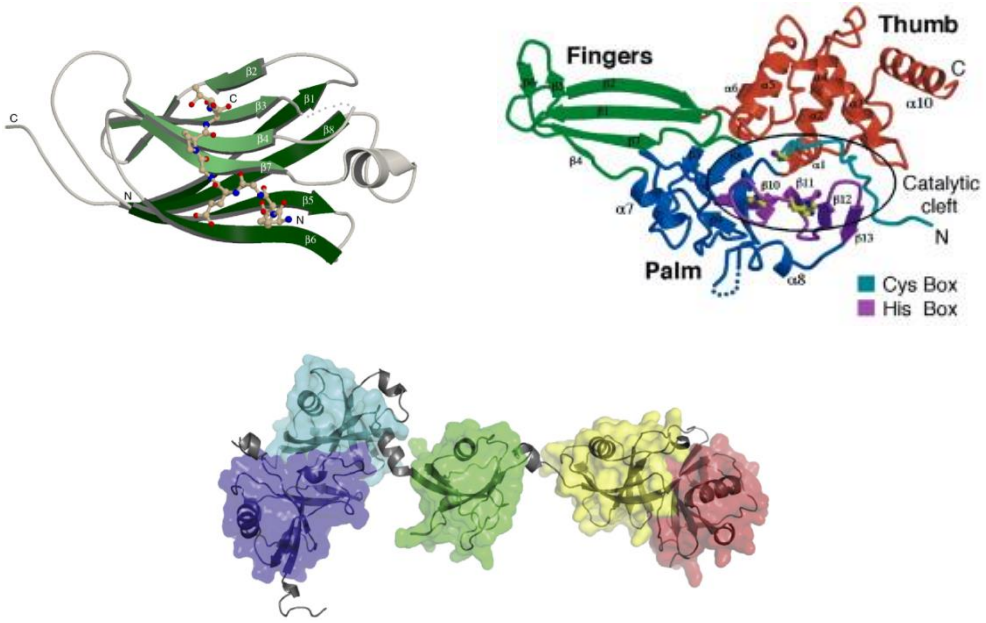

Figure 1.4. X-ray crystal structures of N-terminal (top left), catalytic domain (top right) and C-terminal (bottom) of USP7 have been determined by (Saridakis et al. 2005), (Hu et al. 2002), (Faesen et al. 2011), respectively.

1.6 Focus of this project

Proteomics studies have revealed that USP7 interacts with two proteins - minichromosome maintenance complex binding protein (MCM-BP) (Sowa et al. 2009) and checkpoint with forkhead and ring finger domain (CHFR) (Oh et al. 2007). These proteins contain the P/AXXS substrate recognition motif and it is hypothesized that these proteins will interact with USP7-NTD and the mechanism will be similar to what has been previously observed in interactions with USP7-NTD involving the recognition motif. This project thus aims to further investigate the involvement of this motif in order to understand the molecular mechanism underlying these interactions.

1.7 Preliminary work

The objectives of this project included determining the site of interaction between USP7, and CHFR and MCM-BP. Both the proteins consist of multiple P/AXXS sites, and through preliminary work (La Delfa, unpublished) it was determined that ^{177}PSTS^{180} and ^{155}PSTS^{158} from CHFR and MCM-BP, respectively, were responsible for interaction with USP7. Following this, mutational studies were used to confirm these sequences (La Delfa, unpublished).

Using peptide array studies with USP7-NTD and peptides from CHFR and MCM-BP containing the PSTS motif, it was discovered that the two proteins interact with USP7-NTD via the established substrate recognition motif, PSTS. The left panel in figure 1.5 shows the peptide array for CHFR wild type and mutant peptides. In a peptide array, the appearance of a spot indicates positive interaction (La Delfa, unpublished)

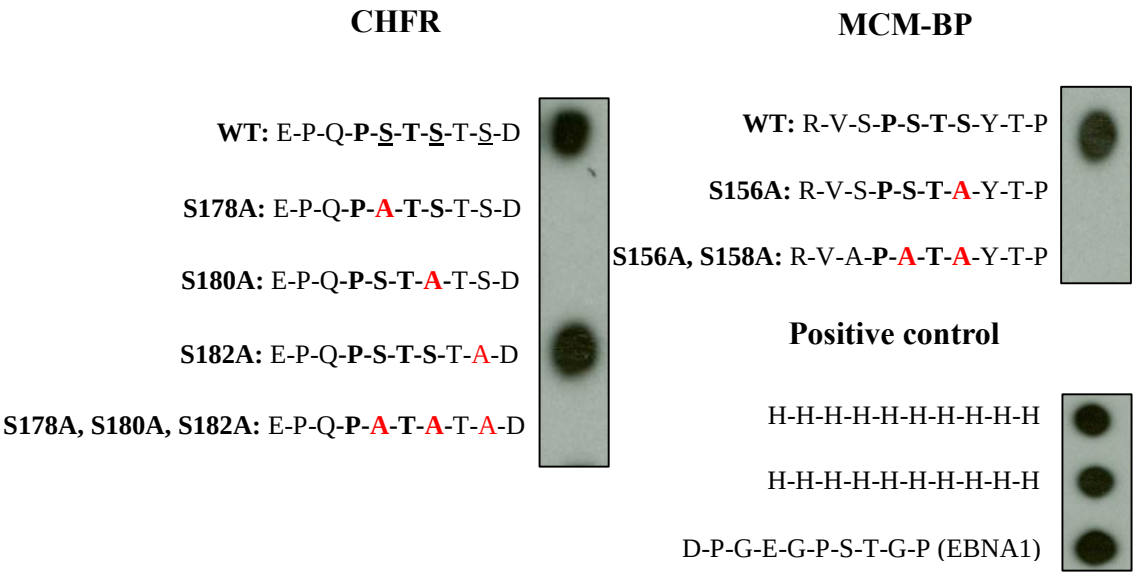

Figure 1.5: PSTS motif in CHFR and MCM-BP involved in interaction with USP7-NTD. A. P/AXXS substrate recognition sites in CHFR and MCM-BP were identified to be PSTS using peptide spot arrays. 10-mer peptides containing the motif were used for the arrays (^{174}EPQPSTSTSD^{183} and ^{152}RVSPSTSYTP^{161}, respectively). Interaction was observed for wild type peptides, as can be seen by the first spot on the arrays for CHFR and MCM-BP. Interaction was abolished when any of the serines were mutated within the motif (PSTS), however mutation of serine outside the motif did not affect binding. Positive controls for the arrays included poly-His and a previously published EBNA1 peptide.
(La Delfa, unpublished)

A spot appeared for the wild type peptide ^{174}EPQPSTSTSD^{183} but the interaction was abolished when the serines within PSTS were mutated to alanines (S178A and S180A). However, when a serine outside the motif was mutated, interaction was reinstated and a spot appeared for the S182A mutation. Similarly, the wild type MCM-BP peptide ^{152}RVSPSTSYTP^{161} displayed interaction, while the mutants did not. An EBNA1 peptide, which was previously shown to interact with USP-NTD, and Poly-His were used as positive controls (La Delfa, unpublished).

	Peptide	Dissociation Constant (Kd µM)
CHFR	^{174}EPQPSTSTSD^{183}	1.6
MCM-BP	^{152}RVSPSTSYTP^{161}	9.4
	^{152}RVSPSTAYTP^{161}	102

Figure 1.6: Intrinsic tryptophan fluorescence assay to demonstrate affinity of USP7-NTD for PSTS motif. The binding affinity of USP7 with CHFR and MCM-BP peptides was determined using intrinsic tryptophan fluorescence assay. Peptides with PSTS motif bound NTD-USP7 with high affinity. Mutation of serine in PSTS of MCM-BP resulted in lowered affinity, with a dissociation constant of 102 uM, compared with 9.4 uM for wild type PSTS.
(La Delfa, unpublished)

Interaction of CHFR and MCM-BP with USP7-NTD using the PSTS motif was further demonstrated, as shown in figure 1.6, using an intrinsic tryptophan fluorescence assay using the same peptides as the peptide spot array. The smaller dissociation constants for the wild type peptides as compared with a mutant for MCM-BP signals the use of the PSTS motif for binding to USP7-NTD (La Delfa, unpublished).

CHAPTER 2: INTERACTION STUDY BETWEEN USP7 AND CHFR

2.1 Introduction

Chromosomal instability and propagation of mutations are major events that can lead to cellular transformation. As such, it is important for the cell to be able to prevent mitotic errors, which is achieved through various checkpoints in the cell. Upon stress or DNA damage, checkpoint proteins are responsible for delaying the cell cycle progression to prevent a compromised genome from being propagated.

2.1.1 CHFR – the antephase checkpoint

One such checkpoint is CHFR, which is involved in the initial response to DNA damage by delaying entry into mitosis. Its N-terminal domain consists of an FHA (forkhead – associated) domain, it has a cysteine-rich C-terminus as well as a central RING domain. The function of the FHA domain is still under investigation, although Fukuda and colleagues demonstrated that the FHA domain is essential for the anti-proliferative effect of CHFR (Fukuda et al. 2008) and may be involved in its interaction with phosphorylated proteins (Li et al. 2002). The RING finger domain however, is well studied and renders an E3 ubiquitin ligase activity to the protein, which is utilized in its role in DNA damage by delaying the cell cycle progression. The known substrates of CHFR E3 ligase activity are PLK1, Aurora A, Kif22, HDAC1 and PARP1 (Privette and Petty 2008).

CHFR is a cytoplasmic protein, expressed ubiquitously in normal tissues, but is transported into the nucleus when it senses spindle or chromosomal damage or radiation induced stress (Derks et al. 2013). It functions at the antephase stage of the cell cycle, which is a point near late G2 when the chromosomes are beginning to condense.

However, if the cell is introduced to certain stressors, it is able to revert back to the previous stage temporarily, thus delaying entry into mitosis. If the cell goes past the antephase into prometaphase where chromosome condensation is completely achieved with the breakdown of the nuclear envelope, the cell can no longer revert to a previous stage and is committed to mitosis (Chin and Yeong 2010).

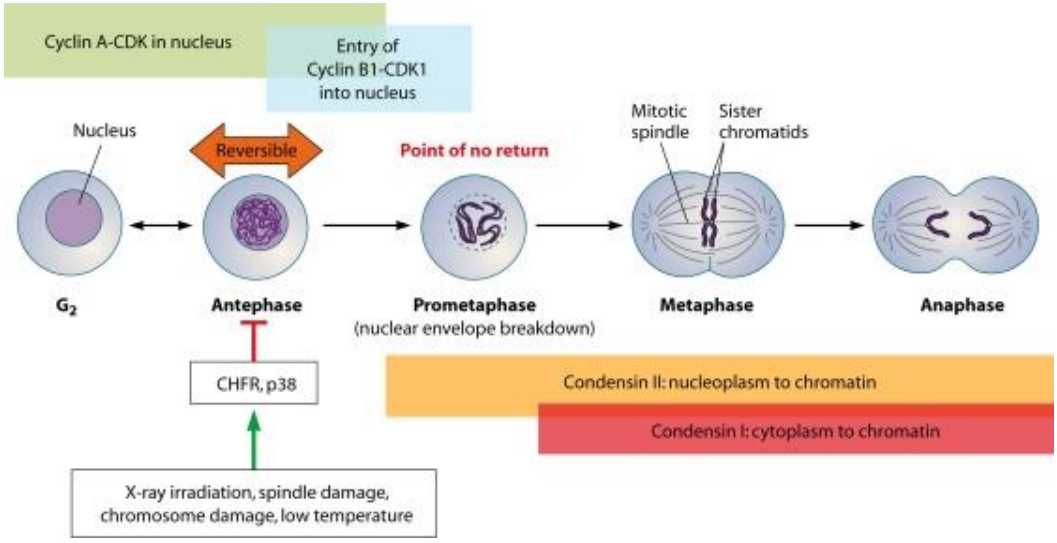

Figure 2.1. CHFR is an antephase checkpoint. Prior to chromatin condensation, if the cell encounters a stress, various checkpoints are activated to deal with the interruption to avoid the propagation of corrupt genome. One such checkpoint protein is CHFR, which acts at the antephase, by preventing the activation of the cyclinB1-CDK1 complex and reverting the cell to the previous phase with uncondensed chromatin and an intact nuclear envelope, thus delaying the cell cycle.

2.1.2 Proteasomal E3 ligase activity of CHFR

The cyclinB1-Cdk1 pathway

Chromosomal condensation and nuclear envelope breakdown are achieved by the action of a complex of kinases, cyclinB1-Cdk1. This complex is not present in an active stage throughout the cell cycle; it gets activated before mitosis near the end of antephase. CyclinB1 is always present in the cytoplasm in an unphosphorylated state, but is transported into the nucleus before mitosis by phosphorylation. In addition, Cdk1 remains phosphorylated in an inactive state, but gets dephosphorylated by Cdc25, allowing it to form an active complex with cyclinB1 in the nucleus (Derks et al. 2013, Berry and Gould 1996, Hagting et al 1999). Cdc25 is also regulated by its phosphorylation state and is activated to carry out its function in the cyclinB1-Cdk1 pathway by PLK1 (Polo-like kinase 1). Finally, PLK1 is itself phosphorylated and activated by the action of another kinase at the top of this pyramid, called Aurora A (Derks et al 2013).

By activating the cyclinB1-Cdk1 pathway, Aurora A and PLK1 have established an essential role in the commitment of the cell to mitosis, with no possibility for return to a previous phase. The E3 ligase activity of CHFR is involved in the ubiquitin-mediated destabilization of Aurora A and PLK1 (Kwon et al. 2013). By targeting the proteins for degradation, CHFR is able to prevent the activation of the cyclinB1-Cdk1 pathway resulting in cell cycle delay, allowing for the DNA damage response to be undertaken.

Besides directly being involved in the regulation of the cyclin-cdk1 pathway, CHFR also plays a role in maintaining another G1 checkpoint protein p21. p21 is a cyclin-dependent

kinase inhibitor that directly inhibits the activity of the cyclinB1-Cdk1 pathway, amongst others. p21 is transcriptionally inhibited by the activity of HDAC1 (histone deacetylase 1), which is a substrate of CHFR. By ubiquitinating HDAC1, CHFR is able to inhibit HDAC1, allowing for the expression of p21 and restoring the G1checkpoint (Derks et al. 2013, Gartel and Radhakrishnan 2005).

The PAR-PARP1 DNA damage response

Another aspect of the E3 ligase activity of CHFR involves its recruitment to the site of DNA damage. PolyADP-ribose (PAR) is covalently bound to the site of damage and along with PAR polymerase 1 (PARP1) is involved in recovery from the damage (Liu et al. 2013, Ahel et al. 2008). PARP1 is continuously recycled and activated in the process unless removed from the DNA. Hyper-active PARP1 can cause genomic instability and thus its eviction from the DNA during the repair response is central to a normal recovery (Liu et al. 2013). PAR is recognized by a PAR-recognition motif in the C-terminus of CHFR. This results in the recruitment of CHFR to the site of damage where it ubiquitinates PARP1 for proteasomal degradation and regulates its levels for a balanced DNA damage response, avoiding further genomic instability (Kashima et al. 2012).

2.1.3 Proteasome-independent E3 ligase activity of CHFR

In addition to its proteasome-dependent ubiquitination, CHFR employs proteasome-independent ubiquitination to achieve various blocks in the cell cycle progression, including activating a p38 kinase pathway that decondenses chromosomes, as well as MAD2 which is a spindle assembly checkpoint (Derks et al. 2013).

2.1.4 Regulation of CHFR

Analysis of cancer cell lines for CHFR expression has revealed that most tumor cells either undergo promoter-methylation dependent silencing of CHFR or express a mutated form (Toyota et al. 2003). Although its function is well understood, its regulation in the cell is still under investigation. Since it has functions in so many pathways as a checkpoint protein, it is imperative to understand how its levels are modulated in the cell.

Every E3 ubiquitin ligase partners up with multiple E2 ubiquitin conjugating enzymes to perform their ubiquitination function. There are several known E2 partners of CHFR including UbE2D1, UbE2D2 and UbE2D3 for its K48-linkage polyubiquitination and a heterodimer enzyme complex of UbE2N-MMS2 for the K63-linked polyubiquitin chains (Privette and Petty 2008). However, this list is not exhaustive, and there are E2 enzymes that haven't been tested with CHFR yet. RNF8 is a CHFR homolog that is also involved in the DNA damage response, and contains FHA and RING domains similar to CHFR. Interestingly, the two RING domains are interchangeable and in fact use similar E2 partners (Liu et al. 2013). One of the E2 partners of RNF8 is UbE2E1 (Ito et al. 2001), and since RNF8 shares a RING domain with CHFR, this could also be a potential E2 partner of CHFR.

Being an E3 ligase, CHFR is capable of auto-ubiquitination targeted towards keeping a low level of itself in normal cells, and is one of the key events involved in a normal mitotic entry (Kim et al. 2011). Interestingly, USP7 was found to interact with CHFR (Oh et al. 2007), providing a link to its method of regulation.

2.1.5 Objectives

CHFR contains a P/AXXS (PSTS) motif and the purpose of this project is to determine if it interacts with the N-terminal domain of USP7, and to structurally determine if the recognition motif in CHFR is responsible for the interaction.

Further, *in vivo* expression levels of CHFR in the absence of USP7 were tested using HEK293T cells in which CHFR is endogenously expressed, with USP7 silenced using siRNA. As a result, the effect of USP7 on CHFR stability can be determined, confirming a role for USP7 directly at a mitotic checkpoint.

This project also aimed to determine if UbE2E1 is a ubiquitin-conjugating partner of CHFR using a co-immunoprecipitation assay.

2.1.6 Techniques employed to achieve objectives

In order to test whether CHFR interacts with the N-terminal domain of USP7, a GST pull-down assay was used with USP7-NTD expressed as a GST-fusion protein and cell lysate expressing CHFR was applied to it to pull-down CHFR.

The method employed to test the stability of CHFR is called a protein turnover assay. This technique monitors the half-life a protein after blocking the translational machinery. The translation machinery is blocked by a chemical called cycloheximide, which is derived from *Streptomyces griseus* and inhibits the elongation stage of protein translation in eukaryotes (Schneider-Poetsch et al. 2010). The advantage of this technique is that the half-life of proteins can be visualized without the need to account for newly synthesized protein.

The interaction between CHFR and UbE2E1 was tested using a co-immunoprecipitation assay. In this assay, a protein of interest is isolated from a cell lysate using antibody specific to the protein, bound to beads to immobilize it and blotted for a second interacting protein that is being tested. If the two proteins interact, the interacting protein would have co-immunoprecipitated with the protein of interest and could be visualized in the same fraction. However, if the two proteins don't interact, the interacting protein would be recovered in a separate unbound fraction.

2.1.7 Hypotheses

It is hypothesized that CHFR will interact with USP7-NTD and that the PSTS motif is responsible for this interaction, where the mechanism of interaction will be similar to what has previously been observed with interaction of USP7 and p53, Hdm2, HdmX and EBNA1.

In the *in vivo* protein turnover assay, it is expected that in cells lacking USP7, endogenous CHFR will get degraded faster, or have a shorter half-life, than in the presence of USP7 due to the lack of deubiquitinating activity of USP7.

In determining whether RNF8 and CHFR share the E2 ubiquitin conjugating enzyme, it is expected that UbE2E1 will interact with CHFR.

2.2 Materials and Methods

2.2.1 PCR amplification of CHFR

A plasmid encoding for the human CHFR cDNA was obtained from the Mammalian Gene Collection (Clone ID: 4650348). The cDNA was PCR amplified using forward primer 5'-GCA CTC GAG CTA TGG AGC GGC CCG AGG AA-3' and reverse primer 5-CAG GGT ACC GTT TTT GAA CCT TGT CTG TTC ACA-3', with XhoI and KpnI digestion sites incorporated into the primers, respectively. Eight annealing temperatures were used to test for optimal product. Each reaction was performed in a final volume of 50 µl and contained 3mM $MgSO_4$, 0.3mM each of the dNTPs, 1XPfu Buffer (20mM Tris-HCl pH 8.8, 1mM $MgSO_4$, 10mM KCl, 10mM $(NH_4)_2SO_4$, 0.1% Triton X-100, 0.1 mg/ml nuclease-free BSA), 50 pmol each of forward and reverse primers, DNA template and 0.05U/µl Pfu DNA polymerase. A thermocycler with a temperature gradient block was used to set up the PCR. Following is the PCR program used:

Step	Temperature (^oC)	Time	No. of Cycles
Initial Denature	95	10 min	1
Denature	95	1 min	30
Annealing	X	1 min	
Extension	72	5 min	
Final Extension	72	20 min	1

"X" under Annealing Temperature refers to a gradient of the annealing temperatures used: 56.1^{0}C, 56.7^{0}C, 58.1^{0}C, 59.0^{0}C, 59.9^{0}C, 60.9^{0}C, 61.9^{0}C, 63.0^{0}C

The PCR products were separated on a 1% agarose gel for 40 mins at 100V (5 µl sample + 1 µl 6xDNA dye) to test for the presence of a 1.9 kb DNA band representing the amplified DNA. The PCR products were then gel purified to isolate the desired DNA.

2.2.2 Isolation of amplified CHFR DNA

The amplified DNA was isolated by separating the products on a 1% agarose gel, excising the desired band and extracting the DNA using the illustra GFX PCR DNA and Gel Band Purification Kit (GE Healthcare). The DNA was eluted in 50 µl ddH_2O.

2.2.3 Cloning CHFR into pCMV3FC mammalian vector

The gel extracted CHFR DNA was serially digested using XhoI (NEB) in 1XNEB1, 1XBSA, and using 1µg DNA in a 50 µl volume at 37°C overnight, followed by heat inactivation at 65°C for 20 minutes and digesting with KpnI with the same conditions as that for XhoI in a 60 µl reaction volume at 37°C for 10 minutes. The digested DNA was subjected to a reaction cleanup using the illustra GFX PCR DNA and Gel Band Purification Kit (GE Healthcare) and eluted with 50 µl ddH_2O. The digested DNA was ligated with XhoI/KpnI digested pCMV3FC mammalian vector (encoding for a C-terminal 3XFlag) using T4 DNA Ligase (NEB), incubated overnight at 37°C.

The ligated DNA was electroporated into *Escherichia coli* DH5α electrocompetent cells (1 µl DNA + 25 µl cells), plated onto LB agar plates with 50 ng/ml kanamycin for selection and incubated overnight at 37°C. Of the resulting colonies, 8 were picked and cultured overnight in 5 ml of LB broth with 50 ng/ml kanamycin at 37°C. Plasmid DNA

was isolated from the resulting culture using the QIAprep Spin Miniprep Kit and the DNA was eluted with 50 µl ddH_2O. To check for the presence of the correct insert, a XhoI/KpnI serial double digest was set up as before and the resulting samples were separated on a 1% agarose gel. The positive clone was confirmed with sequencing and the plasmid encoded for Flag-CHFR.

2.2.4 Testing interaction of CHFR with USP7-NTD using GST pull-down

The interaction between CHFR and the N-terminus of USP7 (amino acid residues 54-205) was tested using GST pull-down, with GST-tagged USP7-NTD.

E. coli BL21 (DE3) MGK cells with a pGEX2tk plasmid encoding for GST-USP7-NTD were cultured in Terrific Broth (TB, Bioshop) with 100 ng/ml ampicillin and 50 ng/ml kanamycin and protein expression was induced using 0.4mM IPTG (Bioshop), overnight at 16°C. The cells were harvested at 7,446 x g for 30 minutes in a Beckman-Coulter centrifuge with rotor JLA 9.1 at 4°C. 0.5 g of the resulting pellet was lysed using 2 ml of 1XPBS with 1XProtease inhibitor cocktail (0.05mM phenylmethylsulfonyl fluoride (PMSF), 0.1mM benzamide, cold absolute ethanol) at 30% amplitude, 20 sec ON 15 sec OFF for a total ON time of 80 seconds. The lysed cells were centrifuged at 21,339 x g for 10 minutes at 4°C. A 50 µl sample of the lysate was stored to be used for analysis, and the remaining lysate was subjected to glutathione beads equilibrated with 1XPBS. The protein was allowed to bind to the GST resin for 1 hour at 4°C with rotating. The resulting unbound fraction was collected and the resin was washed three times with 1 ml of 1XPBS. The last wash was collected and the resin was ready to be used for the GST

pull-down. This exact procedure was also carried out for GST protein to be used as a negative control.

HEK293T cells were cultured with DMEM media supplemented with 5% FBS and transfected with 10 µg of the Flag-CHFR plasmid using Lipofectamine 2000 Transfection Reagent (Life Technologies). The cells were harvested 48 hours post transfection by washing three times with 1XPBS. The resulting cell pellet was lysed using 50mM Tris pH 8, 150mM NaCl, 0.5% NP-40, 1XProtease inhibitor cocktail and 1XProtease inhibitor tablet (Roche cOmplete ULTRA Tablets). The cells were allowed to lyse for 15 minutes at 4°C with rotating followed by sonication at 10% amplitude with 1 sec ON 1 min OFF for a total ON time of 3 seconds. The lysed cells were centrifuged at 17,000 x g for 10 minutes at 4°C. 50 µl of the resulting lysate was stored as input. The NaCl concentration in the remaining lysate was diluted to 50mM with 50mM Tris pH 8 to prevent interference during interaction. 1XPBS was also diluted 3 times to reduce the salt concentration.

Diluted Flag-CHFR lysate (250 µl) with 300 µl of diluted PBS, 250 µl of ddH_2O and 1XProtease inhibitor cocktail were added to the GST-USP7-NTD and GST resins and were left rotating overnight at 4°C. The resulting unbound fractions were collected and the resin was washed three times with 500 µl of diluted PBS. A sample of the beads was taken at this point (beads pre-E) and the GST-tagged proteins were eluted with 20mM reduced glutathione (GSH) by incubating the resin with 500 µl with rotating at room

temperature for 15 minutes. The beads were then centrifuged and the supernatant collected as elution. A sample of the beads was also taken post elution (beads post-E).

A 10% SDS gel was run with 10 µg of Flag-CHFR lysate and samples from the unbound fraction, beads pre-E, elution (E) and beads post-E, for both the pull-downs. The gel was run at 70V for the first 30 minutes (through the stacking gel) and 195V for the next 40 minutes. The proteins were transferred to a PVDF membrane at 100V for 75 minutes at 4°C. The membrane was blocked for an hour with 5% milk in PBS at room temperature and blotted overnight with an anti-Flag primary antibody (Sigma F3165) at 1:1000 dilution. The membrane was washed 3 times with 1XPBS-T for 5 minutes each, with rinsing with 1XPBS in between each wash. It was then blotted with an anti-mouse HRP secondary antibody for 1 hour at room temperature at 1:20,000 dilution, followed by three washes of 15 minutes each. The membrane was incubated in ECL solution (GE Healthcare) for 1 minute, exposed onto a film for 30 seconds and the film developed to visualize Flag-CHFR. The membrane was then stripped of the current antibodies by boiling it with 50mM Tris pH 6.8, 2% SDS, 100mM β-Me and washed for 10 minutes 3 times. The blotting was repeated at before with an anti-GST primary antibody (Novagen 71097) at a 1:4000 dilution and an anti-mouse HRP secondary antibody at a 1:20,000 dilution. The film was exposed for 1 minute and developed to visualize GST-USP7-NTD and GST proteins.

2.2.5 Molecular basis of interaction between USP7-NTD and CHFR

Expression and purification of USP7-NTD

E. coli BL21 (DE3) cells containing a plasmid encoding for 6xHis-tagged USP7-NTD were cultured in TB with 100 ng/ml ampicillin and expression was induced overnight using 0.4mM IPTG at 16°C. The cells were harvested at 7,446 x g for 30 minutes at 4°C. The resulting pellet was lysed with 4 ml of Lysis Buffer per gm of pellet (100mM Hepes pH 7.5, 500mM NaCl, 10% glycerol, 10mM Imidazole, 0.5mM TCEP, 1XProtease inhibitor cocktail). The cells were sonicated at 30% amplitude, 15 sec ON 10 sec OFF for a total ON time of 6 minutes, with a pause after 3 minutes. The lysed cells were centrifuged at 41,287 x g for 30 minutes at 4 °C. A sample was taken from the supernatant for SDS PAGE analysis and the remaining lysate was incubated with Ni^{2+} agarose beads equilibrated with the Lysis Buffer, with gentle rocking at 4°C for 2 hours. The proteins left unbound after binding were collected and the resin was washed with 100 ml of Wash Buffer (100mM Hepes pH 7.5, 500mM NaCl, 10% glycerol, 25mM Imidazole, 0.5mM TCEP). The wash was collected and the isolated protein was eluted with Elution Buffer (100mM Hepes pH 7.5, 500mM NaCl, 10% glycerol, 250mM Imidazole, 0.5mM TCEP).

Samples obtained from lysate, unbound proteins, wash and elute (16 µl sample + 4 µl 5XSDS dye) were resolved on a 10% SDS gel at 195V for 65 minutes and a PageRuler Prestained Protein Ladder was used as a MW reference.

The purified 6xHis-USP7-NTD contains a thrombin cleavage site between the His-tag and the protein. To cleave the 6xHis-tag, the protein was incubated with 0.5 units thrombin (Sigma T6884) per mg protein and 2.5mM $CaCl_2$ for 72 hours at 4°C. Samples of the protein were taken before and after cleavage (His-uncleaved and His-cleaved, respectively) and resolved on a 15% SDS gel run at 220V for 35 minutes. The marker used was PageRuler Prestained Protein Ladder.

The His-cleaved USP7-NTD was then subjected to size exclusion chromatography HiLoad 16/60 Superdex 200 prep grade column (GE Healthcare) on an AKTA Purifier (GE Healthcare) to further remove impurities from the protein and to exchange the protein into 20mM Hepes pH 7.5, 500mM NaCl. The cleaved dialyzed protein was used for protein crystallization trials.

Co-crystallization trials of USP7-NTD with CHFR^{PSTS} peptide

USP7-NTD was concentrated to 100 mg/ml and mixed with 5-fold molar excess of CHFR peptide ^{174}EPQPSTSTSD^{183} with N-terminal acetylation and C-terminal amidation (synthesized by CanPeptide Inc.) and incubated overnight at 4°C. Co-crystal trials were set up using micro-seeding with USP7-NTD:HdmX as seeds in 0.1 M Tris pH 8.5, 30% PEG 4000, and 0.2 M Lithium Sulfate.

X-ray data collection and molecular structure determination

A USP7:CHFR crystal was frozen and X-ray diffraction data was collected at 100K on a Rigaku MicroMax007 rotating anode diffractometer with a 944+ CCD (charge-coupled-device) detector. HKL2000 was used to integrate and scale the diffraction data and

molecular replacement was used to determine the structure (Otwinowski and Minor 1997). USP7 54-205 (PDB identifier [ID] 1YY6) without any peptide was used as the search model in CNS program (version 1.3) (Brunger 2007). The electron density was visualized and the model was rebuilt using the molecular graphics program O (Jones and Kjeldgaard 1997). CNS 1.3 was used for refinement and $2F_o$-F_c and F_o-F_c maps were inspected for further refinement and model rebuilding in O. Water molecules were picked using CNS 1.3 and verified in O. The figures were created using the software program PyMOL (version 1.3).

2.2.6 Determining cellular effect of USP7 on CHFR

Comparing the stability or turnover of CHFR in the presence and absence of USP7

For the turnover assay, cells were harvested at six time points (0, 2, 4, 8, 24, 48 hour); thus the experiment was carried out in 6-well plates with a 2 ml working volume per well. Two sets of 6-well plates were used - one for experimental (siUSP7) and one for negative control (siNC).

HEK293T cells were transfected separately with siRNA for USP7 (siUSP7) and negative control (siNC) using 30nM siRNA and LipoJet In Vitro Transfection Kit (SignaGen Laoratories). The cells were incubated for 72 hours post transfection to allow for sufficient silencing of USP7. The cells were then split into 6-well plates, allowed to settle for 3 hours and subjected to 50 µg/ml cycloheximide treatment. The cells were harvested at 0, 2, 4, 8, 24 and 48 hour time points post cycloheximide treatment, washed three times with 1XPBS.

The resulting cell pellet was lysed with 50mM Tris pH 8, 150mM NaCl, 0.5% NP-40, 1XProtease inhibitor cocktail and 1XProtease inhibitor tablet (Roche cOmplete ULTRA Tablets) for 15 minutes at 4°C with rotating, followed by sonication at 10% amplitude with 1 sec ON and 1 min OFF for a total ON time of 3 seconds. The lysed cells were centrifuged at 17,000 x g for 10 minutes at 4°C. 10 µg of the lysates were subjected to SDS PAGE on 10% SDS gels (four gels) at 195V for 65 minutes. The proteins were then transferred to PVDF membranes and subjected to Western Blotting at 100V for 1 hour.

The membranes were cut to allow for separate blotting of CHFR and GAPDH which was used as a loading control. They were blocked for 1 hour with 5% milk in 1XPBS and blotted with anti-CHFR (Abcam, 1:100 dilution) and anti-GAPDH primary antibodies for 1 hour and washed with 1XPBS-T three times for 5 minutes each with rinses with 1XPBS between each wash. They were then blotted with anti-mouse HRP secondary antibody for 45 minutes and washed with 1XPBS-T three times for 15 minutes each. The membranes were incubated with ECL solution for 1 minute and a film was exposed to the membranes. The membranes were then stripped and re-probed with anti-USP7 primary antibody (Bethyl, 1:10,000 dilution) and anti-rabbit HRP secondary antibody.

2.2.7 Testing if UbE2E1 and CHFR are interacting partners

Co-immunoprecipitation (Co-IP) with endogenous UbE2E1 and over-expressed CHFR

10 µg Flag-CHFR was transfected in HEK293T cells and harvested 48 hours post transfection and lysed with 50mM Tris pH 8, 150mM NaCl, 0.5% NP-40, 1XProtease inhibitor cocktail and 1XProtease inhibitor tablet (Roche cOmplete ULTRA Tablets), as

described previously. The proteins were immunoprecipitated with Flag and blotted for Flag and UbE2E1. To accomplish this, 1 mg of lysate was incubated with 2 µg of rabbit anti-ECS (DDDK or Flag) antibody and 2 µg of anti-IgG antibody (negative control), separately, and left rotating at 4°C overnight. This was applied to 15 µl of Protein A/G Plus-Agarose beads pre-cleared with 5% BSA in 1XPBS and incubated for 1 hour with rotating at 4°C to immobilize the immunoprecipitated protein (Flag-CHFR and IgG) and any protein bound to it. After incubation the unbound protein fraction was collected by centrifuging the samples at 8,000x g for 1 minute and collecting the supernatant. The beads were then washed four times with 0.5 ml of 50mM Tris pH 8, 150mM NaCl, 0.5% NP-40, 1XProtease inhibitor cocktail and 1XProtease inhibitor tablet (Roche cOmplete ULTRA Tablets) and the last wash was collected. 30 µl of 5XSDS dye was added to the samples, boiled for 3 minutes, centrifuged at 8,000 x g for 1 minute and the supernatant was collected as the eluate.

Two 10% SDS gels were run with the same samples (from IP: Flag and IP: IgG) and subjected to Western blotting to visualize Flag-CHFR and UbE2E1 separately. The gel that was blotted for Flag-CHFR had 10 µg of the lysate (input), 10 µl each of the unbound and wash samples and 5 µl of the eluate. The gel that was blotted for endogenous UbE2E1 contained 30 µg of input, 20 µl each of the unbound and wash and 25 µl of the eluate. The gels were run at 195V for 65 minutes, the transfer was set up at 100V for 1 hour and the membranes were blotted with mouse anti-Flag and anti-UbE2E1 primary antibodies and anti-mouse HRP secondary antibodies.

2.3 Results

2.3.1 E3 ligase CHFR interacts with the N-terminal domain of USP7

CHFR cDNA was amplified using PCR (Figure 2.1A), digested with XhoI and Kpn1, cloned into pCMV3FC mammalian expression vector and the ligated product was electroporated into *E. coli* DH5α cells. Plasmids were isolated from the resulting colonies and digested with Xho1 and Kpn1 to test for the presence of the correct 1.9 kb CHFR insert. As seen in figure 2.1B, of the eight colonies tested, one yielded a positive insert at 1.9 kb along with the plasmid backbone.

GST pull-down using GST-USP7-NTD and Flag-CHFR

To determine if the interaction of CHFR is with the N-terminal domain of USP7 (USP7-NTD), a GST pull-down of Flag-CHFR (lysate from HEK293T cells expressing Flag-CHFR) with GST-USP7-NTD was performed. A pull-down of Flag-CHFR with GST was also performed to serve as a negative control. Figure 2.2 displays a western blot of the samples taken from the pull-downs. Lanes 3 and 5 contain samples of beads taken pre-elution and post-elution, respectively, and these contain any protein that was bound to the beads. The membrane was blotted with anti-Flag and anti-GST to visualize Flag-CHFR and GST-tagged proteins, respectively. Even though a small fraction of Flag-CHFR is seen in the unbound fraction in the pull-down with USP7-NTD, Flag-CHFR is evident in lanes 3 and 5, as well as a faint band present in the eluate in lane 4; GST-USP7-NTD is also present in the same samples. However, in the pull-down with GST, Flag-CHFR is

not present in the samples with GST (lanes 7 and 8), only in the unbound fraction, suggesting that CHFR bound to GST-USP7-NTD.

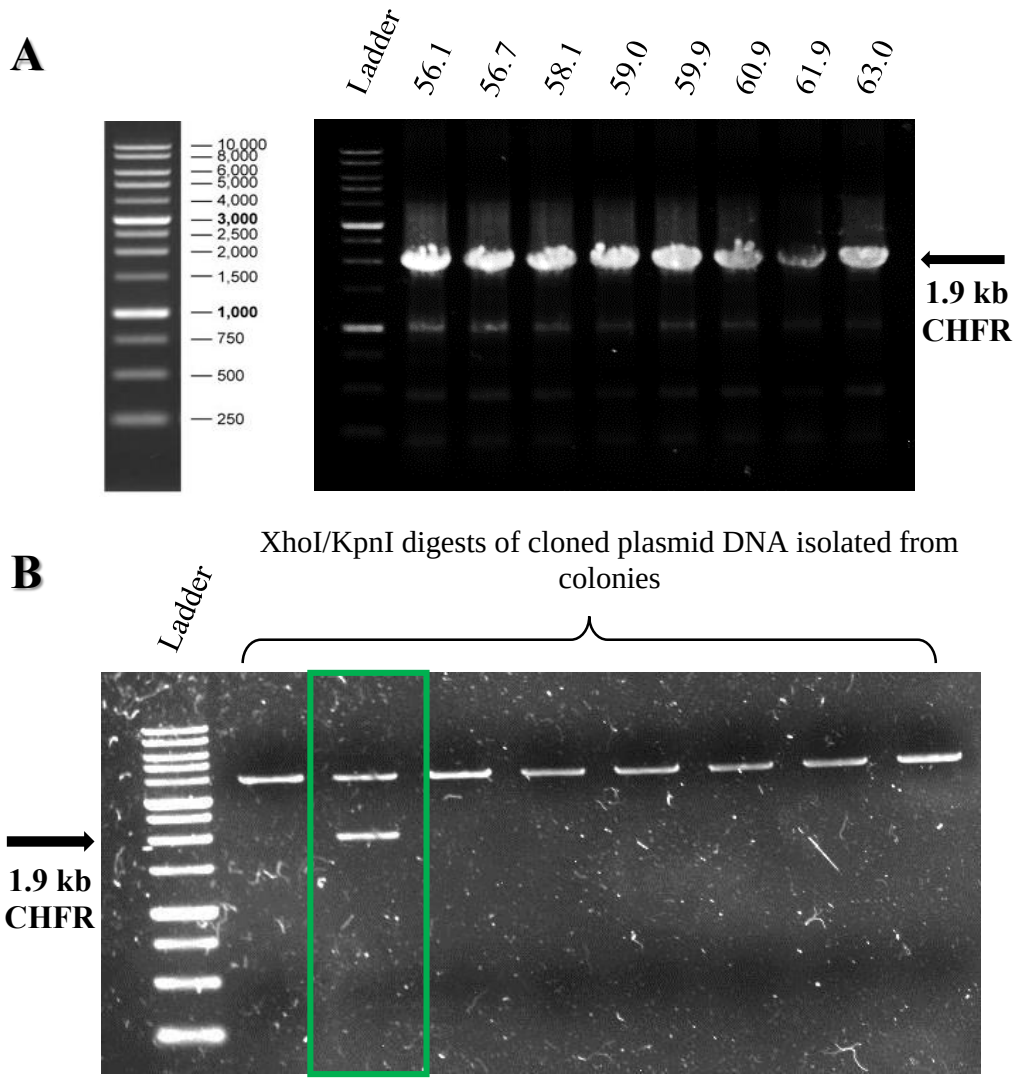

Figure 2.2: PCR amplification and cloning of CHFR into mammalian expression vector pCMV3FC. A) CHFR cDNA was PCR amplified at eight annealing temperatures to test for optimal product. It could be amplified at all the temperatures except 61.9^{0}C. XhoI and KpnI digestion sites were incorporated into the primers. The PCR products were gel purified to isolate the desired DNA at 1.9 kb, digested with XhoI and KpnI and ligated with cut pCMV3FC vector. The resulting plasmid was cloned into *E. coli* DH5α cells. **B)** Plasmids were obtained from resulting colonies and digested with XhoI/KpnI to test for positive insert. Seven of the tested colonies were false positives, whereas one showed an insert at 1.9 kb, highlighted in green in the figure. The positive clone was confirmed with sequencing. The samples were separated on a 1% agarose gel, run at 100 V. The ladder used was GeneDireX 1 kb RTU DNA Ladder.

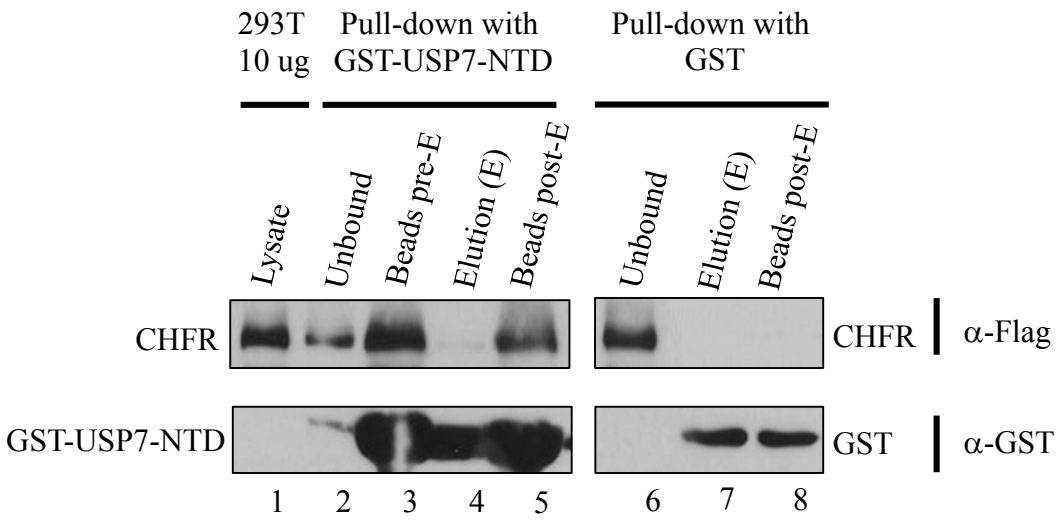

Figure 2.3: GST pull-down shows interaction between CHFR and USP7-NTD. Cell lysate from HEK293T cells overexpressing Flag-CHFR was subjected to glutathione beads bound to GST-USP7-NTD and interaction was allowed to happen overnight. GST was used in place of GST-USP7-NTD as a negative control. The unbound fractions containing proteins that did not interact with USP7-NTD or GST were collected (lanes 2, 6). The beads were washed with PBS and eluted with 20 mM GSH (lanes 4, 7). Beads pre-E (lane 3) and post-E (lanes 5, 8) refer to a sample of beads taken before and after elution, respectively. A 10 ug lysate sample from 293T cells was used as input (lane 1). The samples were resolved by SDS-PAGE and transferred to a PVDF membrane for Western Blotting. Ant-flag antibody was used to detect Flag-CHFR (top panel), the membrane was stripped and anti-GST antibody was used to detect GST-USP7-NTD and GST (bottom panel). Flag-CHFR can be seen present on the beads with GST-USP7-NTD in lanes 3 and 5 along with a small amount seen in elution in lane 4. Note: low amount of flag-CHFR in elution was due to insufficient elution, as can be seen from GST-USP7-NTD left on the beads after elution as well. However, when compared with GST and the absence of flag-CHFR in elution (lane 7) and beads post-E (lane 8), it is evident that CHFR interacts with USP7-NTD.

2.3.2 Molecular basis of interaction of USP7 with CHFR^{PSTS} involves its ^{164}DWGF^{167} binding pocket

Purification of His-USP7-NTD

To determine the molecular basis of interaction, co-crystal structure of USP7-NTD with a peptide from CHFR (^{174}EPQPSTSTSD^{183}) was determined using X-ray crystallography. USP7-NTD was purified using Ni^{2+} affinity chromatography (Figure 2.3A) and exposed to thrombin to cleave the 6xHis tag (Figure 2.3B). The small difference in sizes of uncleaved and cleaved proteins in figure 2.3B (18.5 kDa and 17.8 kDa, respectively), show successful removal of the 6xHis tag from the protein.

Co-crystallization trials and molecular structure determination

The cleaved USP7-NTD was successfully co-crystalized with 5-fold excess of CHFR peptide in 0.1M Tris pH 8.5, 30% PEG 4000 and 0.2M Lithium Sulfate using micro-seeding with crystals from the USP7-NTD:HdmX complex as seeds to produce long, rod-shaped crystals as seen in figure 2.4. These crystals were used to diffract X-rays and the diffraction patterns were used to determine the three-dimensional structure of the complex. Figure 2.6 displays one of the diffraction images collected for a complete data set. The first image (figure 2.6A) is lighter to show the reflections in the medium resolution shells. Spots can clearly be seen until the 2.44Å shell. However, reflections at higher resolutions can be viewed in figure 2.6B, with a magnified region around 2.1Å. Each spot on the image is a reflection created by the constructive interference of X-rays when they get diffracted through a crystal.

Using molecular replacement, the USP7-NTD:CHFR^{PSTS} structure was solved to 1.6Å. Table 2.1 lists the X-ray data collection and refinement parameters for the structure. The space group was $P4_1$ with a = b = 70.0 Å and c = 45.7 Å unit cell parameters. At the highest resolution shells the data was found to be 50%. The Ramachandran plot values with 97.3% of the residues at their favored regions signals the validity of the determined structure.

CHFR binds to the β-7 strand of USP7

Figure 2.7A displays the molecular structure, with USP7-NTD depicted as a ribbon diagram in chocolate brown and the peptide represented in yellow (CHFR) in stick-form. The N-terminal domain of USP7 consists of an anti-parallel beta-sandwich of eight β-strands that resembles a TRAF domain. This domain was modelled from residues 63-205 instead of 54-205 since the initial residues were too disordered to assign an atomic structure. The CHFR peptide interacts with the β7 strand of USP7-NTD and is situated such that it hugs the two beta-sheets along its length. The orientation of the structure, as visualized in figure 2.7A, will be referred to as the frontal view since it provides the optimal view of the peptide and protein together. Figures 2.7B and C represent surface and electrostatic charge diagrams of the structure, respectively, both in frontal view.

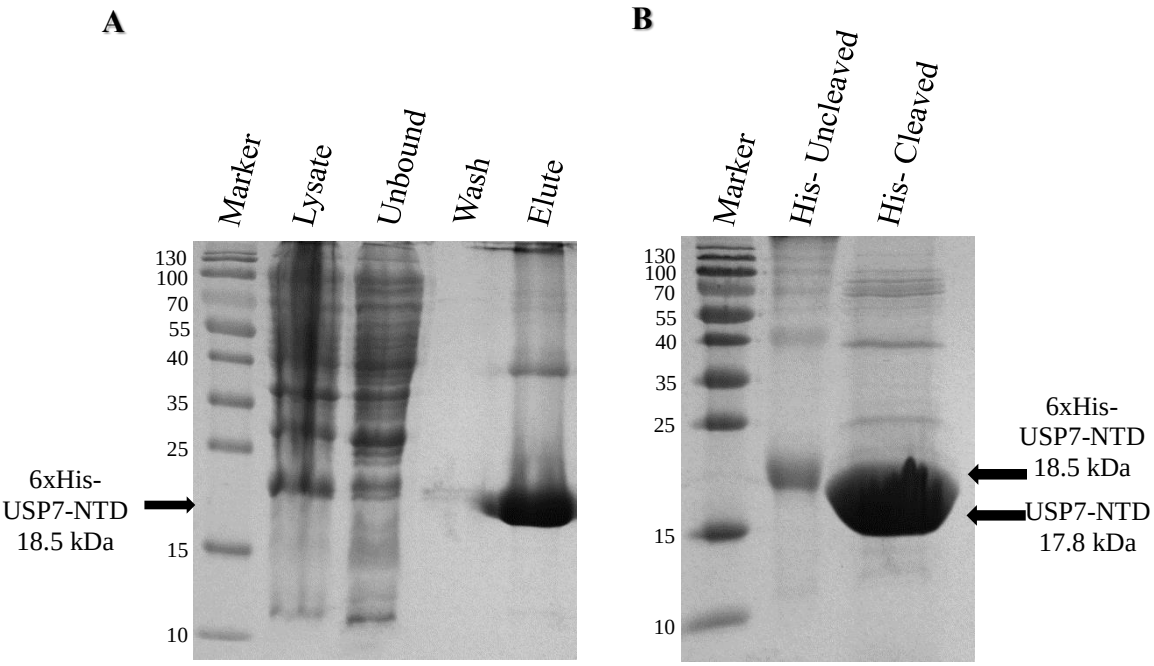

Figure 2.4: Purification of USP7-NTD using Ni2+ affinity chromatography. A) 6xHis tagged N-terminal domain of USP7 (residues 54-205) was overexpressed in *E. coli* cells and purified using Ni2+ affinity chromatography. Samples from lysate, unbound proteins, wash and elute were collected and separated on a 15% gel at 195V for 65 minutes A band can be seen in Elute at ~18.5 kDa, representing 6xHis-USP7-NTD. **B)** The purified protein was incubated with thrombin for ~72 hrs at 4^0C to cleave the 6xHis tag. The difference in MW of uncleaved and cleaved protein can be seen at 18.5 kDa and 17.8 kDa, respectively. The cleaved protein was subjected to size exclusion chromatography for use in X-ray crystallography. Samples were separated on a 15% gel at 220V for 35 minutes. The ladder used for both the gels was PageRuler Prestained Protein Ladder.

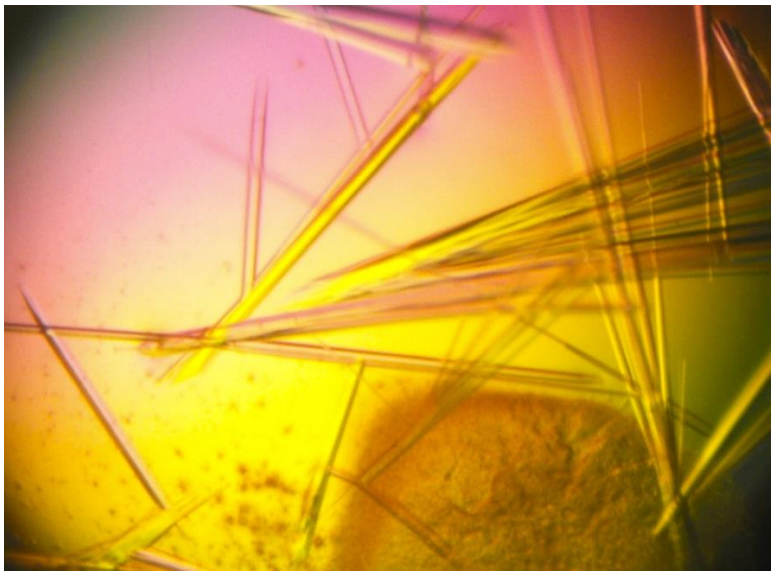

Figure 2.5: Protein crystals of USP7-NTD complexes with CHFR peptide. 100 mg/ml USP7-NTD was incubated with approximately 5-fold excess of CHFR^{PSTS} peptide. Co-crystal trials were set up using micro-seeding with USP7-NTD:HdmX as seeds in 30% PEG 4000, 0.1 M Tris pH 8.5 and 0.2 M Lithium Sulfate. Crystals were obtained in the dark at 4^0C and used to collect X-ray data and solve the three-dimensional structures of the USP7-NTD:CHFR^{PSTS} complex. Shown here are the long rod-shaped crystals obtained from complex of USP7-NTD with CHFR peptide ^{174}EPQPSTSTSD^{183}

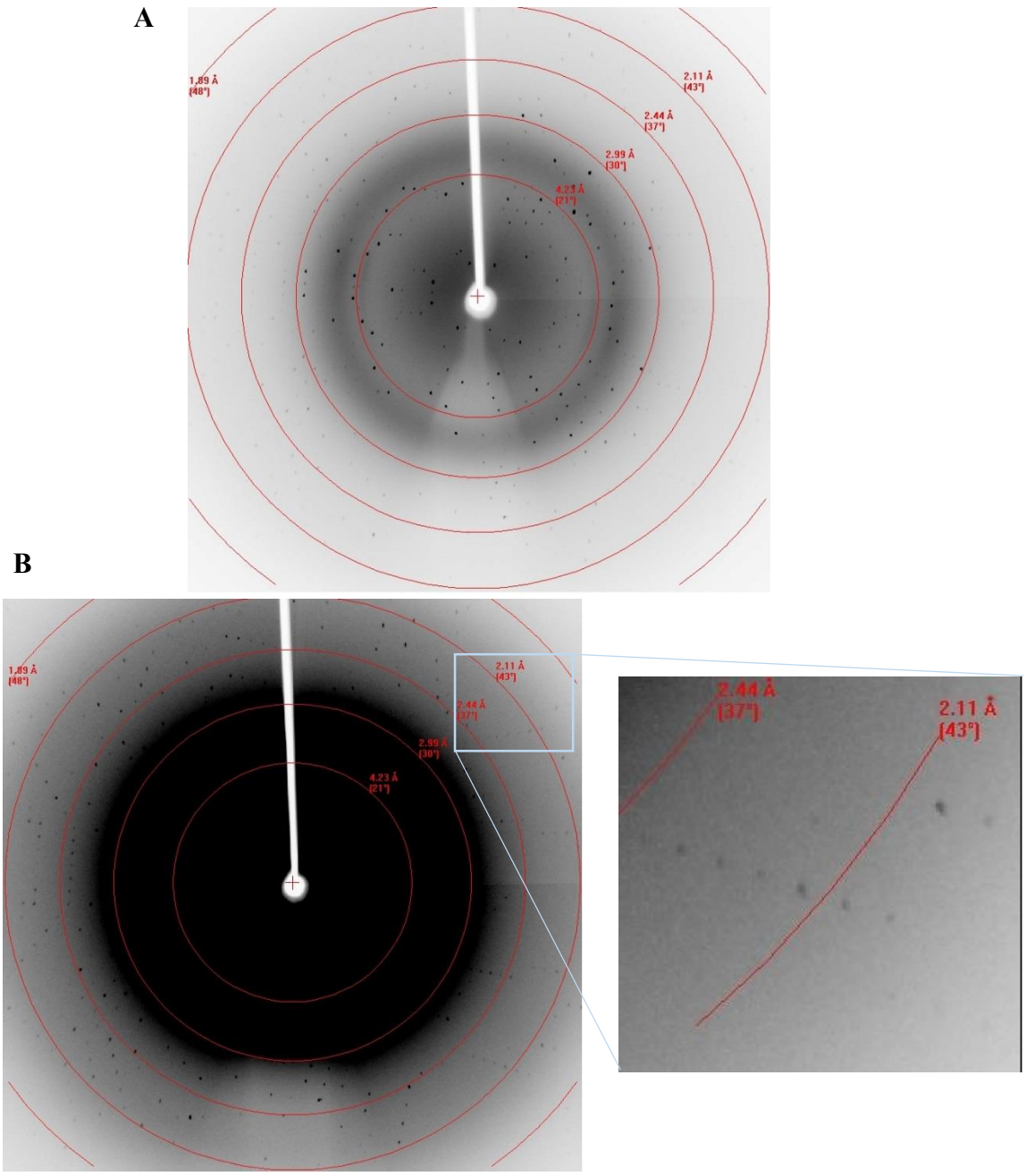

Figure 2.6: X-ray diffraction pattern from a USP7:CHFR complex crystal. X-ray data from a Rigaku MicroMax007 rotating anode diffractometer with a 944+ CCD (charge-coupled-device) detector was collected at 100K from a frozen protein crystal. When the X-rays pass through the crystal, a constructive interference of the X-rays produce reflections on the detector, which as seen as spot on the images. **A.** Image of the diffraction pattern displaying reflections at the low-medium resolution shells. **B.** Image showing the reflections at the higher resolution shells, with a magnified section around 2.11Å.

Table 2.1. X-Ray data collection and refinement parameters for USP7:CHFR complex structure

X-Ray Data	USP7-NTD: $CHFR^{PSTS}$	Refinement	USP7-NTD: $CHFR^{PSTS}$
Space Group	$P4_1$	R_{work}	0.191
Resolution (Å)	50.0 – 1.60	R_{free}	0.226
Unit Cell Axes ($Å^3$)	69.9 x 69.9 x 45.7	Protein Atoms (#)	1246
Molecules/AU	1	Water Molecules (#)	193
Total Observations (#)	100 595	rmsd bonds (Å)	0.005
Unique Reflections (#)	23 151	rmsd angles (^{0})	1.36
Intensity (I/σ<I>)	32.8 (2.6)	rmsd dihedrals (^{0})	2.3
Completeness (%)	78.2 (49.6)	rmsd improper (^{0})	0.78
$^aR_{sym}$	0.063 (0.570)	Thermal factors ($Å^2$)	18.4
		Ramachandran Plot	
		Most Favoured	97.3
		Additionally Allowed	12.7

Numbers in brackets refer to the highest resolution shell, 1.60 Å for the $CHFR^{PSTS}$ data. $^aR_{sym}$ = S |I-<I>| /SI where I is the observed intensity and <I> is the average intensity from multiple observations of symmetry-related reflections.

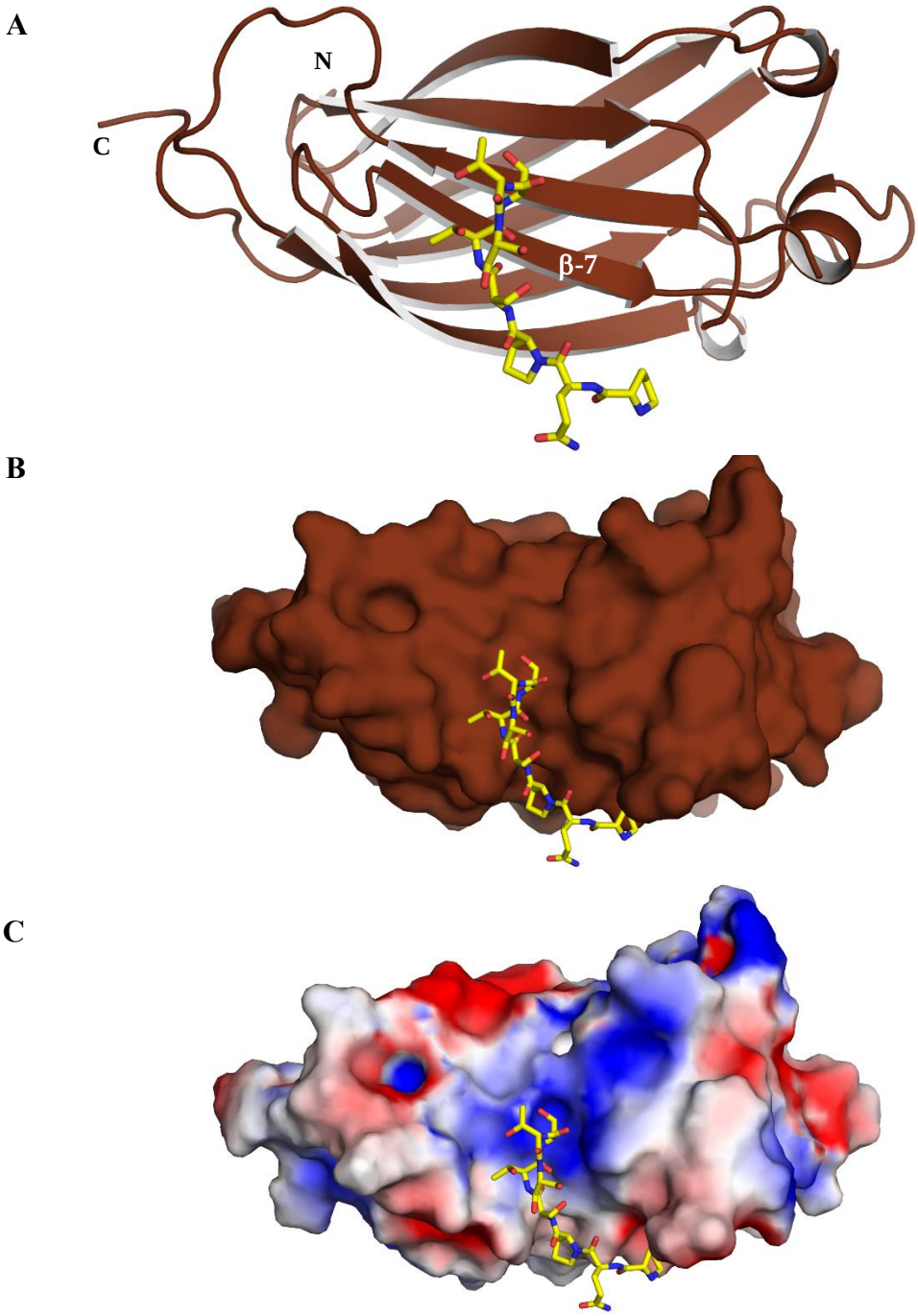

Figure 2.7: Crystal structure of USP7-NTD bound to CHFR ^{174}EPQ<u>PSTSTSD</u>^{183}. A. The CHFR peptide in yellow stick form is seen bound to the β-7 strand of USP7, which is represented in a chocolate ribbon diagram. **B.** Surface diagram and **C**. Electrostatic surface representation of the crystal structure. The complex structure was solved at a resolution of 1.6 Å.

By binding to the β-7 strand, CHFR sits in a shallow groove on the surface of USP7

To view the structure from a different angle, it was rotated 90° on its x-axis from the frontal view, as seen in figure 2.8. Figure 2.8A displays this in ribbon diagram, whereas 2.8B represents USP7 in surface diagram. In the surface diagram, upon rotation, a groove on the surface of USP7 is evident in which CHFR fits. The corresponding ribbon diagram shows that the β-7 strand of USP7 is a part of the base of this groove.

The interaction site – S180 of CHFR makes most contacts with D164 of USP7

The CHFR peptide was aligned with USP7 and a detailed look was taken at the interaction site. From figure 2.9A, it is evident that the tight binding between CHFR and USP7 is owed to two interactions. Figure 2.9B and C are rotated views of 2.9A to provide clarity and highlight each individual interaction. The most important bonding that takes place is between S180 (Ser180) of CHFR and D164 (Asp 164) of USP7. The carboxyl groups of the side chain of D164 form direct hydrogen bonds with the hydroxyl of the serine side chain of S180 as well as the amide of S180 (figure 2.9B). The other interaction that aids in binding are water-mediated hydrogen bonds between S178 of CHFR with USP7 (figure 2.9C). The groove on the surface of USP7 is lined by residues ^{164}DWGF^{167}, and it is these interactions that allow the peptide to bind in the groove.

To provide orientation clarity, the orientation of the peptide observed in figure 2.9B is considered as the standard orientation, and will be used with every depiction of the peptide, along with a rotated view to provide the optimal visualization of the site of

interest. Figure 2.9A is an electron density map of the peptide, also in the standard orientation.

CHFR peptide forms a beta-strand anti-parallel to β-7 of USP7

In order to see if there is any secondary structure relation between USP7 and the CHFR peptide, CHFR was displayed as a strand and compared with its stick-form. This is shown in the frontal view of the complex structure, as well as a rotated view in three dimensions to better observe their alignment. Figure 2.10A shows these two orientations with CHFR in stick form. In the rotated view, the peptide is seen to lie adjacent to the β-7 strand of USP7. Interestingly, with the peptide in ribbon diagram, in figure 2.10B, it forms an anti-parallel strand to USP7.

Comparing the substrate recognition motif of CHFR with USP7 interacting peptides

Figures 2.11-2.13 compare the CHFR peptide with other USP7-NTD interacting peptides from MDM2, p53 and EBNA1, respectively, by aligning these peptides with CHFR. The PSTS motif of CHFR is compared with the respective motifs of the other proteins. MDM2 uses a PSSS motif, which differs only by one residue from the PSTS motif of CHFR, and the motifs can thus be seen to align well. The PGGS of p53 only shares the proline and last serine with CHFR, but still maintains the P/AXXS conservation. EBNA1, however, uses EGPS, which deviates from the P/AXXS used by CHFR as well as the other proteins. This peptide in general does not align with CHFR, except for the last serine in the motif which interacts with D164 of USP7, which is conserved and aligns perfectly.

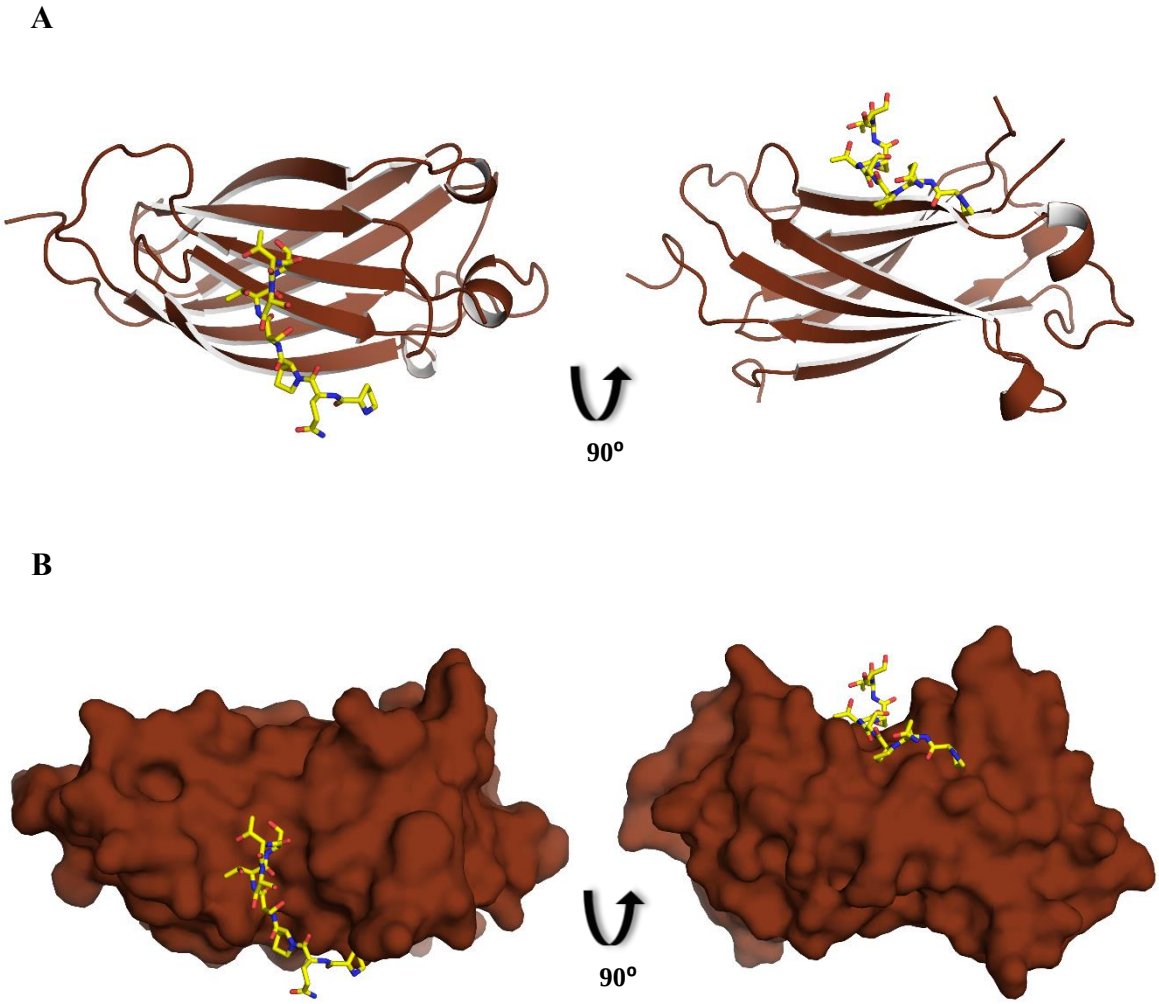

Figure 2.8: CHFR binds to a shallow groove on the surface of USP7. The figures on the left in **A** and **B** depict the frontal view of the structures, with a clear view of both the USP7-NTD structure as well the peptide bound to it. Upon rotating the structure on the x-axis at a 90° angle, the CHFR peptide is observed to be sitting in a shallow groove on the surface of USP7. At the base of the groove is the β-7 strand of the anti-parallel beta-sheets of the N-terminal domain of USP7. **A.** Cartoon and **B.** Surface representations of the frontal view as well as the rotated, to allow for visualization of the binding groove. The peptide is represented in yellow stick form.

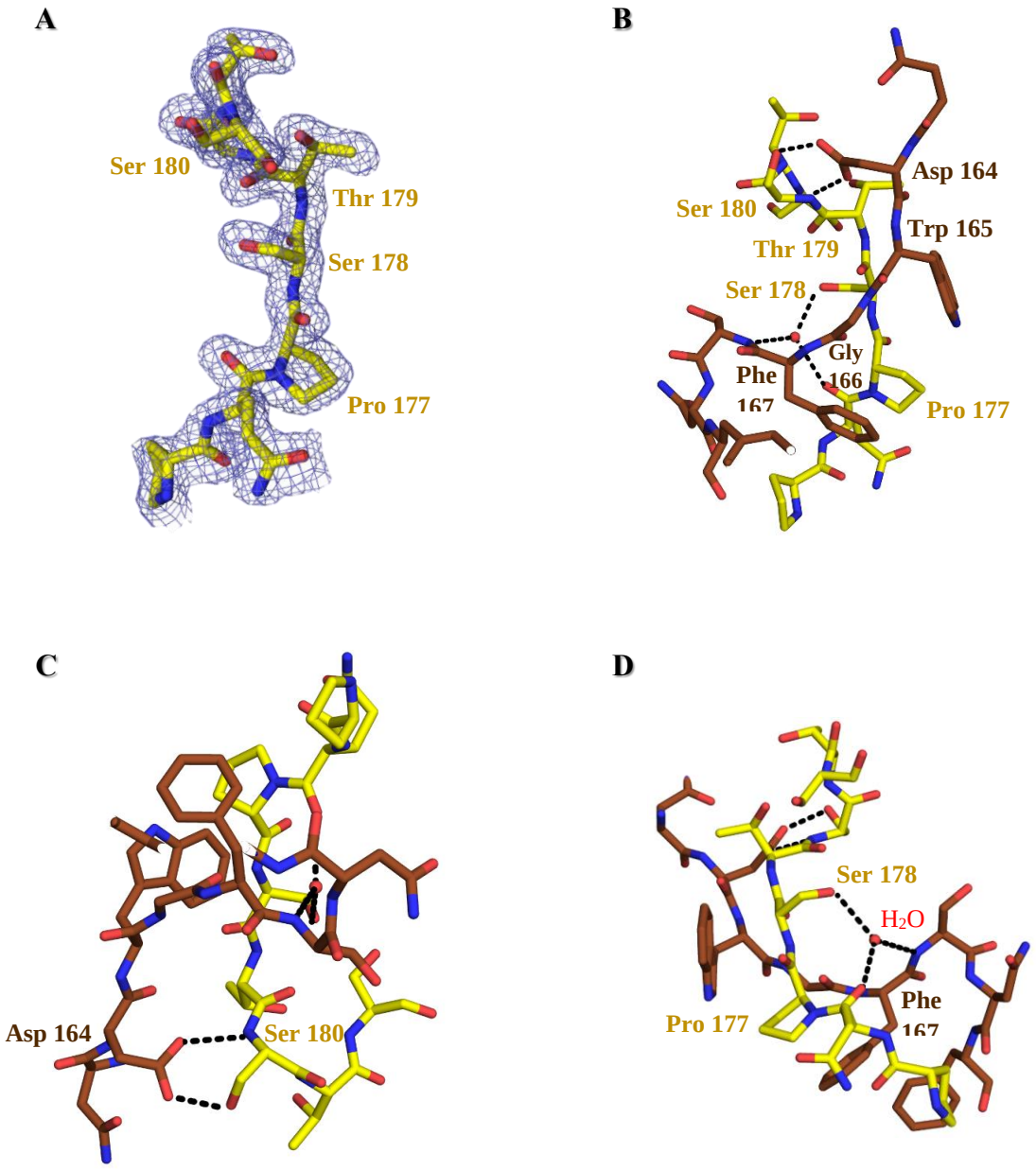

Figure 2.9: CHFR ^{177}PSTS^{180} interacts with ^{164}DWGF^{167} in the binding groove of USP7. A. The electron density map (2fo-fc) of the CHFR peptide. **B.** The peptide in yellow aligned with the interacting residues of USP7, in chocolate. **C.** Direct hydrogen bonds are made between the peptide and protein using S180 (Ser180) of CHFR and D164 (Asp164) of USP7. **D.** Additional interaction is established by water-mediated hydrogen bonding using S178 of CHFR with USP7. **C**. and **D.** are rotated views of **A**, to better display the S158-D164 and the water-mediated interactions, respectively.

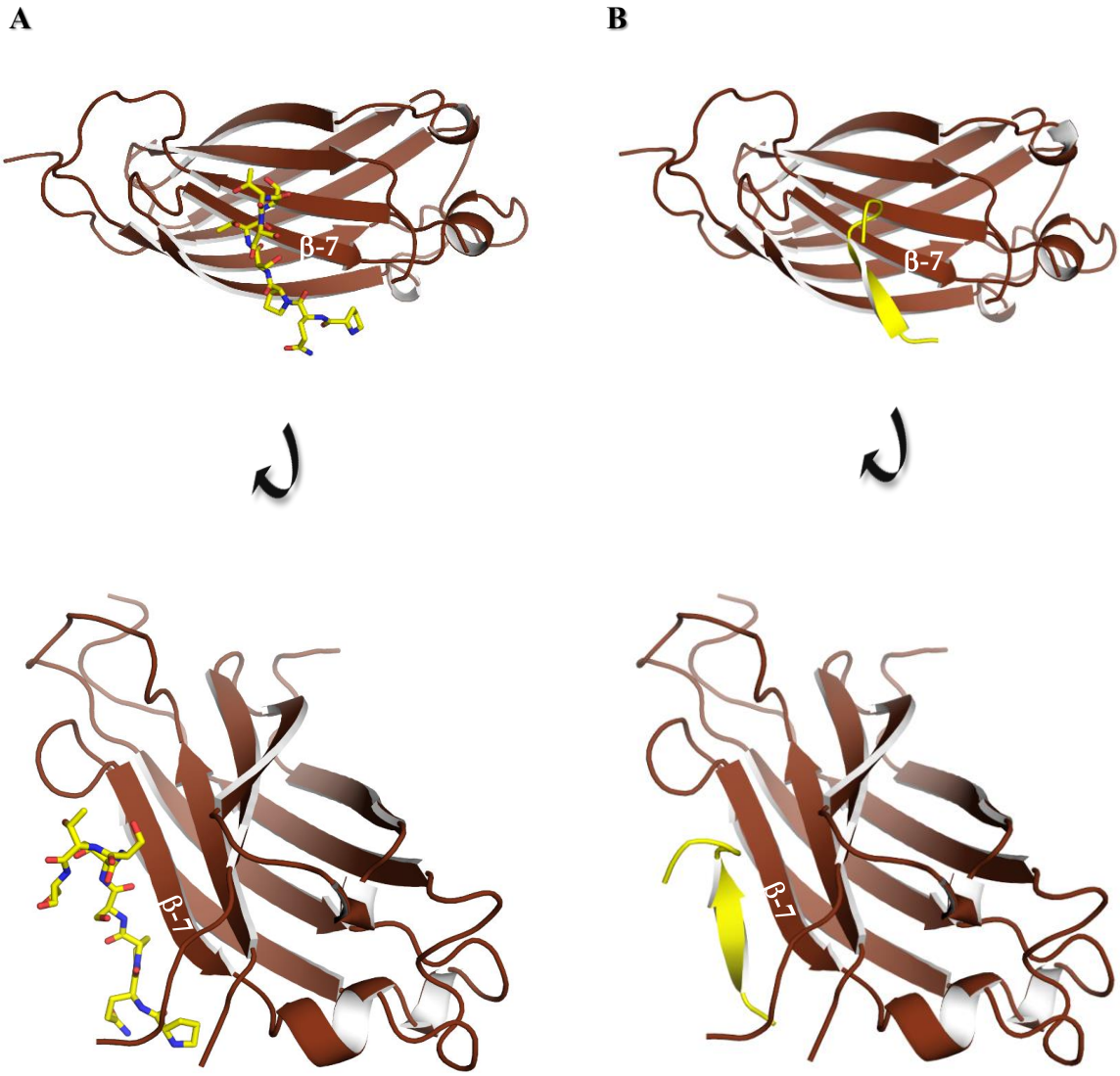

Figure 2.10: The CHFR peptide forms an antiparallel strand. A. When the USP7:CHFR structure is rotated from its frontal view in three dimensions, the peptide, in stick form, is seen to line up against the upper beta-sheet of USP7. Viewing the peptide as a strand instead of stick-model, as seen in **B**, enables visualization of it as forming an anti-parallel strand to the β-7 strand of USP7.

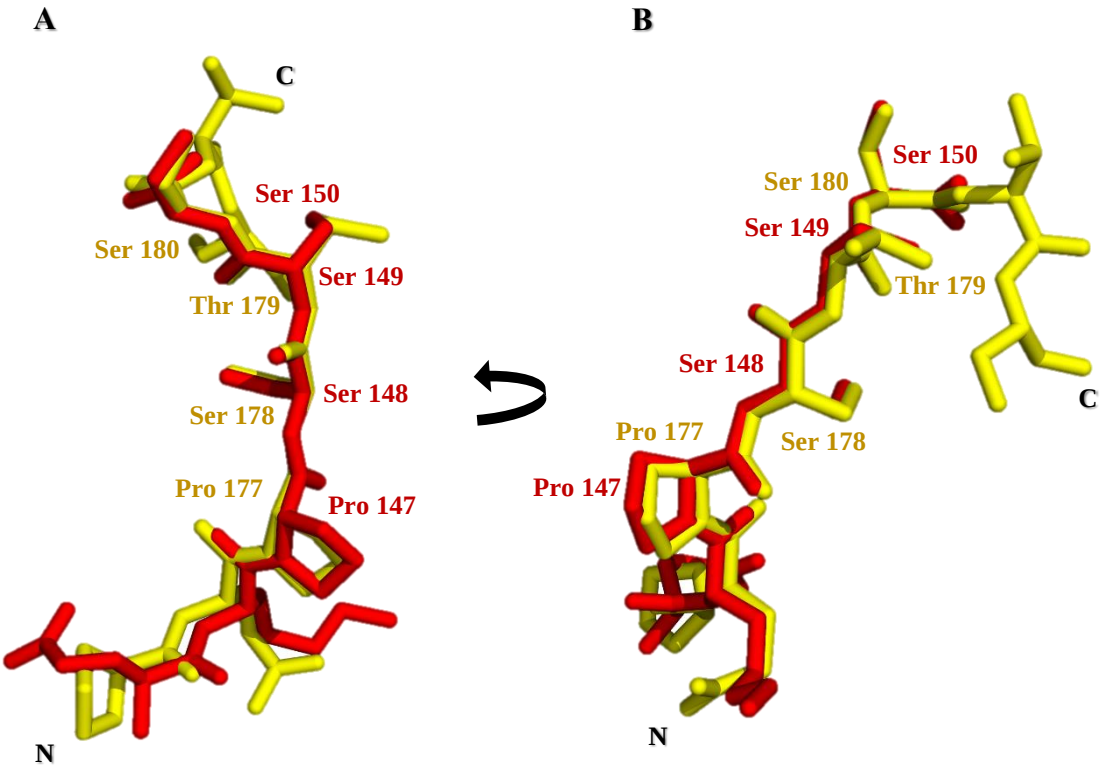

Figure 2.11: The USP7 binding motif of CHFR ^{177}PSTS^{180} compared with that of MDM2 ^{147}PSSS^{150}. A. An orientation of the CHFR peptide used to provide a standard view amongst peptide comparisons. **B.** Rotated view to best portray a comparison of the residues involved in the motifs. The PSTS motif of CHFR is aligned with PSSS of MDM2. The difference in T179 of CHFR and S149 of MDM2 can be seen, with CHFR in yellow and MDM2 in red. The most important residues, CHFR S180 and MDM2 S150 align well.

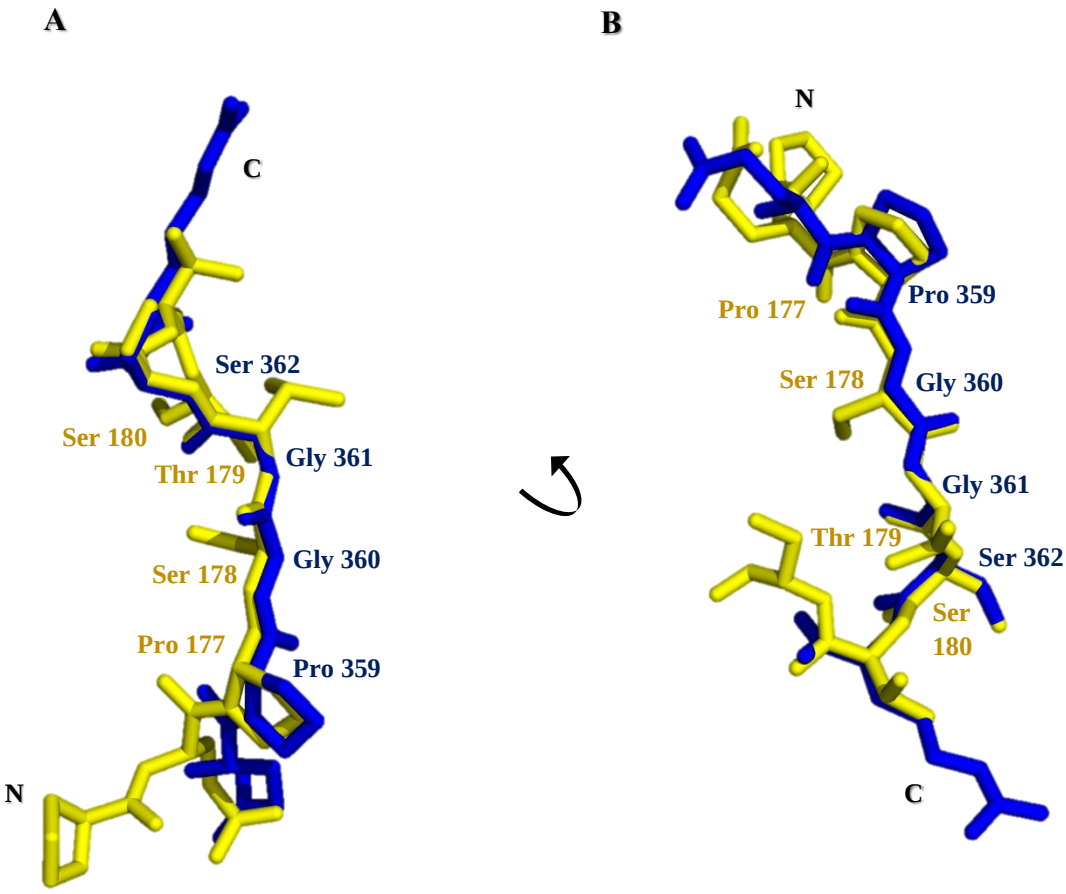

Figure 2.12: The USP7 binding motif of CHFR ^{177}PSTS^{180} compared with that of p53 ^{359}PGGS^{362}. A. An orientation of the CHFR peptide used to provide a standard view amongst peptide comparisons. **B.** Rotated view to best portray a comparison of the residues involved in the motifs. CHFR has a PSTS motif, whereas p53 has PGGS, which is still a P/AXXS motif. Even though p53 contains two glycines instead of a serine and threonine, the most essential residues, S180 and S362 of CHFR and p53, respectively, are conserved and align perfectly. CHFR is displayed in yellow, and p53 in blue.

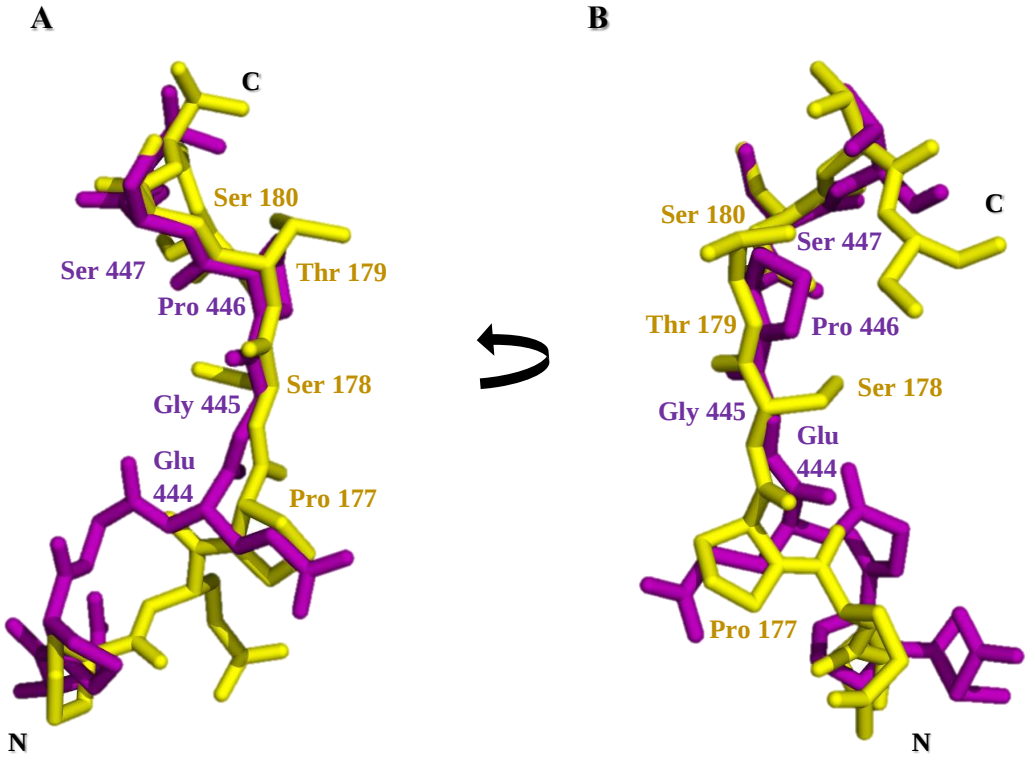

Figure 2.13: The USP7 binding motif of MCM-BP ^{177}PSTS^{180} compared with that of EBNA1 ^{444}EGPS^{447}. A. An orientation of the CHFR peptide used to provide a standard view amongst peptide comparisons. **B.** Rotated view to best portray a comparison of the residues involved in the motifs. The EGPS of EBNA1 in purple deviates completely from PSTS of CHFR in yellow except for the last serine. S180 in CHFR and S447 in EBNA1 align perfectly, as compared with the rest of the peptide which deviates at every residue.

2.3.3 USP7 is involved in the stability of endogenous CHFR

A protein turnover assay for CHFR was performed in two cell lines of HEK293T cells – silenced USP7 (siUSP7) and negative control (siNC) - to compare the stability of CHFR in the absence and presence of USP7. USP7 was silenced using siUSP7 or left at endogenous levels with siNC. Cycloheximide treatment was administered to the cells after silencing USP7 and the level of CHFR was compared with cells in which USP7 was not silenced. Cells were harvested at the time points shown in figure 2.14 to analyze the amount of protein present in the two cell lines. The top two panels in figure 2.14A are blots showing a decreased level of USP7 in cells with siUSP7 as opposed to siNC. The curve in figure 2.14B displays quantified levels of USP7, with more than 50% of USP7 knocked down in siUSP7 cells. From these figures it is also seen that USP7 stability is not affected over the 48 hours post-cycloheximide treatment in either experiment.

The two blots in the center in figure 2.14A show the level of CHFR at each time point in the presence and absence of USP7. The expression levels were quantified and plotted as relative expression levels, in figure 2.14C. The amount of protein at the 0-time point was established as the reference level, at 100% for each cell line individually, and the stability of the protein was analyzed by comparing the levels at the consecutive time points with the reference level in that cell line. CHFR decreases steadily over the 48 hours in siUSP7 cells, as opposed siNC cells where it remained close to a 100% until the 24-hour mark where it started to decrease. It is evident that the stability of endogenous CHFR was affected by the reduction in USP7 levels in the cell.

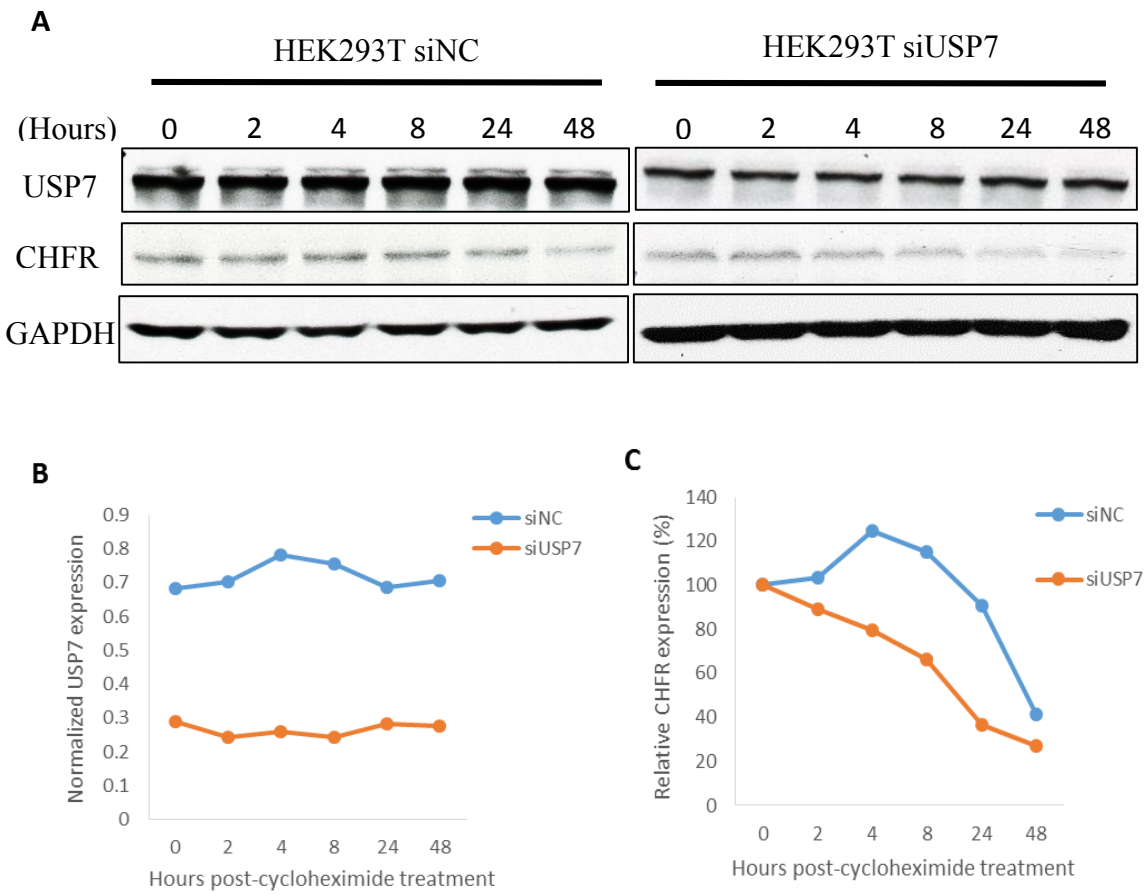

Figure 2.14: Stability of endogenous CHFR is affected by silencing USP7. A. USP7 was silenced in HEK293T cells by transfection with 30nM siRNA (USP7 and negative control) for 72 hours. The cells were treated with cycloheximide (50 ug/ml) for 0, 2, 4, 8, 24 and 48 hours post transfection. 100 ug of lysates for the respective cell lines were subjected to Western Blot analysis. Expression levels of endogenous CHFR over time were detected using anti-CHFR antibody, USP7 was detected using anti-USP7 antibody and anti-GAPDH was used to detect GAPDH as the loading control. **B.** Bands for USP7 siUSP7 and siNC obtained from Western blotting were quantified using ImageJ (national Institute of Health). USP7 expression level post-cycloheximide treatment remains constant for each cell line; expression was knocked down in cells treated with siUSP7 (orange) compared with siNC cells (blue). **C.** Bands obtained from western blotting were quantified using ImageJ software (National Institute of Health) and plotted as the relative expression of CHFR at each time point post-cycloheximide treatment. The expression level at the 0-hour point is set as the reference (100%), and the expression at each of the following time points is calculated as a percentage of the reference. CHFR degrades faster in USP7 knockdown cells (orange steeper curve) as compared with the negative control (blue curve).

2.3.4 UbE2E1 is not the ubiquitin conjugating enzyme associated with CHFR E3 ligase

CHFR is an E3 ligase, with its respective E2 ubiquitin conjugating enzyme. UbE2E1 is an E2 and to determine if it's the E2 for CHFR, a co-IP was performed from cells over-expressing Flag-CHFR. The IP was performed with anti-Flag and anti-IgG (negative control), and western blotted for Flag (Flag-CHFR) and UbE2E1, as seen in figure 2.15. Both Flag-CHFR and UbE2E1 were seen in the lysate. However, UbE2E1 did not co-immunoprecipitate with CHFR, since it is present only in the unbound sample, not in the eluate, indicating that it is not associated with CHFR.

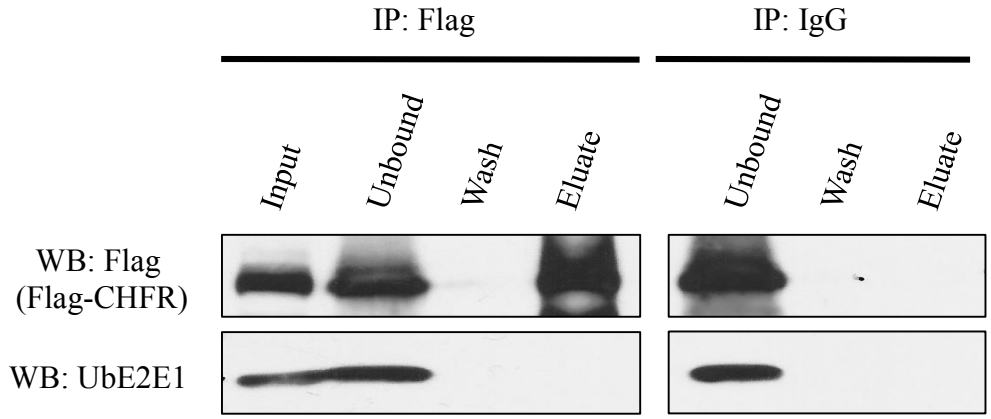

Figure 2.15: UbE2E1 is not the ubiquitin conjugating enzyme associated with CHFR E3 ligase. Flag-CHFR was overexpressed in HEK293T cells. The cells were harvested after 48 hours and the lysate was immunoprecipitated with anti-Flag and anti-IgG (negative control) beads. The unbound and wash fractions were collected and the proteins bound to the beads were eluted by boiling with 5XSDS dye. The co-immunoprecipitated samples were resolved on a 10% SDS gel and subjected to Western Blotting. Flag-CHFR and UbE2E1 were detected with anti-Flag and anti-UbE2E1 antibodies, respectively. UbE2E1 did not co-immunoprecipitate with CHFR in the eluate and was recovered only in the unbound fraction.

2.4 Discussion

2.4.1 CHFR binds to the N-terminus of USP7

In a previous study, CHFR was established as a substrate of USP7 (Oh et al. 2007) using a co-immunoprecipitation assay. The aim of this project was to determine the site of interaction, starting with determining the domain of USP7 that binds to CHFR. This was accomplished using a GST pull-down with GST-tagged USP7-NTD and Flag-CHFR. The result of this pull-down was compared with that of a control, whereby the GST protein was used instead of GST-USP7-NTD and the data is shown in figure 2.1. CHFR was successfully pulled-down with USP7-NTD. A portion of both CHFR and USP7 remained on the beads after elution, which could be due to insufficient elution. This data narrowed down the region that binds to CHFR to be the N-terminal domain of USP7, which has not been established prior to this project. This result was used for further experiments to determine the site of interaction on CHFR as well as the mode of interaction that allows the binding to occur.

2.4.2 PSTS motif in CHFR involved in interaction with USP7-NTD

Once a positive interaction was established, it was important to determine the site of interaction between the proteins. CHFR contains a PSTS-motif, which resembles the established P/AXXS substrate recognition motif found in substrates or interacting partners of USP7 (Sheng et al. 2006). This motif is recognized by a binding pocket in the N-terminus of USP7. Data from a peptide spot array and intrinsic tryptophan fluorescence assay helped confirm that this motif is responsible for binding to USP7.

Having determined the site of interaction in CHFR, the molecular mechanism was established using X-ray crystallography. Co-crystal trials were set up with USP7-NTD and peptides containing the PSTS motif in CHFR (^{174}EPQPSTSTSD^{183}), using microseeding with seeds from a previously crystallized complex of USP7-NTD:HdmX. HdmX, which is a negative regulator of p53, is also associated with USP7 using a P/AXXS motif. The complex of USP7-NTD:CHFR^{PSTS} crystallized in the dark at 4°C, and the crystals were used to determine the molecular structures at a resolution of 1.6 Å.

By aligning the CHFR peptide with USP7-NTD, it is seen that the peptide binds to the shallow groove on the surface of USP7, which is lined by the residues ^{164}DWGF^{167}. S180 in CHFR makes the most contacts with D164 in USP7, with additional water-mediated hydrogen bonding between S178 in CHFR with USP7. By doing so, the peptide binds to the β-7 strand in USP7-NTD and hugs the two anti-parallel beta-sheets created by the eight beta-strands.

This mechanism of interaction is not unique to CHFR, but has been shown for almost all the proteins that bind to the N-terminal domain of USP7, such as p53, Hdm2, HdmX and EBNA1. This, along with the fact that the conserved residues of the motifs of these proteins align well with those of CHFR, adds CHFR to a growing pool of proteins that make use of the substrate recognition motif and highlighting the importance of this mode of interaction for USP7.

2.4.3 USP7 is associated with the stability of CHFR

CHFR is a mitotic checkpoint protein that is down regulated in a wide variety of cancers. It thus becomes essential to understand the mechanism revolving around its stability in the cell. USP7 was found to interact with CHFR, and being a deubiquitinating enzyme it was expected to be responsible for the stability of CHFR. It was hypothesized that the levels of CHFR would decay faster in the absence of USP7. Using a protein turnover assay in HEK293T cells, which express endogenous CHFR, USP7 was silenced or knocked down to less than 50% using siRNA, and the turnover of CHFR was observed. The half-life of CHFR was much shorter in cells with silenced USP7 than that with complete USP7 expression. Quantification of the bands obtained from western blots help to demonstrate this in figure 2.14C, where CHFR level in siUSP7 cells fall steadily, even within the first two hours after blocking the translational machinery, as opposed to those with siNC where the level remained close to a 100% for the first 24 hours.

Theoretically it would be ideal to study endogenous CHFR in cancer cell lines, but given its lost and/or low expression in most tumor cells, it is difficult to detect changes, if any, in these cells. HEK293T cells, which are human embryonic kidney cells, were thus used for studying endogenous CHFR. Since this is not a cancer cell line, it also has the benefit of allowing to study the effect of USP7 depletion on CHFR in its normal unstressed environment.

Oh et al. (2007) first detected the interaction between USP7 and CHFR. They also studied the effect of USP7 on the stability of CHFR, and found that USP7 was able to

stabilize CHFR. However, they used exogenous CHFR and exogenous USP7, and they used increasing amount of USP7 to detect increased overall levels of CHFR. This project, on the other hand, demonstrated that silencing USP7 de-stabilized CHFR over a certain time period, and more importantly, used endogenous proteins instead of ectopic thus eliminating the uncertainty of the behavior of an exogenously expressed protein.

2.4.4 Perspective

The interaction of USP7 with CHFR is still a novel interaction that researchers are beginning to explore. This project has determined the site of interaction of USP7 with CHFR, which was previously unknown. CHFR interacts with USP7 in the binding groove-dependent manner, and has been established as a substrate. The molecular mechanism that governs this interaction has been seen previously with p53, Hdm2, HdmX and EBNA1, where a substrate recognition motif present in the substrates or interacting partners is recognized by a binding pocket on the surface of the N-terminal domain of USP7.

The implications of USP7 and its involvement in the regulation of a checkpoint protein can be vast. This project has confirmed that the USP7:CHFR interaction involves the ability of USP7 to stabilize CHFR. CHFR is a checkpoint protein that is able to revert the cell cycle upon a signal of cellular stress and prevent the propagation of corrupted DNA. It makes sense that it's seen to be either deleted or is expressed very poorly in most tumors. Exploiting the interaction between USP7 and CHFR could have potential to stabilize CHFR and prevent its degradation as a part of preventative therapy. It could

also be used to stabilize the existing pool of CHFR in tumors that have low expression of CHFR, which may help in preventing the tumor from growing further. However, the interacting pair needs further examination, especially in terms of the network of proteins that must exist around CHFR's checkpoint function. USP7 could play a role in the stability of proteins regulated by CHFR E3 ubiquitin ligase activity such as Aurora A and Plk-1. Aurora A and Plk-1 support mitosis, and as a part of its checkpoint function, upon stress CHFR ubiquitinates these proteins to prevent the cell from entering mitosis. It would thus be interesting to observe the effects of USP7 on Aurora A and Plk-1 stability and this may contribute to a network of regulation and feedback provided by USP7.

CHAPTER 3: INTERACTION STUDY BETWEEN USP7 AND MCM-BP

Some of the results presented in this chapter have been published in Molecular and Cellular Biology (MCB) under A Role for USP7 in DNA Replication. Jagannathan M, Nguyen T, Gallo D, Luthra N, Brown GW, Saridakis V, Frappier L. (Appendix A)

3.1 Introduction

The transfer of genetic material from parent to daughter cell involves a complete and error-free replication of the genome. To accomplish this, eukaryotes have developed a highly complex, sensitive and regulated mechanism to carry out its DNA replication, starting with the recognition of origins of replication, loading the pre-RC (pre-replicative complex) and assembling the CMG helicase.

3.1.1 Initiation of DNA replication

During late M or early G1 phase, the origin recognition complex (ORC) locates the origin of replication and commences the assembly of a stable and inactive pre-RC (pre-replicative complex) starting with CDC6, which recruits Cdt1 and together they recruit MCMs 2-7 to the DNA. This event licences the origin of replication and in late G1 or early S phase, the MCM 2-7 complex gets activated by cyclin-dependent kinases (CDKs) and a Dbf4-dependent kinase (DDK). The activated MCMs2-7 play a role in the recruitment and loading of CDC45 to the DNA, which is a DNA polymerase-α loading factor (Bochman and Schwacha 2009). In addition, a complex of four subunits called the GINS complex, which is also a replication factor, is recruited to the replication site. Together, CDC 45, MCMs 2-7 and the GINS complex form a CMG helicase, responsible for unwinding the DNA double helix ahead of the replication fork and allowing for replication to occur in the S phase (Bryant and Aves 2011).

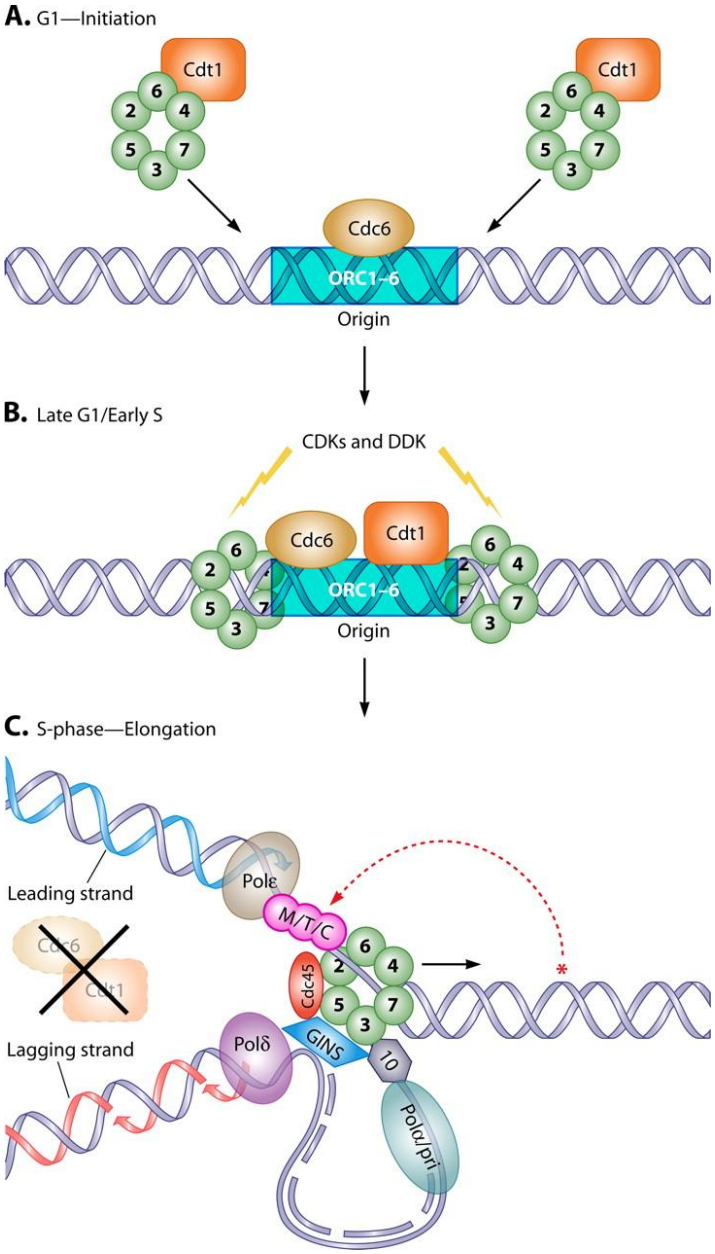

Figure 3.1: DNA replication initiation. In early G1 phase, the ORC complex initiates the licencing of the origin of replication by recruiting Cdt1, Cdc6 and the MCM 2-7 complex to the DNA to form a stable pre-replicative complex. At late G1 or early S phase, CDKs and DDK activate the MCM-complex, leading to the recruitment of other replication factors to the DNA to form an active CMG helicase, which allows for replication to start in the S phase. (Bochman and Schwacha 2009)

The faithful propagation of genetic material should only happen once per cell cycle, and there are a large number of checks present in the cell that prevent re-initiation of replication. The pre-RC gets unloaded from replicated DNA to ensure it doesn't start a second round. Once unloaded, there are multiple overlapping mechanisms that prevent the pre-RC from being re-assembled, where in one way or another the components of the complex are downregulated or kept away from each other (Nguyen et al. 2011).

3.1.2 MCM-BP - unloading the MCM-complex

The mechanism revolving around the displacement of the MCM helicase was unclear, until a protein sharing limited homology with MCM proteins was discovered in 2007 called MCM-BP (minichromosome maintenance complex binding protein). It was observed to have the ability to replace MCM2 in the complex providing evidence for an alternate form of the complex (Sakwe et al. 2007). This alternate complex was found to be involved in the unloading of the pre-RC from replicated DNA.

MCM-BP is imported into and accumulates in the nucleus in the late S phase, towards the end of replication. Coincidentally, this is when MCM2-7 was known to dissociate from the chromatin, and MCM-BP depletion was shown to result in delayed disassociation of the MCM proteins, as well as impaired mitotic entry (Nishiyama et al. 2011). The clearing of the pre-RC from replicated DNA can have various implications, including the prevention of re-initiation of replication as well as successful chromosome segregation, thus providing evidence for MCM-BP to be a key player in maintaining genomic integrity (Nishiyama et al. 2011).

3.1.3 Objective and hypothesis

A proteomic study identified an MCM-complex of 7-8 proteins to be a USP7 interacting partner (Sowa et al. 2009). The purpose of this interaction is yet to be understood. A sequence analysis revealed the presence of a P/AXXS motif on MCM-BP. Using structural studies, the purpose of this project is to determine if the USP7:MCM-BP interaction is via this recognition motif. The structure will enable us to visualize the location of interaction. By comparing this with previously established USP7-substrate protein interactions such as the USP7-p53 complex and combining with interaction assays can help us determine the purpose and mechanism of this interaction, thereby demonstrating a role of USP7 in the DNA replication process.

It is expected that MCM-BP will interact with USP7-NTD using its substrate recognition motif, and that the mechanism will be similar to what has been observed in established USP7-NTD interactions.

3.2 Materials and Methods

3.2.1 Expression and purification of MCM-BP and USP7

6xHis-MCM-BP (73 kDa) and 6xHis-USP7 (128 kDa) were expressed in *Spodoptera frugiperda* Sf9 cells using the baculovirus expression system, cultured at 27°C in Sf-900 II SFM media (Life Technologies) supplemented with 5% FBS. The cells were harvested 2-3 days post infection at 3000 x g for 10 mins and the pellets were washed three times with 1XPBS.

The proteins were purified using Ni^{2+} affinity chromatography. The cells were lysed by resuspending each gram of pellet in 10 ml Buffer A (20mM Hepes pH 7.5, 500mM NaCl, 1mM β-mercaptoethanol (β-Me), 10% glycerol, 0.5% Nonidet P-40 (NP40), 10mM Imidazole, 1XProtease inhibitor cocktail) and incubating on ice for 45 minutes, followed by sonication for 3 min, 30% Amp, 15 sec ON 10 sec OFF. The suspension was centrifuged at 27,000 x g for 30 mins in a Beckman-Coulter Avanti JE centrifuge with a JA 25.50 rotor. The lysate was applied to Buffer A equilibrated Ni^{2+}-agarose beads and allowed to bind for 60 minutes. Unbound proteins were collected and the resin was washed three times with 150 ml of Buffer B (20mM Hepes pH 7.5, 500mM NaCl, 1mM β-Me, 10% glycerol, 10mM Imidazole, 1XProtease inhibitor cocktail). The protein bound to the resin was eluted using Buffer C (20mM Hepes pH 7.5, 500mM NaCl, 1mM β-Me, 10% glycerol, 500mM Imidazole, 1XProtease inhibitor cocktail) and the eluate was subjected to a size exclusion Hi Load 16/60 Superdex 200 prep grade column (GE Healthcare) on an AKTA Purifier (GE Healthcare) using Buffer D (20mM Hepes pH 7.5, 300mM NaCl, 0.5mM tris(2-chloroethyl)phosphate TCEP).

3.2.2 Testing molar ratio of interaction between MCM-BP and USP7

The interaction between MCM-BP and USP7 was tested with eight different molar ratios of MCM-BP:USP7 – 1:0, 0:1, 1:1, 1:1.5, 1:2, 1:5, 2:1, and 5:1. The NaCl concentration of both proteins was diluted to 50mM from 300mM using 20mM Hepes pH 7.5 to avoid salt interference during interaction. The proteins were combined in their respective ratios; 20mM Hepes pH 7.5 was used to substitute for each of the absent protein in the controls

(1:0 and 0:1). The reaction mixture was incubated at room temperature for 60 minutes, following which the samples were concentrated using a VivaSpin6 50 kDa MWCO (GE Healthcare) concentrator to a final volume of 250 µl and subjected to size exclusion chromatography using a Superdex 200 10/300 GL column (GE Healthcare) on an AKTA Purifier (GE Healthcare). Two major peaks were obtained for each run at fractions D10 and E8, and samples taken from fractions C9, 11, 12, D2, 4, 6, 8, 10, 12, E2, 4, 6, 8, 10, 12, F2, 4, 6 and G6 were resolved on a 10% SDS gel (20 µl sample with 5 µl 5XSDS dye). A GeneDireX PINK Plus Prestained Protein Ladder was used as a MW reference and the gel was run at 195V for 75 minutes.

2.2.5 Molecular basis of interaction between USP7-NTD and MCM-BP

Expression and purification of USP7-NTD

E. coli DE3 cells containing a plasmid encoding for 6xHis-tagged USP7-NTD were cultured in TB (Terrific Broth, Bioshop) with 100 ng/ml ampicillin and expression was induced overnight using 0.4mM IPTG at 16°C. The cells were harvested at 7,446 x g for 30 minutes at 4°C. The resulting pellet was lysed with 4 ml of Lysis Buffer per gm of pellet (100mM Hepes pH 7.5, 500mM NaCl, 10% glycerol, 10mM Imidazole, 0.5mM TCEP, 1XProtease inhibitor cocktail). The cells were sonicated at 30% amplitude, 15 sec ON 10 sec OFF for a total ON time of 6 minutes, with a pause after 3 minutes. The lysed cells were centrifuged at 41,287 x g for 30 minutes at 4 °C. A sample was taken from the supernatant for SDS PAGE analysis and the remaining lysate was incubated with Ni^{2+} agarose beads equilibrated with the Lysis Buffer, with gentle rocking at 4°C for 2 hours.

The proteins left unbound after binding were collected and the resin was washed with 100 ml of Wash Buffer (100mM Hepes pH 7.5, 500mM NaCl, 10% glycerol, 25mM Imidazole, 0.5mM TCEP). The wash was collected and the isolated protein was eluted with Elution Buffer (100mM Hepes pH 7.5, 500mM NaCl, 10% glycerol, 250mM Imidazole, 0.5mM TCEP).

Samples obtained from lysate, unbound proteins, wash and elute (16 µl sample + 4 µl 5XSDS dye) were resolved on a 10% SDS gel at 195V for 65 minutes and a PageRuler Prestained Protein Ladder was used as a MW reference.

The purified 6xHis-USP7-NTD contains a thrombin cleavage site between the His-tag and the protein. To cleave the 6xHis-tag, the protein was incubated with 0.5 units thrombin (Sigma T6884) per mg protein and 2.5mM $CaCl_2$ for 72 hours at 4°C. Samples of the protein were taken before and after cleavage (His-uncleaved and His-cleaved, respectively) and resolved on a 15% SDS gel run at 220V for 35 minutes. The marker used was PageRuler Prestained Protein Ladder.

The His-cleaved USP7-NTD was then subjected to size exclusion chromatography using a HiLoad 16/60 Superdex 200 prep grade column (GE Healthcare) on an AKTA purifier (GE Healthcare) to further remove impurities from the protein and to exchange the protein into 20mM Hepes pH 7.5, 500mM NaCl. The cleaved dialyzed protein was used for protein crystallization trials.

Co-crystallization trials of USP7-NTD with MCM-BP^{PSTS} peptide

5-fold molar excess of MCM-BP peptide ^{152}RVSPSTSYTP^{161} with N-terminal acetylation and C-terminal amidation (synthesized by CanPeptide Inc.) was incubated with 100 mg/ml of USP7-NTD, overnight at 4°C. Seeds from crystals of USP7:HdmX complex were used to set up co-crystal trials using microseeding in a crystallization condition of 0.1 M Tris pH 8.5, 30% PEG 4000, and 0.2 M Lithium Sulfate.

X-ray data collection and molecular structure determination

X-ray diffraction data was collected from a frozen USP7:MCM-BP crystal at 100K on a Rigaku MicroMax007 rotating anode diffractometer with a 944+ CCD (charge-coupled-device) detector. HKL2000 (Otwinowski and Minor 1997) was used to integrate and scale the diffraction data and molecular replacement was used to determine the structure. USP7 54-205 (PDB identifier [ID] 1YY6) without any peptide was used as the search model in CNS program (version 1.3) (Brunger 2007). The electron density was visualized and the model was rebuilt using the molecular graphics program O (Jones and Kjeldgaard 1997). CNS 1.3 was used for refinement and $2F_o$-F_c and F_o-F_c maps were inspected for further refinement and model rebuilding in O. Water molecules were picked using CNS 1.3 and verified in O. The figures were created using the software program PyMOL (version 1.3).

3.3 Results

3.3.1 Expression and purification of MCM-BP and USP7

MCM-BP and USP7 were purified from SF9 cells using Ni^{2+} affinity chromatography, followed by a second round of purification using size exclusion chromatography. Figures 3.2 and 3.3 represent samples from both rounds of purifications, for MCM-BP and USP7, respectively. The eluate contains the proteins after Ni2+ affinity purifications, whereas the lanes following that show samples taken from fractions obtained after size exclusion, with the fractions highlighted in green pooled and collected for use in further experiments. MCM-BP is detected at 73 kDa and USP7 at 128 kDa. MCM-BP was concentrated to 0.67 mg/ml while USP7 was concentrated to 1.71 mg/ml.

The yield from the purifications was not high, as is seen from the faint bands observed, but enough was obtained to allow for determining the molar ratio of interaction between the two proteins.

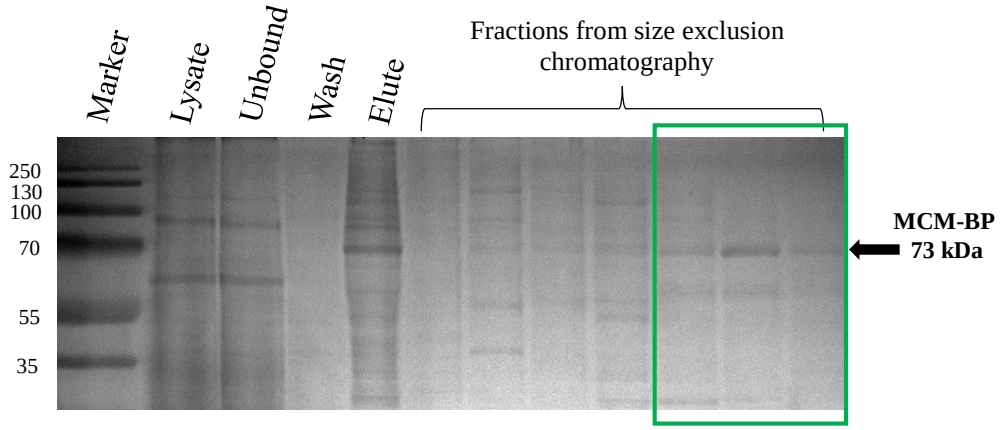

Figure 3.2: Purification of MCM-BP using Ni^{2+} affinity chromatography. 6xHis tagged MCM-BP (642 amino acid residues, 73 kDa protein) was overexpressed in SF9 cells using the baculovirus expression system and purified using Ni2+ affinity chromatography followed by size exclusion chromatography. Samples from lysate, unbound proteins, wash and elute from the first round of replication, as well as from fractions obtained from the second round were collected and separated on a 15% gel at 195V for 65 minutes A band can be seen in Elute at ~73 kDa, representing 6xHis-MCM-BP. Bands at the same position can be seen in the fractions highlighted in green, which were pooled and concentrated to 0.67 mg/ml, to be used in determining the molar ratio of interaction between USP7 and MCM-BP. The ladder used was PageRuler Plus Prestained Protein Ladder.

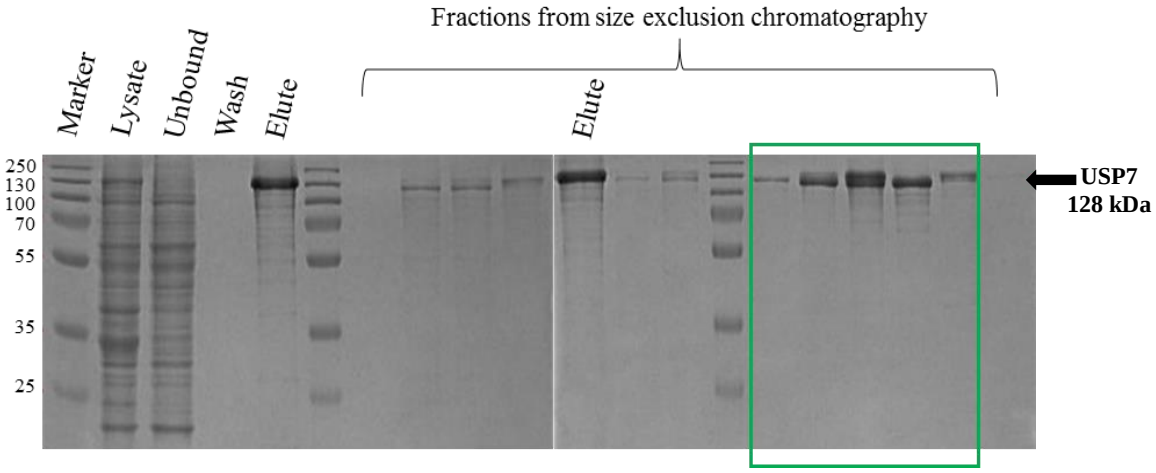

Figure 3.3: Purification of USP7 using Ni^{2+} affinity chromatography. 6xHis tagged USP7 (1102 amino acid residues, ~130 kDa protein) was overexpressed in SF9 cells using the baculovirus expression system and purified using Ni2+ affinity chromatography. Samples from lysate, unbound proteins, wash and elute were collected and separated on a 15% gel at 195V for 65 minutes A band can be seen in Elute at ~130 kDa, representing 6xHis-USP7. The eluate was subjected to size exclusion chromatography, fractions from which were also resolved using SDS-PAGE. The eluate was run again, along with samples from size exclusion, to provide a size comparison for the second gel. The fractions highlighted in green were pooled, concentrated to 1.71 mg/ml and used in determining the molar ratio of interaction between USP7 and MCM-BP. The ladder used was PageRuler Plus Prestained Protein Ladder.

3.3.2 Equimolar and 1:1.5 ratio of MCM-BP: USP7 facilitates interaction

MCM-BP and USP7 were expressed in Sf9 cells using the baculovirus expression system and purified using Ni^{2+} affinity chromatography. They were then mixed in molar ratios of MCM-BP: USP7 - 1:0, 0:1, 1:1, 1:1.5, 1:2, 1:5, 2:1, and 5:1, incubated to allow for interaction and subjected to size exclusion chromatography to separate complexed proteins from fractions with individual unbound proteins. Figure 3.4 displays the size exclusion chromatograms for the various molar ratios tested, where the major peaks observed were at fractions D10 and E8, for USP7 and MCM-BP, respectively (figure 3.4A and B). As the molar ratios are changed, the intensity (height) of the peaks changes respectively.

Fractions from the peaks as well as before and after each peak were resolved using SDS-PAGE to visualize the contents of each peak, as seen in figure 3.5, with USP7 at 128 kDa and MCM-BP at 73 kDa. An interaction between the two proteins is positive if they are present in the same fractions. As controls to determine the location of the two proteins individually, MCM-BP is seen from fractions E6-E10, whereas USP7 is seen mainly from D6-E2, as displayed in the top two panels (1:0 and 0:1). When either protein is in twice the excess, or more, of the other, the two proteins are not visible in the same fractions and thus interaction was not facilitated at these ratios (bottom four panels). However when the two proteins are in an equimolar ratio or a small excess of MCM-BP (1:1 or 1:1.5, respectively), they are present in the same fractions, suggesting a successful interaction between the two proteins at these ratios.

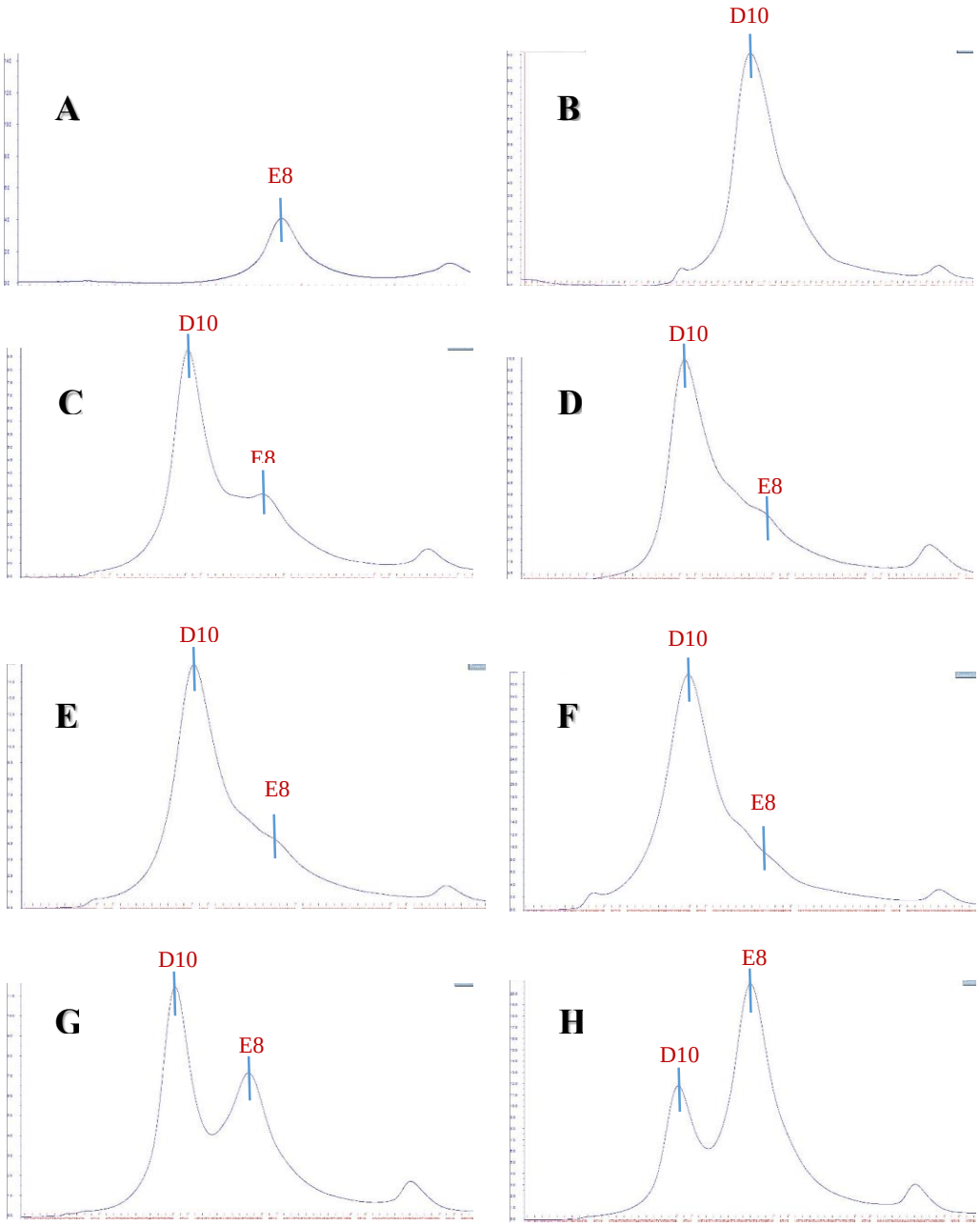

Figure 3.4: Size exclusion chromatographs testing interaction molar ratio between MCM-BP and USP7. Full length USP7 and MCM-BP proteins were purified from *SF9* cells and incubated together in various molar ratios at room temperature for 1 hour to determine optimal ratio for interaction. This was subjected to size exclusion chromatography to separate bound and unbound fractions. A-H represent chromatographs for molar ratios of (MCM-BP:USP7) 1:0, 0:1, 1:1, 1:1.5, 1:2, 1:5, 2:1 and 5:1, respectively. Major peaks were observed at D10 and E8. Fractions from, before, and after each peak were separated using SDS-PAGE.

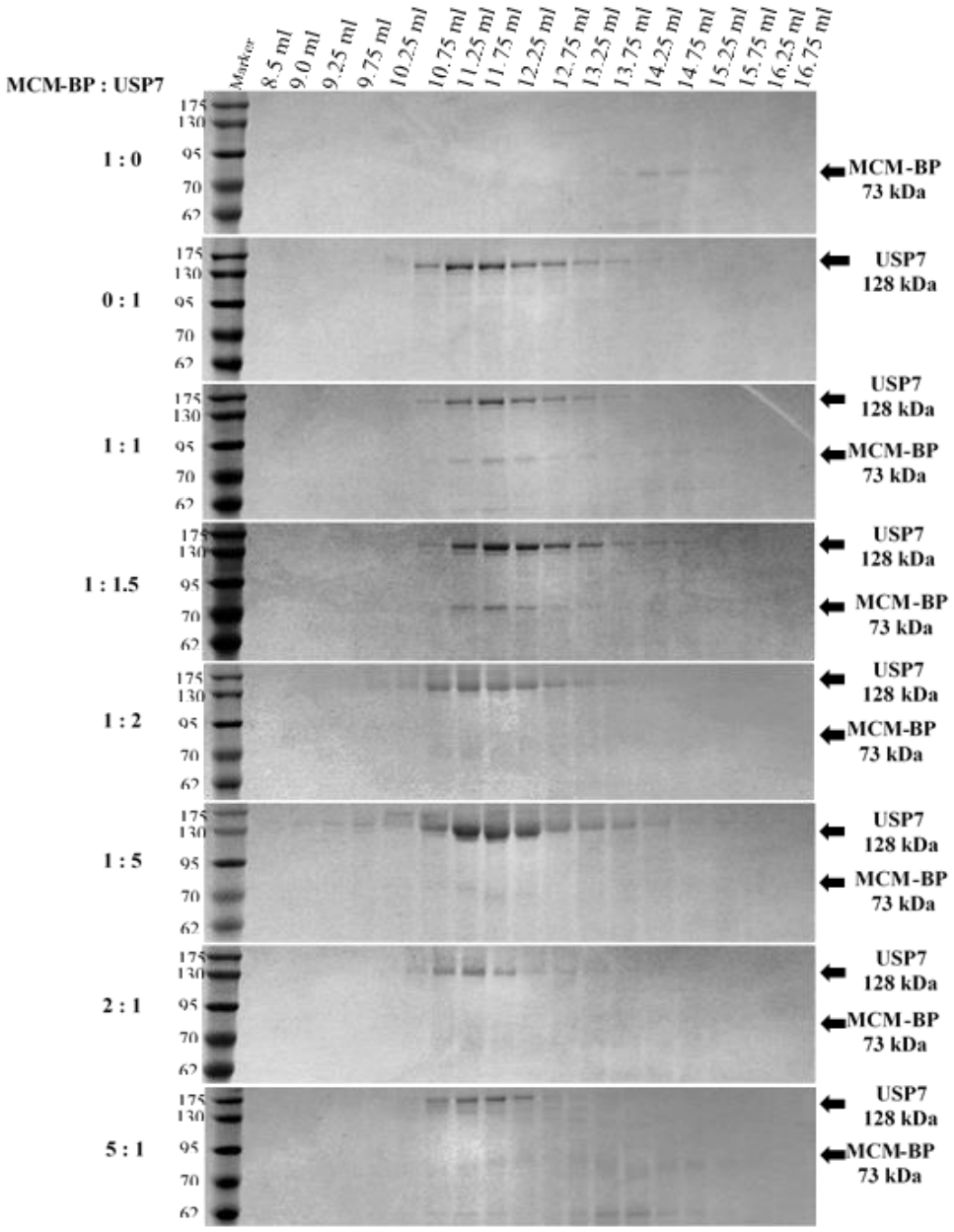

Figure 3.5: Equimolar and 1:1.5 ratio of MCM-BP:USP7 facilitates interaction. USP7 and MCM-BP were purified and incubated together in various molar ratios at room temperature for 1 hour to determine optimal ratio for interaction. This was subjected to size exclusion chromatography and fractions from, before, and after each peak (D10 and E8) were separated using SDS-PAGE on a 10% gel. The top two panels contain MCM-BP and USP7 controls, where the proteins can be seen at 73 kDa and 128 kDa respectively. When the molar ratio is increased more than 1.5 fold, MCM-BP and USP7 do not elute in the same fraction showing that greater than 1:1.5 ratio does not facilitate interaction.

3.3.3 Molecular basis of interaction of USP7 with MCM-BP^{PSTS} involves its ^{164}DWGF^{167} binding pocket

To determine the molecular basis of interaction, co-crystal structure of USP7-NTD with peptide from MCM-BP was determined using X-ray crystallography. USP7-NTD was purified using Ni^{2+} affinity chromatography, as shown in Chapter 2.

Co-crystallization trials and molecular structure determination

5-fold excess of the MCM-BP peptide was successfully co-crystallized with His-cleaved USP7-NTD in 0.1M Tris pH 8.5, 30% PEG 4000 and 0.2M Lithium Sulfate. Microseeding was used to enhance the crystallization process by using crystals from the USP7:HdmX complex as seeds. Figure 3.6 displays long rod shaped crystals obtained from the crystallization trials, similar to what was observed in crystals from the USP7:CHFR complex. Data collected from X-ray diffraction using one crystal was used to determine the three-dimensional structure of the complex. Figure 3.7A is one of the multiple diffraction images collected, with the red rings displaying the resolution shells. Each spot on the image is a reflection of the diffracted X-rays detected by the CCD detector. Figure 3.7B is an intensified version of the original image to show the reflections at higher resolution shells, as shown in the magnified image around the 2.08Å shell.

Molecular replacement was used to solve the structure at a resolution of 1.7 Å. Table 3.1 lists the X-ray data collection and refinement parameters for this structure. The unit cell was found to be $P4_1$ with a = b = 70.0 Å and c = 45.7 Å unit cell parameters. The data

collection was 76.7% complete at the 1.7 Å resolution shell. After refinement, the R_{work} and R_{free} were shown to be 20.7% and 23.3%, respectively, well within acceptable limits. Additionally, 89% of residues were found to be in their most favored regions in the Ramachandran plot, which further signals the validity of the determined structure.

MCM-BP binds to the β-7 strand in a groove on the surface of USP7

Figure 3.8 displays the complex structure, with USP7-NTD in violet depicted as a ribbon diagram (figure 3.8A), surface diagram (figure 3.8B) and electrostatic surface diagram (figure 3.8C), and the MCM-BP peptide represented as a stick diagram in green. USP7-NTD was modeled from residues 63-205, due to residues 54-63 being disordered. The structure consists of an anti-parallel beta-sandwich of eight β-strands that resembles a TRAF domain. The MCM-BP peptide is seen to interact with USP7-NTD by interacting with its β7 strand while hugging the two beta-sheets along its length. The view of the structure as shown in figure 3.8 will, for comparison purposes, be considered as the frontal view, which is the view that best displays the structure as a complex.

When the structure was rotated 90° from its frontal view, a shallow groove on the surface of USP7-NTD was visible, and the MCM-BP peptide was seen to fit well in this groove through its interaction with the β-7 strand which lies at the base of the groove, as depicted in figure 3.9.

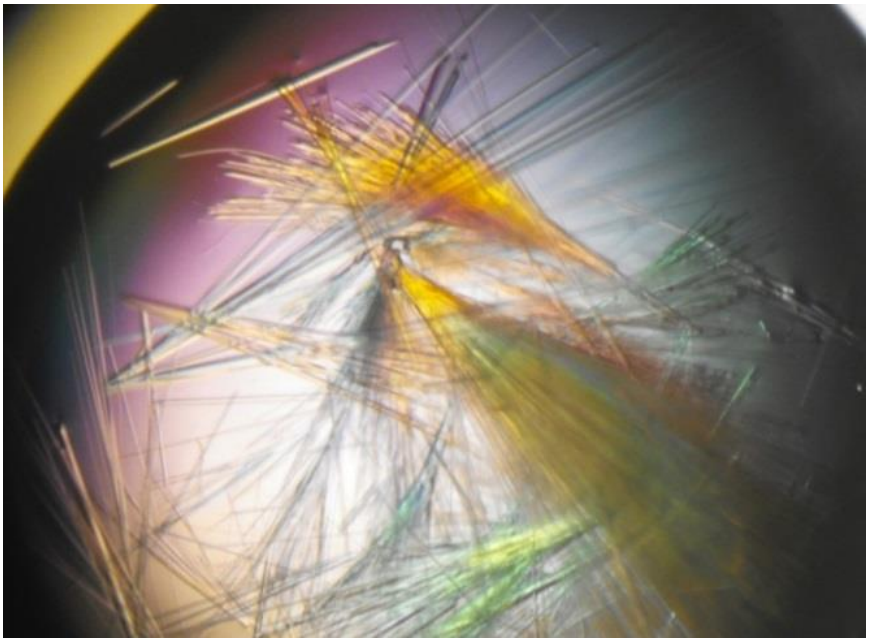

Figure 3.6: Protein crystals of USP7-NTD complex with MCM-BP peptide. 100 mg/ml USP7-NTD was incubated with approximately 5-fold excess of MCM-BP^{PSTS} peptide. Co-crystal trials were set up using micro-seeding with USP7-NTD:HdmX as seeds in 30% PEG 4000, 0.1 M Tris pH 8.5 and 0.2 M Lithium Sulfate. Crystals were obtained from complex of USP7-NTD with MCM-BP peptide ^{152}RVSPSTSYTP^{161} in the dark at 4^{0}C and used to collect X-ray data and solve the three-dimensional structure of the USP7-NTD:MCM-BP^{PSTS} complex.

A

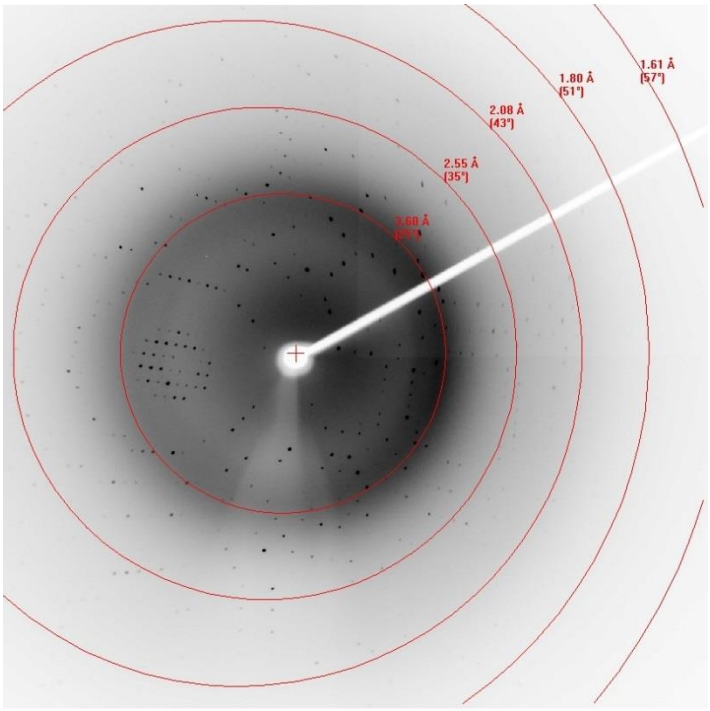

B

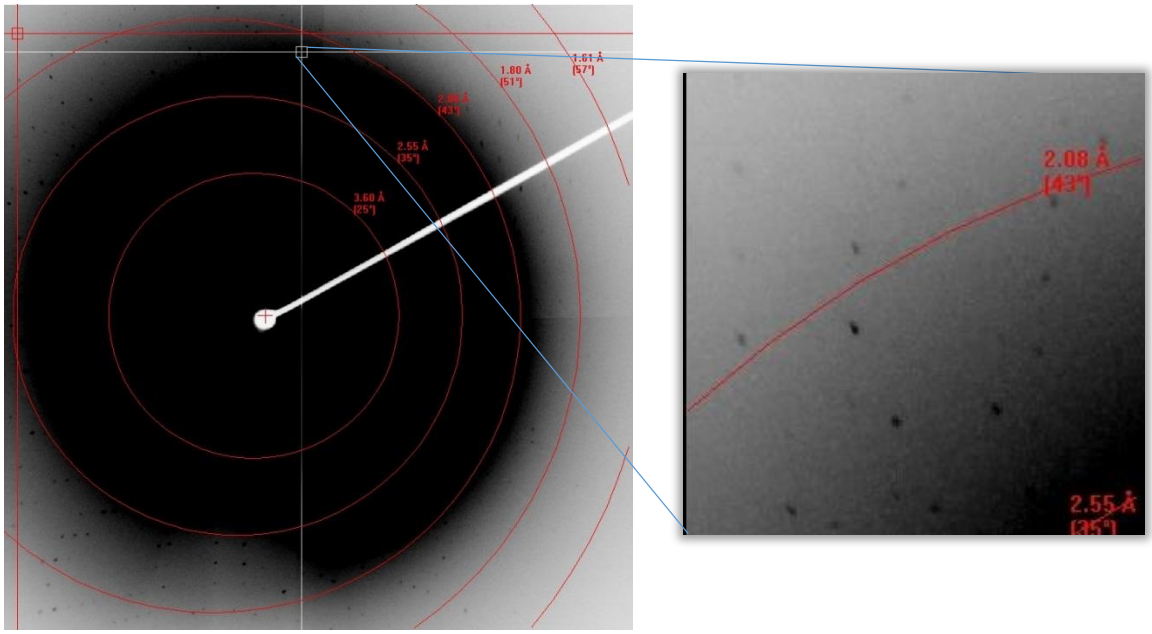

Figure 3.7: X-ray diffraction pattern from a USP7:MCM-BP complex crystal. X-ray data from a Rigaku MicroMax007 rotating anode diffractometer with a 944+ CCD (charge-coupled-device) detector was collected at 100K from a frozen protein crystal. When the X-rays pass through the crystal, a constructive interference of the X-rays produce reflections on the detector, which as seen as spot on the images. **A.** Image of the diffraction pattern displaying reflections at the low-medium resolution shells. **B.** Image showing the reflections at the higher resolution shells, with a magnified section around 2.08Å.

Table 3.1. X-Ray data collection and refinement parameters for USP7:MCM-BP complex

X-Ray Data	USP7-NTD: MCM-BP^{PSTS}
Space Group	$P4_1$
Resolution (Å)	50.0 – 1.70
Unit Cell Axes (Å^3)	69.8 x 69.8 x 45.7
Molecules/AU	1
Total Observations (#)	267 608
Unique Reflections (#)	22 977
Intensity (I/σ<I>)	22.4 (1.5)
Completeness (%)	95.6 (76.7)
$^aR_{sym}$	0.066 (0.509)

Refinement	USP7-NTD: MCM-BP^{PSTS}
R_{work}	0.207
R_{free}	0.233
Protein Atoms (#)	1146
Water Molecules (#)	130
rmsd bonds (Å)	0.006
rmsd angles (^{0})	1.25
rmsd dihedrals (^{0})	25.3
rmsd improper (^{0})	0.87
Thermal factors (Å^2)	19.6
Ramachandran Plot	
Most Favoured	89.1
Additionally Allowed	10.9

Numbers in brackets refer to the highest resolution shell, 1.73 to 1.70 Å for the MCM-BP^{PSTS} data. $^aR_{sym}$ = S |I-<I>| /SI where I is the observed intensity and <I> is the average intensity from multiple observations of symmetry-related reflections.

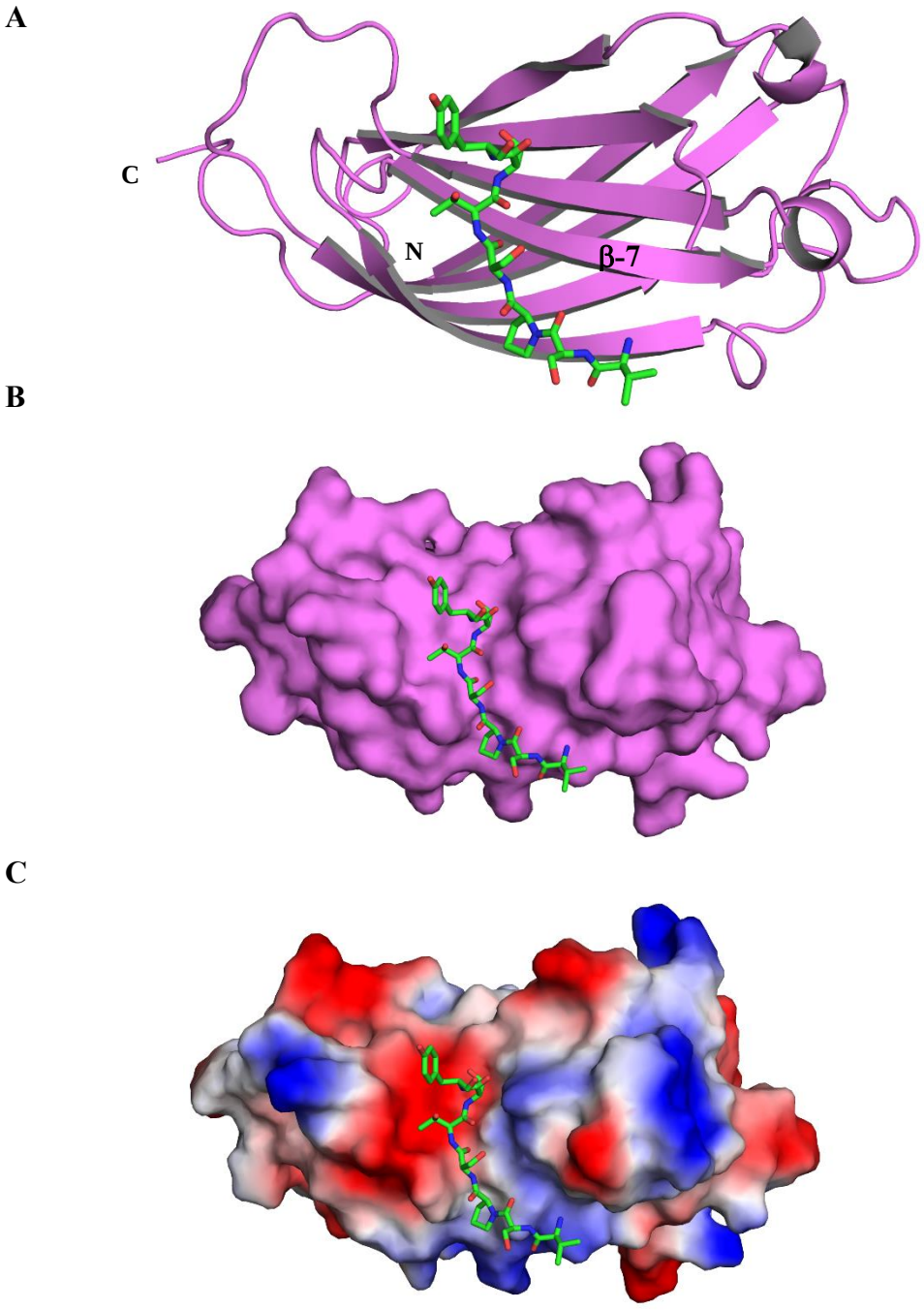

Figure 3.8: Crystal structure of USP7-NTD bound to MCM-BP ^{152}RVSPSTSYTP^{161}. **A.** Cartoon representation of the crystal structure of MCM-BP peptide in green bound to the USP7-NTD in violet ribbon form at its β-7 strand. **B.** Surface diagram and **C**. Electrostatic surface representation of the crystal structure. The complex structure was solved at a resolution of 1.7 Å.

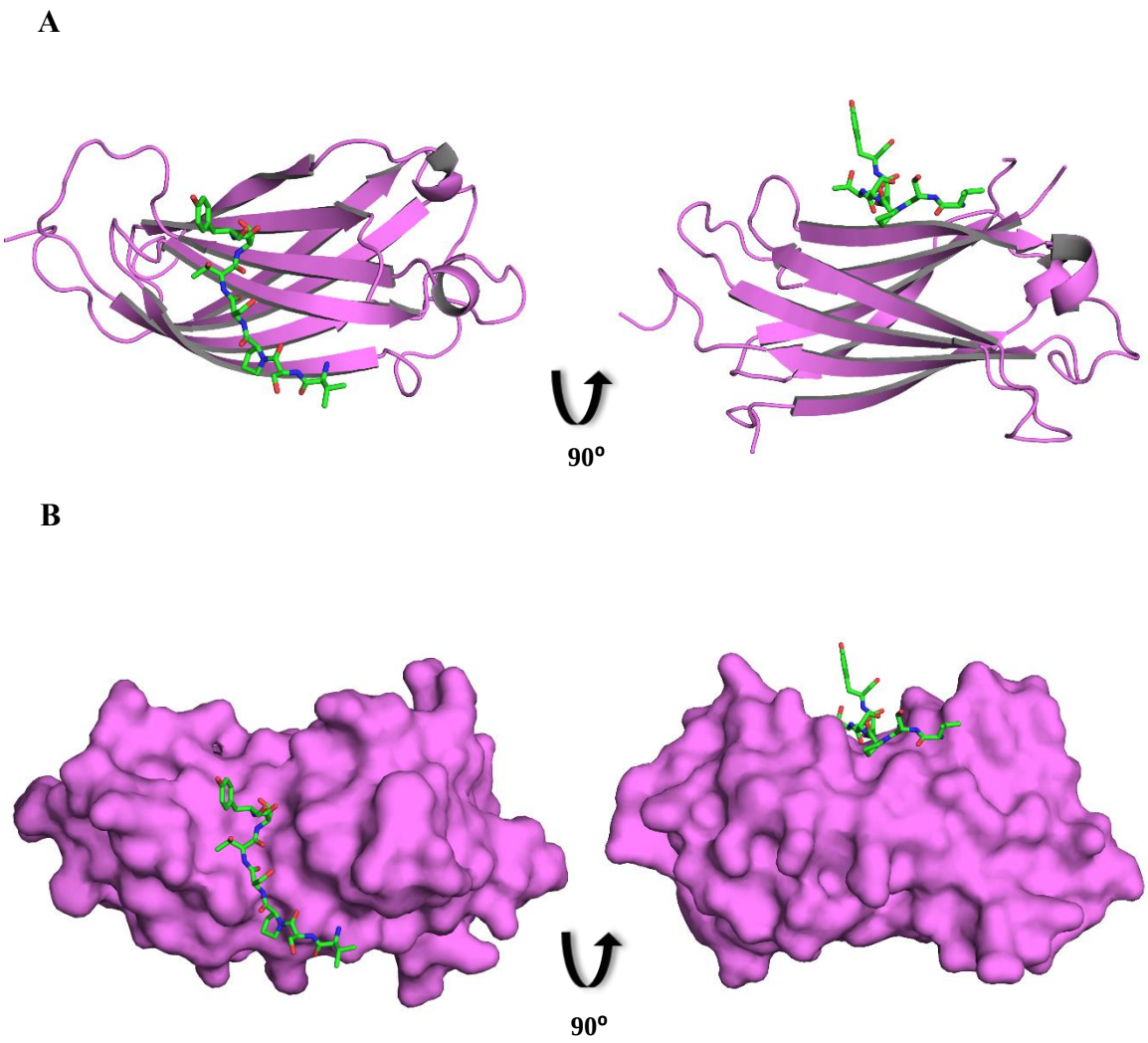

Figure 3.9: MCM-BP binds to a shallow groove on the surface of USP7. Upon rotating the structure on the x-axis at a 90° angle, the MCM-BP peptide is observed to be sitting in a shallow groove on the surface of USP7. At the base of the groove is the β-7 strand of the anti-parallel beta-sheets of the N-terminal domain of USP7. **A.** Cartoon and **B.** Surface representations of the frontal view as well as the rotated, to allow for visualization of the binding groove. The peptide is represented in green stick form.

The interaction site – S158 of MCM-BP makes most contacts with D164 of USP7

To take a closer look at the site of interaction, the MCM-BP peptide is aligned with the interacting residues from USP7, in figure 3.10B. It is clear that there are two interactions that bind the two proteins. By rotating this figure, these interactions are better displayed in figures 3.10C and D. The most essential residues are seen to be S158 in MCM-BP which makes hydrogen bonds with D164 of USP7 (figure 3.10C). The carboxyl groups of the aspartate side chain (D164) in USP7 form hydrogen bonds with the amide of the serine as well as the hydroxyl of the serine side chain (S158) in MCM-BP. Additional binding is achieved through water-mediated hydrogen bonding of S156 with USP7 (figure 3.10D). These interactions allow the peptide to sit in the groove on the surface of USP7 lined by the residues ^{164}DWGF^{167}. Figure 3.10A shows the peptide modelled into its electron density map. At the 1.7Å resolution, the density for the side chains is clear and the side chains fit well.

To provide orientation clarity, the orientation of the peptide observed in figure 3.10A and B is considered as the standard orientation, and will be used with every depiction of the peptide, along with a rotated view to provide the optimal visualization of the site of interest.

MCM-BP peptide forms a ninth beta-strand anti-parallel to β-7 of USP7

Figure 3.11 compares the complex structure with the peptide in stick form with that as a strand. When the frontal view of the structure is rotated in three dimensions, the peptide in stick form is seen to line up against the β-7 strand of USP7. Interestingly, with a part

of the peptide transformed to a ribbon diagram, it is observed to form an anti-parallel strand to the β-7 strand.

Comparing the substrate recognition motif of MCM-BP with USP7 interacting peptides

Figures 3.12-3.15 compare the MCM-BP peptide with other USP7-NTD interacting peptides from CHFR, MDM2, p53 and EBNA1, respectively, by aligning these peptides with MCM-BP. The USP7 substrate recognition motif in MCM-BP is PSTS, which is compared with the motifs in CHFR, MDM2, p53 and EBNA1. Like MCM-BP, CHFR uses PSTS to interact with USP7, so their motifs align perfectly. The motifs in MDM2 and MCM-BP differ by one residue, with MDM2 using PSSS instead of PSTS. p53 only shares the proline and last serine with MCM-BP, but still maintains the P/AXXS conservation. EBNA1, however, does not conform to the P/AXXS, using EGPS. It does not align well with MCM-BP, yet the last serine in the motif which interacts with D164 of USP7 is conserved and aligns perfectly.

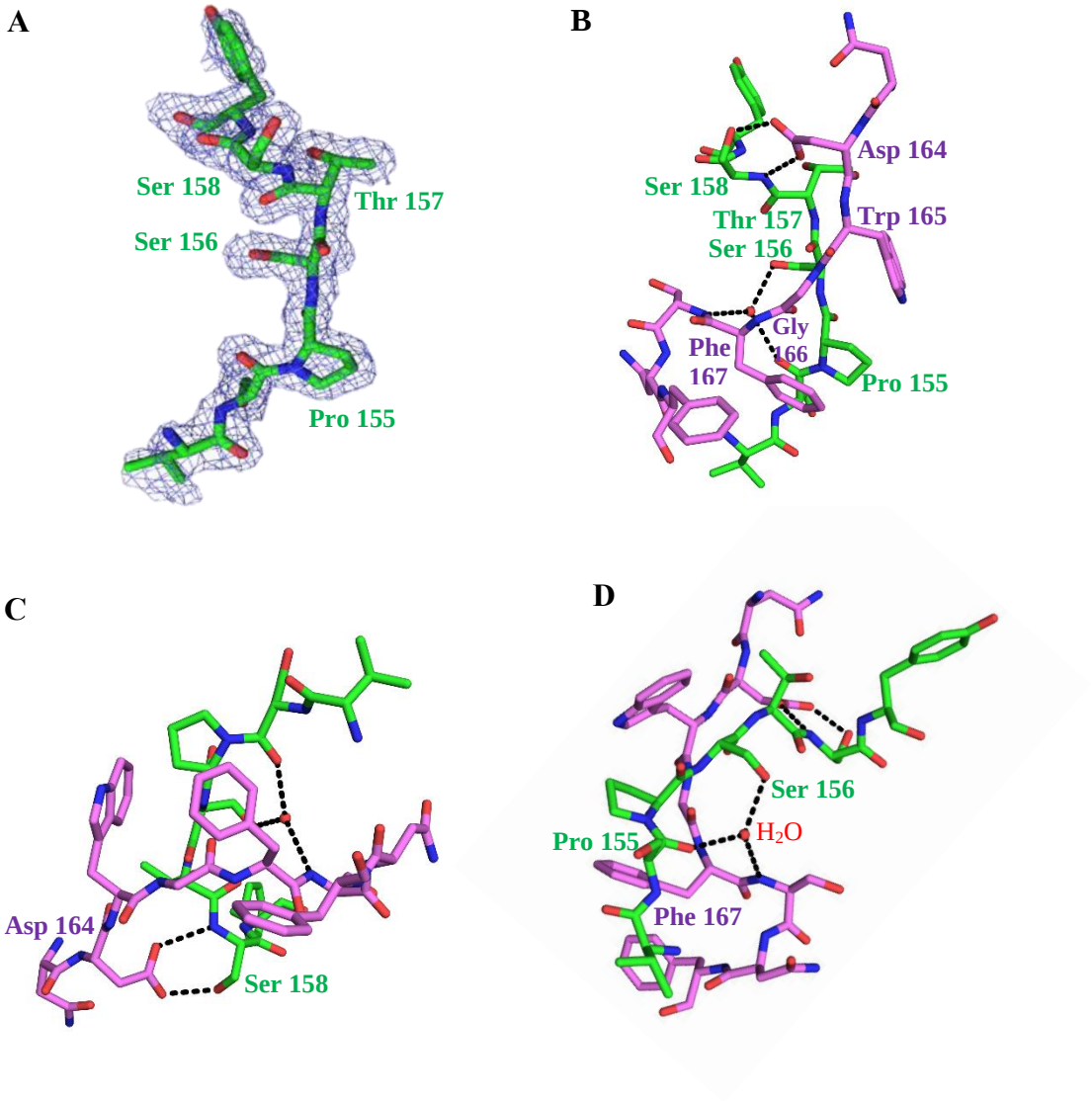

Figure 3.10: ^{155}PSTS^{158} of MCM-BP interacts with ^{164}DWGF^{167} in the binding groove of USP7. A. The electron density map (2fo-fc) of the MCM-BP peptide. **B.** The peptide in green aligned with the interacting residues of USP7, in violet. **C.** MCM-BP S158 (Ser158) makes contacts with D164 (Asp164) of USP7 using hydrogen bonds. **D.** In addition, S156 (Ser156) aids in the interaction by forming water-mediated hydrogen bonds with USP7. **C**. and **D.** are rotated views of **A**, to better display the S158-D164 and the water-mediated interactions, respectively.

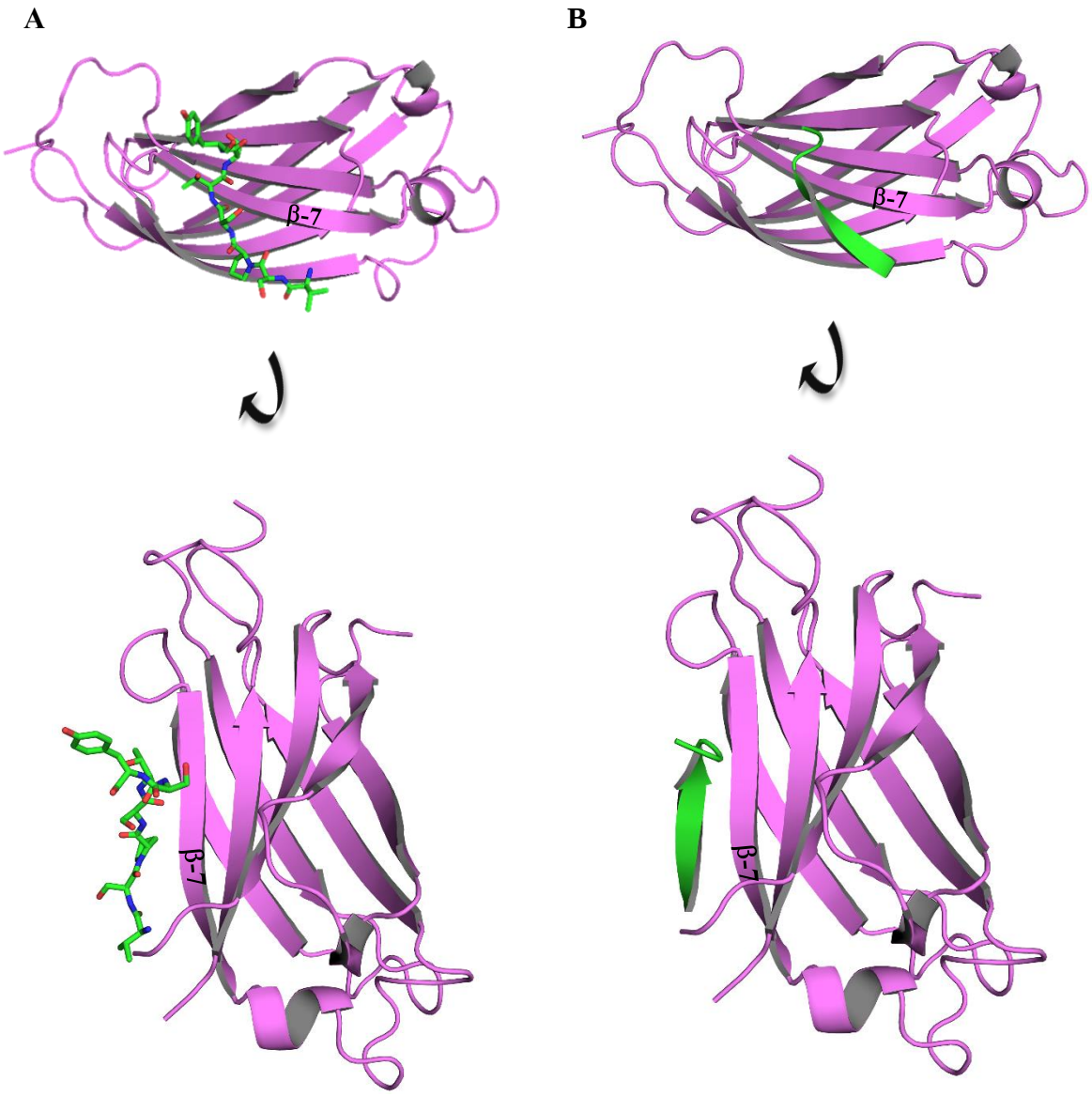

Figure 3.11: The MCM-BP peptide forms an antiparallel strand. A. When the USP7:MCM-BP structure is rotated from its frontal view in three dimensions, the peptide, in stick form, is seen to line up against the upper beta-sheet of USP7. Viewing the peptide as a strand instead of stick-model, as seen in **B**, enables visualization of it as forming an anti-parallel strand to the β-7 strand of USP7.

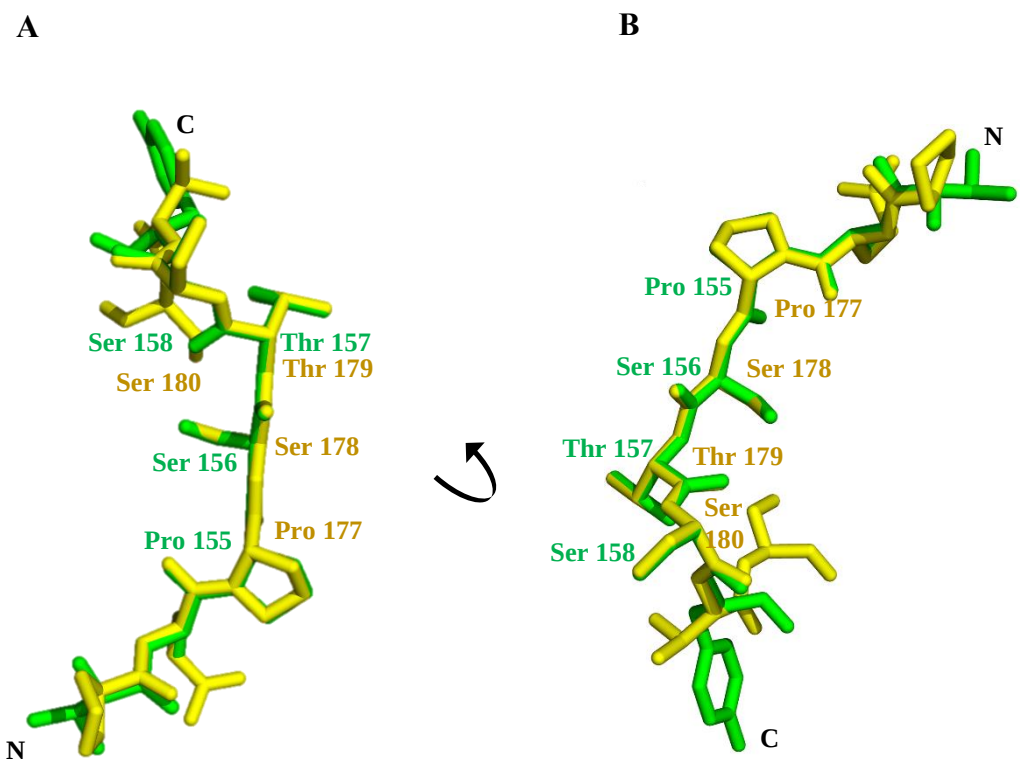

Figure 3.12: The USP7 binding motif of MCM-BP ^{155}PSTS^{158} compared with that of CHFR ^{177}PSTS^{180}. A. An orientation of the MCM-BP peptide used to provide a standard view amongst peptide comparisons. **B.** Rotated view to best portray a comparison of the residues involved in the motifs. MCM-BP and CHFR both have a PSTS motif, hence the peptides line up perfectly at their motifs. MCM-BP in green and CHFR in yellow.

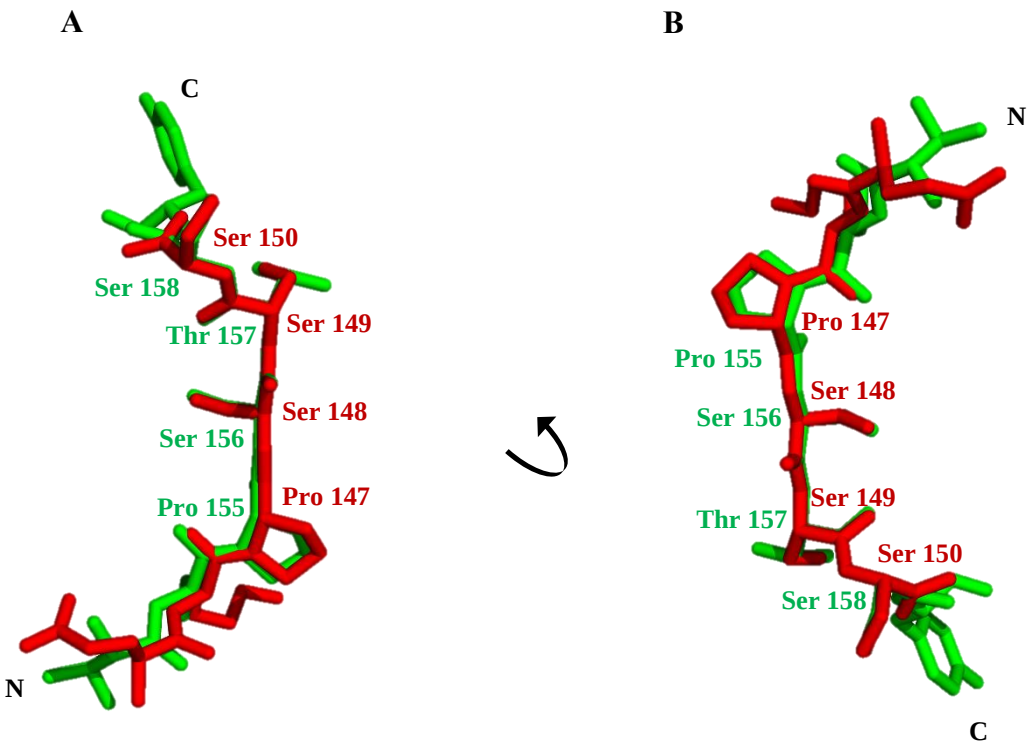

Figure 3.13: The USP7 binding motif of MCM-BP ^{155}PSTS^{158} compared with that of MDM2 ^{147}PSSS^{150}. A. An orientation of the MCM-BP peptide used to provide a standard view amongst peptide comparisons. **B.** Rotated view to best portray a comparison of the residues involved in the motifs. MCM-BP has a PSTS motif, whereas MDM2 uses PSSS. The difference in T157 of MCM-BP and S149 of MDM2 can be seen, with MCM-BP in green and MDM2 in red. The S158 and S150 of MCM-BP and MDM2, respectively, align well.

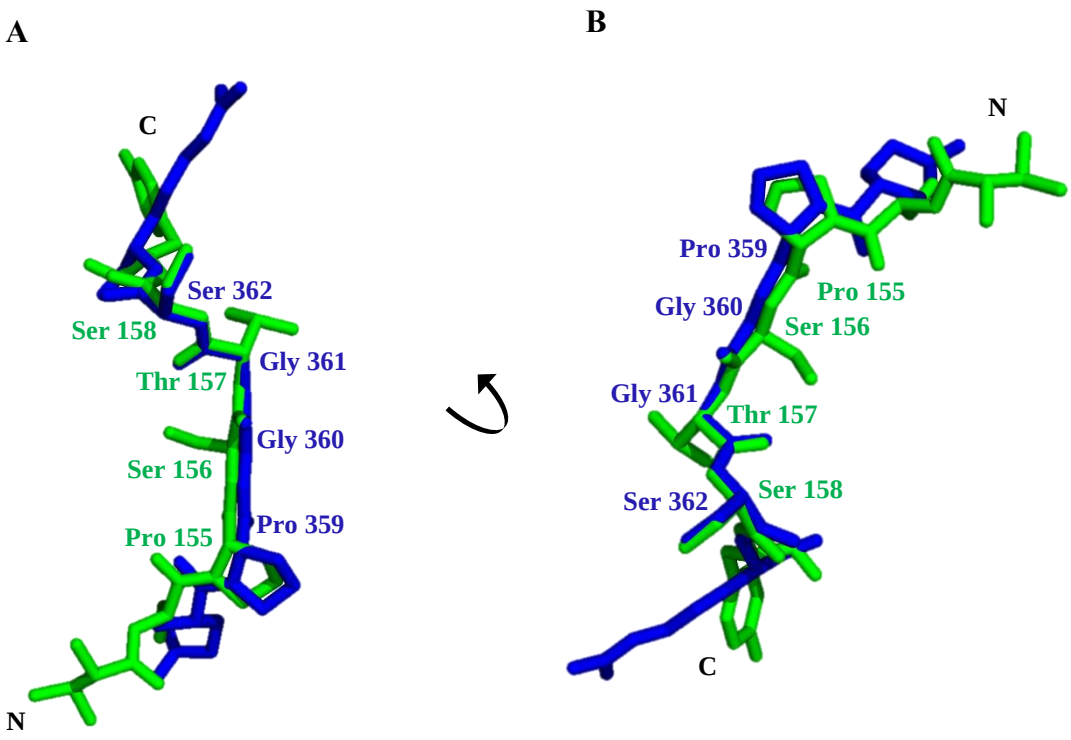

Figure 3.14: The USP7 binding motif of MCM-BP ^{155}PSTS^{158} compared with that of p53 ^{359}PGGS^{362}. A. An orientation of the MCM-BP peptide used to provide a standard view amongst peptide comparisons. **B.** Rotated view to best portray a comparison of the residues involved in the motifs. MCM-BP has a PSTS motif, whereas p53 has PGGS, which is still a P/AXXS motif. Even though p53 contains two glycines instead of a serine and threonine, the most essential residues, S158 and S362 of MCM-BP and p53, respectively, are conserved and align perfectly. MCM-BP is seen in green, and p53 in blue.

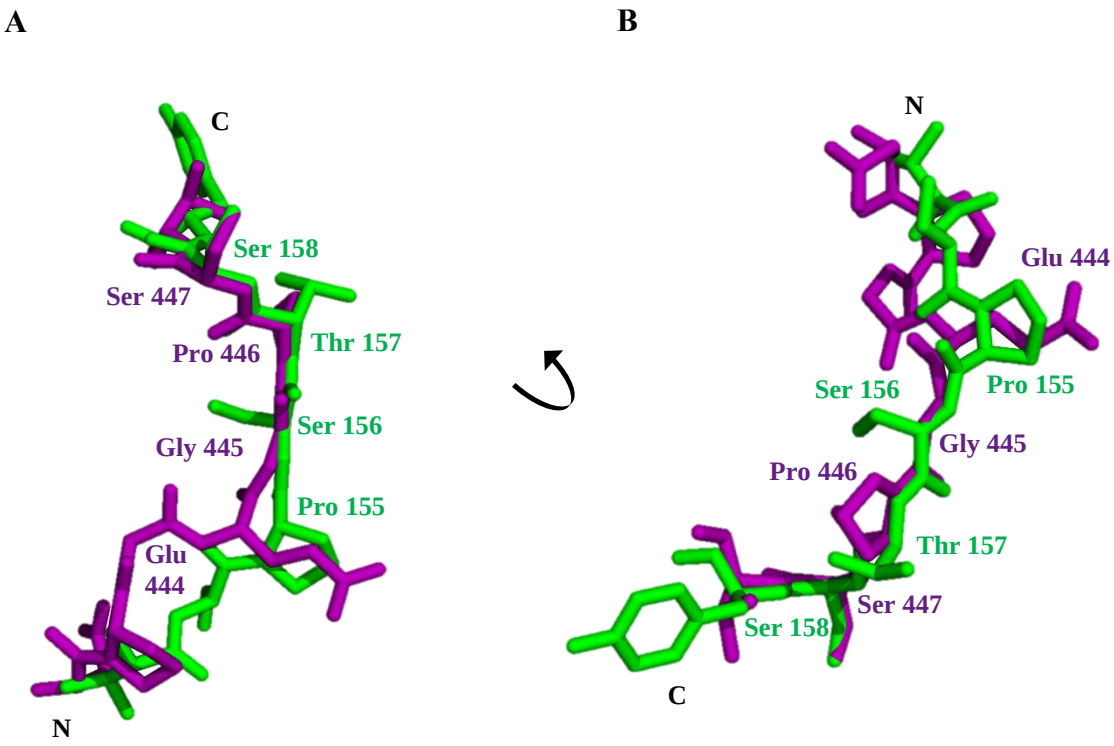

Figure 3.15: The USP7 binding motif of MCM-BP ^{155}PSTS^{158} compared with that of EBNA1 ^{444}EGPS^{447}. A. An orientation of the MCM-BP peptide used to provide a standard view amongst peptide comparisons. **B.** Rotated view to best portray a comparison of the residues involved in the motifs. MCM-BP has a PSTS motif, whereas EBNA1 contains EGPS, which is deviates from the MCM-BP motif except for the last conserved serines. S158 in MCM-BP and S447 in EBNA1 in green and purple, respectively, align perfectly, as compared with the rest of the peptide which deviates at every residue.

3.4 Discussion

After a proteomics study revealed that MCM-BP was a possible interacting partner of USP7, this project was undertaken to confirm the interaction and to determine the site and molecular basis of interaction.

3.4.1 MCM-BP binds to USP7 in a 1:1 molar ratio.

The molar ratio of interaction between USP7 and MCM-BP was tested to determine optimal interaction conditions. It was expected that, if interacting, the optimal ratio would be 1:1, which is validated by the data that shows that the proteins bind when present in a 1:1 as well as 1:1.5 ratio of MCM-BP:USP7. A successful binding is suggested when the two proteins being tested co-elute in the same peak or fractions from a size exclusion column. This is visualized by a shift in the peaks in a chromatogram when compared to the peaks of the individual proteins (figure 3.4) as well as on a SDS-PAGE gel with samples from fractions of and around the peaks (figure 3.5). As seen in figure 3.5, at ratios other than 1:1 and 1:1.5, no binding was observed, as the proteins were not present in the same fractions. Ideally, the proteins would bind only in a 1:1 ratio, however binding at 1.1.5 ratio might suggest that the molar ratio requirement may not be as rigid as expected. Jagannathan et al (2014) conducted a similar experiment where they used equimolar concentrations of USP7 and MCM-BP and observed positive binding. However, their experiment differs from this project since they compared the interaction of MCM-BP with different regions of USP7, whereas we compared different ratios of interaction.

3.4.2 PSTS motif in MCM-BP involved in interaction with USP7-NTD

Once a positive interaction was established, it was important to determine the site of interaction between the proteins. MCM-BP contains a PSTS-motif, which resembles the established P/AXXS substrate recognition motif found in substrates or interacting partners of USP7 (Sheng et al. 2006). This motif is recognized by a binding pocket in the N-terminus of USP7. Data from a peptide spot array and intrinsic tryptophan fluorescence assay helped confirm that this motif is responsible for binding to USP7. The serines in the motif were seen to be essential for binding; mutation of either of the serines to alanine abolished binding and the dissociation constant for the interaction resulted in being significantly higher than the wild type.

Having determined the site of interaction in MCM-BP, the molecular mechanism was established using X-ray crystallography. Co-crystal trials were set up with USP7-NTD and peptide containing the PSTS motif in MCM-BP (^{152}RVSPSTSYTP^{161}), using microseeding with seeds from a previously crystallized complex of USP7-NTD:HdmX. The USP7-NTD:MCM-BP^{PSTS} complex crystallized in the dark at 4°C, and was used to determine the molecular structure at a resolution of 1.7Å.

Similar to the mode of binding observed in CHFR, by aligning the MCM-BP peptide with USP7-NTD, it is seen that peptide binds to the same shallow groove on the surface of USP7, lined by the residues ^{164}DWGF^{167}. The last serine in the PSTS motif, S158, is responsible for making contacts with D164 in USP7, with additional hydrogen bonding between the peptide and USP7 facilitated by a water molecule. USP7-NTD makes two

anti-parallel beta-sheets using eight strands, and the peptide is observed to bind to the β-7 strand, while hugging the two beta-sheets. As seen from interaction study with CHFR, this mechanism of interaction is not unique to MCM-BP, but has been shown for almost all the proteins that bind to the N-terminal domain of USP7, such as p53, Hdm2, HdmX and EBNA1.

Upon comparison of MCM-BP with these proteins, despite the neighboring residues of the motifs being different, the motifs themselves align well in MCM-BP with those in CHFR, MDM2 and p53. In EBNA1, only the last serine is conserved, yet the backbone aligns well with the serine lining up perfectly. This highlights the conserved mechanism used by these proteins to interact with USP7, despite their varied functions.

3.4.3 Perspective

The interaction of USP7 with MCM-BP is still a novel interaction that researchers are beginning to explore. MCM-BP is essential in the unloading of the pre-RC from DNA towards the end of replication, helping to prevent the cell from duplicating the DNA more than once. Determining the site and molecular mechanism of interaction between USP7 and MCM-BP has played a role in portraying the importance of USP7 in DNA replication. Jagannathan et al. (2014) have recently shown that by binding to USP7 on the chromatin, MCM-BP is capable of mediating an interaction between USP7 and the MCM proteins leading to their dissociation from the DNA by a still unknown mechanism.

Their study might also indicate a non-catalytic role between USP7 and MCM-BP. Most proteins, such as p53, Hdm2 and HdmX that bind to the binding pocket in the N-terminus

of USP7 are involved as substrates in a catalytic role with USP7. This project has determined MCM-BP to bind USP7 in a similar fashion to these proteins, but may only be an interacting partner, not a substrate for deubiquitination.

CHAPTER 4: SUMMARY AND

FUTURE PROSPECTS

4.1 Summary and conclusion

The aim of this project was to study the interactions of the N-terminal domain of USP7 with MCM-BP and CHFR by determining the molecular mechanism of these interactions *in vitro* and studying the effect of USP7 depletion on CHFR *in vivo*. Using X-ray crystallography, it was found that a PSTS-motif in both MCM-BP and CHFR bind to a shallow groove on the surface of USP7-NTD lined by residues ^{164}DWGF^{167}, with a major interaction established between S158 of MCM-BP and S180 of CHFR with D164 of USP7. Additional water-mediated hydrogen bonds were also formed between USP7 and S156 of MCM-BP and S178 of CHFR. This mechanism underlying this interaction was observed to be similar to those established with the interactions of USP7 with p53, EBNA1, MDM2 and MDMX. The *in vivo* study between USP7 and CHFR confirmed that endogenous CHFR gets degraded faster in the absence of endogenous USP7, concluding that the deubiquitinating activity of USP7 is involved in stabilizing the levels of CHFR. Although previous studies have established the interaction of USP7 with MCM-BP and CHFR, this study was the first to map these interactions to the N-terminus of USP7.

4.2 Future prospects

4.2.1 Expanding the CHFR-USP7 network

USP7 is a key player of the p53-MDM2 pathway, where it is responsible for the deubiquitination of both p53 as well as MDM2, the E3 ligase responsible for ubiquitinating p53. Being the DUB for CHFR, which is an E3 ligase, it is then possible that USP7 also plays a role in the regulation of the substrates of CHFR, such as Aurora A and Plk-1. Aurora A contains three potential USP7 substrate recognition motifs, PSNS, APSS and ANSS, while Plk-1 contains only APSS. Using a combination of mutational analysis, peptide spot array and intrinsic tryptophan assay, one of these motifs can be validated and used for future research with the interaction of the two proteins with USP7. As mentioned, this would pave the way towards expanding the CHFR-USP7 network to understand the pathways that would tightly govern the regulation of such an essential checkpoint protein.

To function in its E3 ligase capacity, CHFR requires E2 ubiquitin conjugating enzymes to ubiquitinate a substrate. Since CHFR shares its RING domain with RNF8, it would be interesting to study its interactions with the E2s associated with RNF8. UbE2E1 was one such E2 that interacts with RNF8 but was found not to be associated with CHFR. Each E3 ligase can pair with a variety of E2 proteins, and there is a constant effort to find novel E2-E3 pairs. As such, the search for E2s to pair with CHFR can continue, with those interacting with RNF8 used as a starting point.

4.2.2 Examine the mechanism involved in USP7-mediated MCM unloading

The interaction between MCM-BP and USP7 has now been characterized and it has been shown by Jagannathan and colleagues (Jagannathan et al. 2014) to be essential for the dissociation of the MCM complex from chromatin. This interaction may not be a catalytic interaction, and both MCM-BP and USP7 are required for successful dissociation. The mechanism of this process is still unclear. USP7 could potentially be involved in deubiquitination of one of the MCM complex proteins. In fact, MCM3 contains residues PSSS, identical to the motif used by MDM2 to bind USP7. MCM5 also includes residues that conform to the general P/AXXS motif – ASPS.

The affinity of these proteins for USP7 can be determined using interaction assays, while the viability of the motifs can be checked using a peptide array and intrinsic tryptophan fluorescence assay. If there is a positive interaction of these proteins with USP7, a combination of experiments can be used to analyze if the interaction is catalytic and further, if this affects the stability of the proteins. Deubiquitination of these proteins as a part of the unloading process (proteasome independent) would mean conformational changes in the MCM protein, which would provide an insight into the mechanism responsible for the dissociation of the complex.

REFERENCES

Ahel I, Ahel D, Matsusaka T, Clark AJ, Pines J, Boulton SJ, West SC. 2008. Poly(ADP-ribose)-binding zinc finger motifs in DNA repair/checkpoint proteins. Nature. 451(7174): 81-85.

Amerik AY, Hochstrasser M. 2004. Mechanism and function of deubiquitinating enzymes. BBA-Mol Cell Res. 1695(1-3): 189-207.

Berry LD, Gould KL. 1996. Progress in cell cycle research. Volume 2. New York: Plenum Press. p 99-105. Chapter 10, Regulation of Cdc2 activity by phosphorylation at T14/Y15.

Bochman ML, Schwacha A. 2009. The Mcm complex: unwinding the mechanism of a replicative helicase. Microbiol Mol Biol Rev. 73(4): 652-683.

Brunger AT. 2007. Version 1.2 of the crystallography and NMR system. Nat Protoc. 2: 2728-2733.

Bryant JA, Aves SJ. 2011. Initiation of DNA replication: functional and evolutionary aspects. Ann Bot. 107(7): 1119-1126.

Chapman HA, Riese RJ, Shi G. 1997. Emerging roles for cysteine proteases in human biology. Annu Rev Physiol. 59: 63-88.

Chin CF, Yeong FM. 2010. Safeguarding entry into mitosis: the antephase checkpoint. Mol Cell Biol. 30(1): 22-32.

Ciechanover A. 2005. Proteolysis: from the lysosome to ubiquitin and the proteasome. Nat Rev Mol Cell Biol. 6: 79-87.

Ciechanover A, and Saadon RB. 2004. N-terminal ubiquitination: more protein substrates join in. Trends Cell Biol. 14(3): 103-106.

Daubeuf S, Singh D, Tan Y, Liu H, Federoff HJ, Bowers WJ, Tolba K. 2009. HSV ICP0 recruits USP7 to modulate TLR-mediated innate response. Blood. 113(14): 3264-3275.

Derks S, Cleven AHG, Melotte V, Smits KM, Brandes JC, Azad N, van Criekinge W, de Bruine AP, Herman JG, van Engeland M. 2013. Emerging evidence for CHFR as a cancer biomarker: from tumor biology to precision medicine. Cancer Metastasis Rev. [epub ahead of print].

Deshaeis RJ, Joazeiro CAP. 2009. RING domain E3 ubiquitin ligases. Anu Rev Biochem. 78: 399-434.

Epping MT, Meijer LAT, Krijgsman O, Bos JL, Pandolfi PP, Bernards R. 2011. TSPYL5 suppresses p53 levels and function by physical interaction with USP7. Nat Cell Biol. 13: 102–108.

Faesen AC, Dirac AMG, Shanmugham A, Ovaa H, Perrakis A, Sixma TK. 2011. Mechanism of USP7/HAUSP activation by its C-terminal ubiquitin-like domain and allosteric regulation by GMP-Synthetase. Mol Cell. 44(1): 147-159.

Faesen AC, Luna-Vargas MPA, Sixma TK. 2012. The role of UBL domains in ubiquitin –specific proteases. Biochem Soc Trans. 40: 539-545.

Fiore PPD, Polo S, Hofmann K. 2003. When ubiquitin meets ubiquitin receptors: a signaling connection. Nat Rev Mol Cell Biol. 4: 491-497.

Fukuda T, Kondo Y, Nakagama H. 2008. The anti-proliferative effects of the CHFR depend on the forkhead associated domain, but not E3 ligase activity mediated by Ring finger domain. PLoS One. 3(3): e1776.

Gartel AL, Radhakrishnan SK. 2005. Lost in transcription: p21 repression, mechanisms and consequences. Cancer Res. 65: 3980.

Goldstein G, Scheid M, Hammerling U, Schlesinger DH, Niall HD, Boyse EA. 1975. Isolation of a polypeptide that has lymphocyte-differentiating properties and is probably represented universally in living cells. Proc Natl Acad Sci USA. 72(1): 11-15.

Haglund K, Dikic I. 2005. Ubiquitylation and cell signaling. EMBO J. 24(19): 3353-3359.

Hagting A, Jackman M, Simpson K, Pines J. 1999. Translocation of cyclin B1 to the nucleus at prophase requires a phosphorylation-dependent nuclear import signal. Curr Biol. 9(13): 680-689.

Hochstrasser M. 2009. Origin and function of ubiquitin-like proteins. Nature. 458(7237): 422-429.

Hu M, Li P, Li M, Li W, Yao T, Wu J, Gu W, Cohen RE, Shi Y. 2002. Crystal structure of a UBP-family deubiquitinating enzyme in isolation and in complex with ubiquitin aldehyde. Cell. 111(7): 1041-1054.

Ito K, Adachi S, Iwakami R, Yasuda H, Muto Y, Seki N, Okano Y. 2001. N-terminally extended human ubiquitin-conjugating enzymes (E2s) mediate the ubiquitination of RING-finger proteins ARA54 and RNF8. Eur J Biochem. 268(9): 2725-2732.

Jagannathan M, Nguyen T, Gallo D, Luthra N, Brown GW, Saridakis V, Frappier L. 2014. A role for USP7 in DNA replication. Mol Cell Biol. 34(1): 132-145.

Jones TA, Kjeldgaard M. 1997. Electron-density map interpretation. Methods Enzymol. 277: 173-208.

Kashima L, Idogawa M, Mita H, Shitashige M, Yamada T, Ogi K, Suzuki H, Toyota M, Ariga H, Sasaki Y, Tokino T. 2012. CHFR protein regulates mitotic checkpoint by targeting PARP-1 protein for ubiquitination and degradation. J Biol Chem. 287: 12975-12984.

Kim JS, Park YY, Park SY, Cho H, Kang D, Cho H. 2011. The auto-ubiquitylation of E3 ubiquitin-protein ligase Chfr at G2 phase is required for accumulation of polo-like kinase 1 and mitotic entry in mammalian cells. J Biol Chem. 286(35): 30615-30623.

Kimura Y, Tanaka K. 2010. Regulatory mechanisms involved in the control of ubiquitin homeostasis. J Biochem. 147(6): 793-798.

Komander D, Clague MJ, Urbe S. 2009. Breaking the chains: structure and function of the deubiquitinases. Nat Rev Mol Cell Biol. 10: 550-563.

Kwon YE, Bae SJ, Kim M, Seol JH. 2013. SUMOylation negatively regulates the stability of CHFR tumor suppressor. Biochem Biophys Res Commun. 430: 213-217.

Jin J, Li X, Gygi SP, Harper JW. 2007. Dual E1 activation systems for ubiquitin differentially regulate E2 enzyme charging. Nature. 447: 1135-1139

Lee JK, Hurwitz J. 2001. Processive DNA helicase activity of the minichromosome maintenance proteins 4, 6, and 7 complex requires forked DNA structures. Proc Natl Acad Sci. 98(1): 54-59.

Li J, Williams BL, Haire LF, Goldberg M, Wilker E, Durocher D, Yaffe MB, Jackson SP, Smerdon SJ. 2002. Structural and functional versatility of the FHA domain in DNA-damage signalling by the tumor suppressor kinase Chk2. Mol Cell. 9(5): 1045-1054.

Li M, Chen D, Shiloh A, Luo J, Nikolaev AY, Qin J, Gu W. 2002. Deubiquitination of p53 by HAUSP is an important pathway for p53 stabilization. Nature. 416(6881): 648–53.

Liu C, Wu J, Paudyal SC, You Z, Yu X. 2013. CHFR is important for the first wave of ubiquitination at DNA damage sites. Nucl Acids Res. 41(3): 1698-1710.

Moll UM, Petrenko O. 2003. The MDM2-p53 Interaction. Mol Cancer Res. 1: 1001-1008.

Nath D, Shadan S. 2009. The ubiquitin system. Nature. 458(7237): 421

Nakamura J, Lou L. 1995. Biochemical Characterization of Human GMP Synthetase. The Journal of Biological Chemistry. J Biol Chem. 270: 7347-7353.

Nguyen VQ, Co C, Li JJ. 2001. Cyclin-dependent kinases prevent DNA re-replication through multiple mechanisms. Nature. 411: 1068-1073.

Nishiyama A, Frappier L, Mechali M. 2011. MCM-BP regulates unloading of the MCM2-7 helicase in late S phase. Genes Dev. 25(2): 165-175.

Oh YM, Yoo SJ, Seol JH. 2007. Deubiquitination of Chfr, a checkpoint protein, by USP7/HAUSP regulates its stability and activity. Biochem Biophys Res Commun. 357(3): 615-619.

Otwinowski Z, Minor W. 1997. Processing of X-ray diffraction data collected in oscillation mode. Methods Ezymol. 276: 307-326.

Planchon SM, Waite KA, Eng C. 2008. The nuclear affairs of PTEN. J Cell Sci. 121: 249-253.

Privette LM, Petty EM. 2008. CHFR: a novel mitotic checkpoint protein and regulator of tumorigenesis. Trans Onc. 1(2): 57-64.

The PyMOL Molecular Graphics System, Version 1.2r3pre, Schrödinger, LLC.

Sakwe AM, Nguyen T, Athanasopoulos V, Shire K, Frappier L. 2007. Identification and characterization of a novel component of the human minichromosome maintenance complex. Mol Cell Biol. 27(8): 3044-3055.

Saridakis V, Sheng Y, Sarkari F, Holowaty MN, Shire K, Nguyen T, Zhang RG, Liao J, Lee W, Edwards AM, et al. 2005. Structure of the p53 binding domain of HAUSP/USP7 bound to Epstein-Barr Nuclear Antigen 1: implications for EBV-mediated immortalization. Mol Cell. 18(1): 25-36.

Sarkari F, La Delfa A, Arrowsmith CH, Frappier L, Sheng Y, Saridakis V. 2010. Further insight into substrate recognition by USP7: structural and biochemical analysis of the HdmX and Hdm2 interactions with USP7. J Mol Biol. 402(5):825-37.

Sarkari F, Wheaton K, La Delfa A, Mohamed M, Shaikh F, Khatun R, Arrowsmith CH, Frappier L, Saridakis V, Sheng Y. 2013. USP7/HAUSP is a regulator of UbE2E1/UbcH6. J Biol Chem. [Epub ahead of print]

Schneider-Poetsch T, Ju J, Eyler DE, Dang Y, Bhat S, Merrick WC, Green R, Shen B, Liu JO. 2010. Inhibition of eukaryotic translation elongation by cycloheximide and lactimidomycin. Nat Chem Biol. 6(3): 209-217.

Sheng Y, Saridakis V, Sarkari F, Duan S, Wu T, Arrowsmith CH, Frappier L. 2006. Molecular recognition of p53 and MDM2 by USP7/HAUSP. Nat Struct Mol Biol. 13(3): 285-291.

Smyth MS, Martin JHJ. 2000. X-ray crystallography. Mol Pathol. 53: 8-14

Song MS, Salmena L, Carracedo A, Egia A, Lo-Coco F, Teruya-Feldstein J, Pandolfi PP. 2008. The deubiquitinylation and localization of PTEN are regulated by a HAUSP-PML network. Nature. 455(7214): 813-817.

Sowa ME, Bennette EJ, Gygi SP, Harper JW. 2009. Defining the human deubiquitinating enzyme interaction landscape. Cell. 138(2): 389-403.

Toyota M, Sasaki Y. Satoh A, Kazuhiro O, Kikuchi T, Suzuki H, Mita H, Tanaka N, Itoh F, Issa JJ, et al. 2003. Epigenetic inactivation of CHFR in human tumors. Proc Natl Acad Sci. 100(13): 7818-7823.

van der Knaap JA, Kumar BRP, Moshkin YM, Langenberg K, Krijgsveld J, Heck AJR, Karch F, Verrijzer CP. 2005. GMP Synthetase stimulates histone H2B deubiquitylation by the epigenetic silencer USP7. Mol Cell. 17(5): 695–707.

van Lint AL, Murawski MR, Goodbody RE, Severa M, Fitzgerald KA, Finberg RW, Knipe DM, Kurt-Jones EA. 2010. Herpes simplex virus immediate-early ICP0 protein inhibits toll-like receptor 2-dependent inflammatory responses and NF-κB signaling. J Virol. 84(20): 10802-10811.

Vijay-Kumar S, Bugg CE, Cook WJ. 1987. Structure of ubiquitin refined at 1.8Å resolution. J Mol Biol. 194: 531-544.

Ye Y, Rape M. 2009. Building ubiquitin chains: E2 enzymes at work. Nat Rev Mol Cell Biol. 10(11): 755-764.

You J, Pickart CM. 2001. A HECT domain E3 enzyme assembles novel polyubiquitin chains. J Biol Chem. 276: 19871-19

APPENDIX A

Molecular and Cellular Biology

A Role for USP7 in DNA Replication

Madhav Jagannathan, Tin Nguyen, David Gallo, Niharika Luthra, Grant W. Brown, Vivian Saridakis and Lori Frappier
Mol. Cell. Biol. **2014, 34(1):132. DOI: 10.1128/MCB.00639-13.**
Published Ahead of Print 4 November 2013.

MCB
Journals.ASM.org

A Role for USP7 in DNA Replication

Madhav Jagannathan,[a] Tin Nguyen,[a] David Gallo,[b] Niharika Luthra,[c] Grant W. Brown,[b] Vivian Saridakis,[c] Lori Frappier[a]

Department of Molecular Genetics, University of Toronto, Toronto, Canada[a]; Department of Biochemistry and Donnelly Centre, University of Toronto, Toronto, Canada[b]; Department of Biology, York University, Toronto, Canada[c]

The minichromosome maintenance (MCM) complex, which plays multiple important roles in DNA replication, is loaded onto chromatin following mitosis, remains on chromatin until the completion of DNA synthesis, and then is unloaded by a poorly defined mechanism that involves the MCM binding protein (MCM-BP). Here we show that MCM-BP directly interacts with the ubiquitin-specific protease USP7, that this interaction occurs predominantly on chromatin, and that MCM-BP can tether USP7 to MCM proteins. Detailed biochemical and structure analyses of the USP7–MCM-BP interaction showed that the ^{155}PSTS^{158} MCM-BP sequence mediates critical interactions with the TRAF domain binding pocket of USP7. Analysis of the effects of USP7 knockout on DNA replication revealed that lack of USP7 results in slowed progression through late S phase without globally affecting the fork rate or origin usage. Lack of USP7 also resulted in increased levels of MCM proteins on chromatin, and investigation of the cause of this increase revealed a defect in the dissociation of MCM proteins from chromatin in mid- to late S phase. This role of USP7 mirrors the previously described role for MCM-BP in MCM complex unloading and suggests that USP7 works with MCM-BP to unload MCM complexes from chromatin at the end of S phase.

The faithful replication of eukaryotic genomes relies on the complex interplay of multiple factors. Starting with the assembly of the prereplicative complex (pre-RC) at replication origins in G_1, the coordinated loading of replication factors onto DNA and origin activation at the start of S phase result in the bidirectional progression of the replication machinery (replisome) to carry out DNA synthesis. The minichromosome maintenance (MCM) complex is a hexameric complex consisting of MCMs 2 to 7 (MCM2-7) and is an essential component of the pre-RC as well as the replisome (1). It is loaded onto DNA as double heterohexamers in G_1 phase through the concerted actions of Cdc6, Cdt1, and ORC (together, the pre-RC) (1). In eukaryotes, the MCM complex is loaded in an ~20-fold excess over the number of replication origins, with only a fraction being required for replication (2–7). At the start of S phase, phosphorylation events mediated by S-CDK (S-phase cyclin-dependent kinase) and DDK (Dbf4-dependent kinase) result in the association of the MCM complex with Cdc45 and the GINS complex (Psf1-3 and Sld5) forming an active "CMG" helicase (8–10). However, only ~10% of loaded MCM double hexamers form active CMG helicases, and the remaining "inactive" MCM complexes are thought to license dormant origins (11). During replication, these "inactive" MCM complexes pose a barrier to replication and must be removed ahead of the replication fork. While Pif1 family helicases have been implicated in this process (12–14), a mechanism for MCM complex unloading from dormant origins and from terminating replisomes at the end of S phase is not well characterized.

Proteomics experiments performed with MCM proteins in human cells revealed a strong interaction with a previously uncharacterized protein, MCM-BP (MCM binding protein), which is conserved in most eukaryotes (with the exception of budding yeast and *Caenorhabditis elegans*) (15). In human cells, we have shown that MCM-BP depletion results in altered nuclear morphology and replication stress, resulting in G_2 checkpoint activation (16). Similarly, inactivation or loss of the MCM-BP homologues in *Schizosaccharomyces pombe* (Mcb1) and *Arabidopsis thaliana* (ETG1) resulted in defects in DNA replication and G_2 checkpoint activation (17–20). MCM-BP may contribute to DNA replication in multiple ways. For example, studies in *S. pombe* support a role for MCM-BP in pre-RC formation (21), and the interaction of human MCM-BP with Dbf4 also suggests a role for MCM-BP at the onset of S phase (22). In addition, a role for MCM-BP in unloading MCM complexes from chromatin at the end of S phase was identified using the *Xenopus* egg extract system, where MCM-BP depletion resulted in increased levels of MCM proteins on chromatin in mid- to late S phase and MCM-BP was shown to disrupt MCM complexes (23). Similar observations were subsequently made for MCM-BP in human cells (16, 22, 23). However, the mechanism by which MCM-BP regulates MCM complex unloading is unclear.

A putative interaction between MCM-BP (also called C10orf119) and the deubiquitylating enzyme USP7 was identified from a proteomic screen of ~100 deubiquitylating enzymes in human cells (24). USP7 (also called HAUSP) was originally discovered as a binding partner of the ICP0 protein of herpes simplex virus and was subsequently shown to be targeted by several viral proteins from different DNA viruses (25–31). USP7 has multiple roles in the cell that impact oncogenesis in a variety of ways (32). For example, USP7 regulates the p53 pathway by binding either p53, MDM2, or MDMX through its N-terminal TRAF domain and cleaving polyubiquitin chains from them with its central catalytic domain (33–38). In addition to cleaving polyubiquitin chains, USP7 reverses the monoubiquitylation of FOXO4 and PTEN, thereby regulating their localization (39, 40). Similarly, USP7, in complex with GMP synthetase, removes monoubiquitin

Received 23 May 2013 Returned for modification 14 June 2013
Accepted 25 October 2013
Published ahead of print 4 November 2013
Address correspondence to Lori Frappier, lori.frappier@utoronto.ca.

doi:10.1128/MCB.00639-13

from histone H2B, impacting gene expression (41, 42). Finally, USP7 can also affect cellular processes independent of its catalytic activity, since its role in regulating the levels of promyelocytic leukemia (PML) proteins and nuclear bodies was shown to involve only its protein interaction domains (43).

In this work, we investigated the interaction between MCM-BP and USP7 and its functional significance. We showed that MCM-BP and USP7 interact directly, and we defined the mechanism of this interaction. We also demonstrated that USP7 functions in DNA replication, and we present evidence that USP7 acts in unloading MCM complexes from chromatin in late S phase in conjunction with MCM-BP.

MATERIALS AND METHODS

Cell lines. HeLa cells were maintained in Dulbecco's minimal essential medium (DMEM) (Gibco) supplemented with 10% fetal bovine serum (FBS). The colon carcinoma HCT116 cell line was obtained from Daniel Durocher and maintained in alpha minimal essential media (Gibco) supplemented with 10% fetal bovine serum. USP7-null HCT116 cells were obtained from Bert Vogelstein and cultured as for HCT116 cells.

RNAi and plasmids. For RNA interference (RNAi) against USP7, we synthesized a previously characterized small interfering RNA (siRNA) targeting USP7 (5′CCCAAATTATTCCGCGGCAAA3′) using Sigma Genosys (44). AllStars negative-control siRNA was obtained from Qiagen. MCM-BP was depleted using short hairpin RNA (shRNA) (corresponding to shMCM-BP1 in the work of Jagannathan et al. [16]) expressed from pRS, which contains a puromycin resistance cassette. For experiments involving MCM-BP transient expression, we first generated pCMV3FC by excising the yellow fluorescent protein (YFP) tag from pEYFP-N1 (Clontech) with BamHI and NotI and replacing it with a triple FLAG tag. MCM-BP was PCR amplified from pMZS3F MCM-BP (16) and subcloned between the SalI and XbaI sites in pCMV3FC. To generate the MCM-BP S158A point mutant, PCR-mediated site-directed mutagenesis was performed on MCM-BP in pCMV3FC using the primer 5′ GTCAGT CCCTCAACAGCCTACACTCCTAGTC 3′.

Antibodies. Antibodies used in this work targeted MCM2 (9839; Santa Cruz), MCM3 (9850; Santa Cruz), MCM4 (22779; Santa Cruz), MCM5 (165993; Santa Cruz), MCM6 (9843; Santa Cruz), MCM7 (22782; Santa Cruz), Flag M2 (Sigma), ECS/DDDDK (A190-102A; Bethyl), bromodeoxyuridine (BrdU)-fluorescein isothiocyanate (FITC) (556028; BD Pharmingen), actin (1616; Santa Cruz), USP7 (A300-033A; Bethyl), Psf2 (16247-1-AP; Proteintech), histone H3 (A300-823A; Bethyl), MEK2 (A302-141A; Bethyl), and MCM-BP (A303-477A; Bethyl). The antibody used to immunoprecipitate MCM-BP has been described previously (15), and FLAG-tagged proteins were immunoprecipitated using FLAG M2 resin (Sigma). All secondary antibodies were obtained from Santa Cruz Biotechnology.

Transfections. Transfections were performed using Lipofectamine 2000 (Invitrogen) according to the manufacturer's protocol. For USP7 silencing, 0.25×10^6 HeLa cells were transfected with 100 pmol Allstars negative-control or USP7-targetting siRNA at time of plating and every 24 h subsequently for a total of 4 separate transfections. Cells were harvested by trypsinization at 144 h after initial transfection. For MCM-BP silencing, 0.5×10^6 to 1.0×10^6 HeLa cells were transfected with 6 μg pRS plasmid expressing shMCM-BP1 (or empty pRS as a negative control). Forty-eight hours later, puromycin was added to a final concentration of 2.5 μg/ml, and cells were grown under selection for 3 days prior to harvesting. For transient expression of MCM-BP and MCM-BP S158A, 1.0×10^6 HeLa cells were transfected with 6 μg of plasmid and harvested 48 h later.

Cell fractionation. Transfected cells were fractionated into soluble and chromatin-bound fractions as described previously (15, 16). Briefly, 2×10^6 cells were resuspended in 150 μl hypotonic lysis buffer (10 mM HEPES [pH 7.9], 10 mM KCl, 1.5 mM $MgCl_2$, 0.34 M sucrose, 10% glycerol, and 0.1% Triton X-100), and after 15 min on ice, the lysate was subjected to centrifugation at 1,300 × *g* for 5 min. The supernatant comprising the soluble protein fraction was removed, and the pellet was washed with the same buffer. Chromatin-associated proteins were released from the pellet using either 150 μl buffer with micrococcal nuclease (Sigma) (0.2 U/ml for 1 min at 37°C) or 150 μl protein sample buffer. Thirty micrograms of the soluble fraction from each sample was analyzed by Western blotting. For the chromatin-associated fraction of each sample, a volume equivalent to that used for the soluble fraction was analyzed by Western blotting. Total cell extracts were prepared by sonicating cells in 9 M urea in 50 mM Tris (pH 6.8) for 15 s at 50% amplitude, and 30 μg of each sample was analyzed by Western blotting.

Coimmunoprecipitation. For immunoprecipitation (IP) from whole-cell extracts, HeLa cells were lysed with 6 volumes of 50 mM Tris, pH 8.0, 150 mM NaCl, 5% glycerol, 2 mM EDTA, and 0.1% Triton X-100 on ice for 30 to 60 min, sonicated at low amplitude for 10 s, and clarified by centrifugation at 15,000 rpm for 10 min. The lysate (1 mg) was incubated with specific antibody against MCM-BP (described in reference 16) overnight at 4°C. Thirty microliters protein A/G-agarose (Sc-2003; Santa Cruz Biotechnology Inc.) was then added for 2 h, and the resin was washed three times with lysis buffer, resuspended in SDS sample buffer, and analyzed by SDS-PAGE and Western blotting. For IP from fractionated HeLa cells, fractions were incubated with specific antibody against MCM-BP followed by protein A/G-agarose as described above. For FLAG IP, HeLa cells were transfected with pMZS3F-LacZ (16) or pCMV3FC expressing MCM-BP or the MCM-BP S158A mutant. Harvested cells were lysed 48 h later as described above, and the lysate was incubated with FLAG M2 resin (Sigma) overnight at 4°C. The resin was washed three times with lysis buffer, resuspended in SDS samples buffer, and analyzed by SDS-PAGE and Western blotting.

Cell synchronization. HeLa cells were transfected with siRNA as described above. Twenty-four hours after the final transfection, thymidine (Sigma) was added to cells to a final concentration of 2 mM for 19 h, followed by two washes in phosphate-buffered saline (PBS) and release into complete DMEM for 10 h. Thymidine was added again to the cells to a final concentration of 2 mM for 17 h, and cells were either harvested directly or released into complete medium for the indicated times.

Flow cytometry. For DNA content analysis, cells were fixed in 70% ethanol overnight at −20°C, washed with PBS with 0.5% bovine serum albumin (BSA), treated with 100 μg/ml RNase A for 1 h at 37°C, and stained with 50 μg/ml propidium iodide. All samples were analyzed using a FACSCalibur flow cytometer (BD Biosciences), and data were collected using CellQuest software. Cell cycle analysis was performed using FlowJo software (Treestar Inc.). For BrdU pulse experiments, HCT116 wild-type (WT) and USP7-null cells were pulsed with 10 μg/ml BrdU for 30 min. The labeled cells were washed twice with PBS and either harvested and fixed or released into BrdU-free complete medium for the indicated times before harvesting and fixation in 70% ethanol overnight at −20°C. DNA was denatured using 2 N HCl at room temperature for 30 min. BrdU was detected using FITC-conjugated anti-BrdU antibody (BD Pharmingen), while DNA was stained with 50 μg/ml propidium iodide.

Expression of MCM-BP proteins in insect cells. Baculoviruses expressing WT or S158A MCM-BP proteins fused to an N-terminal hexahistidine tag were generated using the pFastBacHT system. The MCM-BP proteins were expressed and purified from High Five insect cells as described previously (15).

Purification of His-tagged USP7 proteins for protein interactions. Full-length USP7 was expressed in High Five insect cells and purified using the hexahistidine tag as previously described (45). USP7 fragments coding for amino acids 1 to 205, 1 to 540, and 202 to 540 were PCR amplified and cloned between the NdeI and BamHI sites of pET15b (Novagen). Proteins were expressed in BL21(DE3)pLysS cells after overnight induction with 0.5 mM isopropyl-β-D-thiogalactopyranoside (IPTG) at 18°C. Cells were lysed by sonication in 50 mM Tris, pH 8.0, 500 mM NaCl, 20 mM imidazole, 5% glycerol containing 0.25% Triton X-100, 0.25% 3-[(3-cholamidopropyl)-dimethylammonio]-1-propanesulfonate (CHAPS),

and protease inhibitor cocktail (8340; Sigma). The lysates were clarified by centrifugation for 30 min in an SS34 Sorvall rotor at 15,000 rpm. Clarified lysates were incubated with nickel-nitrilotriacetic acid (Ni-NTA) resin (Qiagen) for 1 h, and after extensive washing with loading buffer lacking detergent, the His-tagged proteins were eluted with 250 mM imidazole and dialyzed against 50 mM Tris, pH 8.0, 150 to 200 mM NaCl, 5% glycerol, 0.1 mM EDTA, and 0.1 mM dithiothreitol (DTT).

Expression and purification of GST-USP7 fragments. USP7 fragments coding for amino acids 1 to 205 (UPS7 1–205), 1 to 540 (USP7 1–540), 1 to 560 (USP7 1–560), 560 to 1102 (UPS7 560–1102), 202 to 560 (USP7 202–560), and 1 to 560 with the D164A and W165A mutations (USP7 1–560 DW) were PCR amplified and cloned between the NdeI and BamHI sites of a modified pGEX-2TK vector (a gift from Yi Sheng). Proteins were expressed in BL21(DE3)pLysS cells after overnight induction with 0.5 mM IPTG at 18°C. Cells were lysed by sonication in PBS containing 1% Triton X-100 and protease inhibitor cocktail (Sigma). The lysates were clarified by centrifugation for 30 min in an SS34 Sorvall rotor at 15,000 rpm. Clarified lysates were incubated with glutathione-agarose (Pierce, Thermo Scientific) for 1 h, and after extensive washing with PBS lacking detergent, the glutathione *S*-transferase (GST)-tagged proteins were eluted with 20 mM glutathione and dialyzed against 50 mM Tris, pH 8.0, 150 to 200 mM NaCl, 5% glycerol, 0.1 mM EDTA, and 0.1 mM DTT. The USP7 1-560 DW mutant was subcloned by PCR amplification from full-length USP7 with D164A and W165A mutations in pCAN (a gift from Yi Sheng [46]).

Gel filtration analysis of MCM-BP–USP7 interactions. Purified MCM-BP (70 μg) was incubated with equimolar amounts of purified his-tagged USP7 fragments for 30 min on ice in 500 μl of 50 mM Tris, pH 8.0, 150 mM NaCl, and 5% glycerol and then loaded on a 10/300 GL Superose 6 column (GE Healthcare) and developed in the same buffer. Forty-eight 500-μl fractions were collected, and 35 μl of each fraction was analyzed by SDS-PAGE and Coomassie staining.

Analysis of MCM-BP interactions with GST-USP7 fusion proteins. Purified GST-USP7 fusion protein (1 nmol) was bound to 30 μl of glutathione-agarose in PBS, and then 1 nmol of purified MCM-BP (70 μg) in 500 μl of 50 mM Tris, pH 8.0, 150 mM NaCl, and 5% glycerol was incubated with the resin for 1 h at 4°C. Unbound proteins were removed with four 500-μl washes in loading buffer, and bound proteins were eluted with two 40-μl incubations in the same buffer containing 25 mM glutathione. One-tenth of the first wash (flowthrough) and 100% of both elutions were analyzed by SDS-PAGE and Coomassie staining.

Expression and purification of USP7 54–205 for crystallization. USP7 fragment 54–205 was expressed from pET15b in *Escherichia coli* BL21(DE3) cells and purified by virtue of the hexahistidine tag as described previously (45). Briefly, the cells were lysed by sonication in 50 mM Tris (pH 7.5), 500 mM NaCl, 10 mM imidazole, 1 mM benzamidine, and 0.5 mM phenylmethylsulfonyl fluoride (PMSF), and the clarified lysate was incubated with Ni-NTA beads (Qiagen). After extensive washing with 50 mM Tris (pH 7.5), 500 mM NaCl, and 30 mM imidazole, protein was eluted with 50 mM Tris (pH 7.5), 500 mM NaCl, and 250 mM imidazole. The His tag was cleaved using thrombin, and USP7 54–205 was further purified by size exclusion chromatography using a Sephacryl S200 16/60 column on a purifier 10 UPC system (GE Healthcare).

Crystallization and structure determination of USP7–MCM-BP complex. USP7 54–205 (100 mg/ml) was cocrystallized with 5-fold-excess MCM-BP (^{152}RVSPSTSYTP^{161}) peptide (synthesized by CanPeptide Inc., with amino-terminal acetylation and carboxy-terminal amidation) using microseeding with USP7-HdmX^{AHSS} crystals (38). The crystals appeared after several days at 4°C in the dark in 30% polyethylene glycol (PEG) 4000, 0.1 M Tris (pH 8.5), and 0.2 M lithium sulfate in crystallization tools (Qiagen). Diffraction data from a frozen USP7–MCM-BP complex crystal was collected at 100 K on a Rigaku MicroMax007 rotating anode diffractometer with a Saturn 944+ charge-coupled-device (CCD) detector. The space group was $P4_1$ with $a = b = 70.0$ Å and $c = 45.7$ Å unit cell parameters. All of the diffraction data were integrated and scaled using the HKL2000 software program (47). The data collection statistics are shown in Table 1. Molecular replacement was used to determine the structure using the CNS program (version 1.3) with USP7 54-205 (PDB identifier [ID] 1YY6) as the search model without any peptide (48). The molecular graphics program O was used for electron density visualization and model building (49). Rigid body, simulated annealing torsion angle, and individual B-factor refinement were performed using CNS 1.3. Several rounds of refinement were combined with model rebuilding in O after inspection of both $2F_o$-F_c and F_o-F_c maps. Water molecules were picked using CNS 1.3 and manually verified. The refinement statistics are shown in Table 1. The figure was prepared using the software program Pymol.

TABLE 1 X-ray data collection and refinement parameters[a]

Parameter[a]	Value for USP7–MCM-BP[b]
X-ray data	
Space group	$P4_1$
Resolution (Å)	50.0–1.70
Unit cell axes (Å^3)	69.8 × 69.8 × 45.7
Molecules/AU	1
No. of total observations	267,608
No. of unique reflections	22,977
Intensity ($I/\sigma<I>$)	21.9 (1.6)
Completeness (%)	94.3 (80.1)
R_{sym}[c]	0.066 (0.509)
Refinement	
R_{work}	0.207
R_{free}	0.233
No. of protein atoms	1,146
No. of water molecules	130
RMSD, bonds (Å)	0.006
RMSD, angles (°)	1.3
RMSD, dihedrals (°)	25.3
RMSD, improper (°)	0.87
Thermal factors (Å^2)	19.6
Ramachandran plot	
Most favored	0.891
Additionally allowed	0.109

[a] RMSD, root mean square deviation; AU, arbitrary units.
[b] Numbers in parentheses refer to the highest-resolution shell, 1.73 Å to 1.70 Å.
[c] $R_{sym} = \Sigma|I - <I>|/\Sigma I$, where "$I$" is the observed intensity and "$<I>$" is the average intensity from multiple observations of symmetry-related reflections.

Assay of USP7 interaction with MCM5 and MCM7. High Five insect cells in a 15-cm plate were coinfected with baculovirus expressing WT or S158A MCM-BP proteins and FLAG-tagged MCM5 or MCM7 as described previously (22). Some of the infections also included baculovirus expressing full-length USP7. Cells were lysed 3 days postinfection in 1 ml of 50 mM Tris, pH 8.0, 150 mM NaCl, 5% glycerol, 2 mM EDTA, and 0.1% Triton X-100 on ice for 30 min. Lysates were clarified by centrifugation at 13,000 rpm for 10 min and then incubated with 25 μl FLAG-M2 Resin (Sigma) for 1 h at 4°C. The resin was washed three times with 1 ml of lysis buffer, and then proteins were eluted with sample buffer containing 2% SDS, analyzed by SDS-PAGE, and stained with Coomassie blue.

Assay of USP7 ubiquitin cleavage activity. Purified USP7 (0.2 μg) was incubated with purified MCM-BP (0 to 4.0 μg) in 5 μl of the reaction buffer (40 mM Tris-HCl (pH 8.0), 100 mM NaCl, 2 mM EDTA, 10 mM DTT) on ice for 30 min and then at 37°C for 10 min. At the same time, the 3 μg of K48-linked diubiquitin substrate (catalogue no. UC-200; Boston Biochem) in 5 μl of reaction buffer was incubated at 37°C for 10 min. The reaction was started by combining the USP7 and diubiquitin samples and quenched with sample buffer after a 10-min incubation. Products were

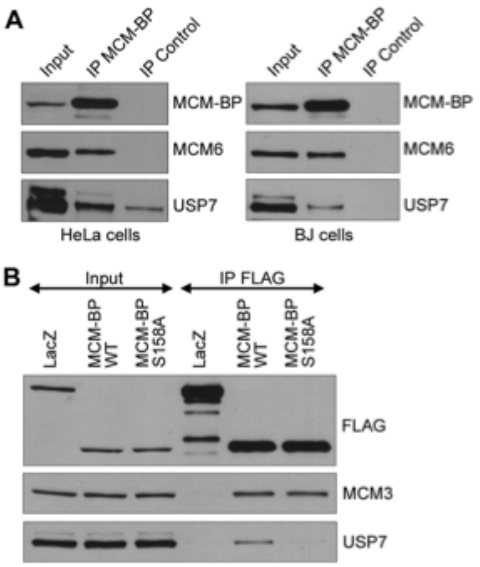

FIG 1 Coimmunoprecipitation of USP7 with MCM-BP. (A) Equal amounts of whole-cell extracts from HeLa cells or BJ cells were incubated with antibody against MCM-BP or nonspecific IgG (control). Immunoprecipitants were analyzed by Western blotting against the indicated proteins. Note that USP7 is known to run as a doublet due to the presence of two isoforms (69). (B) HeLa cells were transfected with FLAG-LacZ, FLAG–MCM-BP, and FLAG–MCM-BP S158A expression plasmids and 48 h later were subjected to anti-FLAG immunoprecipitation. Western blots for the indicated proteins are shown for the immunoprecipitates (IP FLAG) and the starting cell lysates (5% input).

analyzed by SDS-PAGE on NuPAGE Novex 4 to 12% Bis-Tris gels (Invitrogen), followed by Coomassie blue staining.

Molecular combing. Molecular combing of DNA fibers was performed as previously described (50) with the following exceptions. Cells were cast into 1% low-melting-grade agarose plugs to a final concentration of 2.5×10^6. Agarose plugs were melted in two steps at 74°C. At least 70 interorigin distances and 130 fork rates were measured per experiment, and reported values are pooled distributions for 2 independent replicates.

Protein structure accession number. Coordinates and structure factors for the USP7–MCM-BP structure have been deposited in the RCSB PDB under PDB identifier (ID) 4KG9.

RESULTS

MCM-BP binds directly to the USP7 TRAF domain. A genome-wide study of protein interactions with human deubiquitylating enzymes detected an interaction between USP7 and MCM-BP (called C10orf119) in 293 cells (24). To determine if this interaction could be verified by other methods and in other cell lines, we immunoprecipitated endogenous MCM-BP from HeLa cells and BJ primary fibroblasts and examined recovery of USP7. Immunoprecipitated MCM-BP consistently recovered USP7 from both cell lines at levels above that seen with nonspecific IgG (Fig. 1A). As expected, MCM6 was also recovered with MCM-BP, serving as a positive control.

Having verified the USP7–MCM-BP interaction, we next asked whether this interaction was direct. To this end, human MCM-BP and USP7 (shown in Fig. 2A) were expressed and purified from insect cells and analyzed by gel filtration individually and after combining them at equal molar concentrations. As expected, the migration of MCM-BP on its own was slower than that of USP7 due to its smaller size (Fig. 2B, top 2 panels). When the two proteins were combined, a significant proportion of both proteins comigrated at a faster-migrating position, consistent with the formation of a complex (Fig. 2B, bottom panel). This interaction also occurred when the same assay was performed using MCM-BP and the N-terminal half of USP7 (1–540) containing both the TRAF and catalytic domains (Fig. 2A), as evidenced by their size shift (relative to individual proteins) and comigration (Fig. 2C).

We further investigated the requirements for the USP7 TRAF and catalytic domains for MCM-BP binding, initially by repeating the gel filtration analyses with USP7 fragments containing either the N-terminal TRAF domain (1–205) or the catalytic domain (202–540). However, neither of these USP7 fragments caused an obvious shift in the migration of MCM-BP (Fig. 2D and E), suggesting that stable complex formation involved interactions with both USP7 domains. We then investigated whether these domains individually mediate transient interactions with MCM-BP using a GST pulldown assay, which can detect more transient interactions than gel filtration. In this assay, purified USP7 domains linked to GST were immobilized on glutathione resin and then incubated with purified full-length MCM-BP and eluted with glutathione (Fig. 3). Consistent with the gel filtration analysis, MCM-BP was retained on the resin by USP7 1–540 or UPS7 1–560 (Fig. 3E and F) but not by the USP7 catalytic domain (Fig. 3C) or GST alone (Fig. 3A). However, in this assay, some interaction of MCM-BP with USP7 1–205 was detected (Fig. 3B), suggesting that MCM-BP interacts weakly with the USP7 TRAF domain and that this interaction is stabilized by additional contacts with the catalytic domain. We also detected some weak binding to the USP7 C-terminal half (560 to 1102) (Fig. 3D). Other proteins that bind the USP7 TRAF domain do so through a binding pocket that involves contacts with D164 and W165 (28, 36, 38). To further examine the importance of TRAF domain contacts for MCM-BP binding to USP7 1–560, we repeated the GST pulldown assays with USP7 1–560 containing the D164A and W165A point mutations (Fig. 3G). These mutations abrogated the interaction with MCM-BP, confirming the importance of the TRAF binding pocket.

We have previously identified a P/AxxS consensus sequence that mediates the interaction of p53, Mdm2, and MdmX with the USP7 TRAF binding pocket (28, 36, 38). There are five putative P/AxxS motifs in MCM-BP (^{135}PGES^{138}, ^{155}PSTS^{158}, ^{266}PVLS^{269}, ^{299}PPAS^{302}, and ^{397}PRNS^{400}), but ^{155}PSTS^{158} was the only one that exactly matched known USP7 binding sequences (^{156}PSTS^{159} and ^{397}PSTS^{400} from Mdm2) and therefore seemed most likely to mediate the USP7 interaction. To test the importance of ^{155}PSTS^{158} for USP7 binding, we generated MCM-BP with an S158A point mutation and tested its ability to bind USP7 in the gel filtration assay (Fig. 2F) and USP7 1–560 in the GST pulldown assay (Fig. 3H). In both cases, this mutation greatly decreased the interaction with MCM-BP relative to that seen with the WT protein, indicating that this PxxS motif is part of the USP7 binding sequence. This result further supports the importance of the TRAF domain contacts for the MCM-BP–USP7 interaction. Finally, we verified that S158 is important for MCM-BP binding to USP7 by expressing FLAG-tagged WT or S158A versions of MCM-BP in HeLa cells, recovering the tagged protein with anti-FLAG resin, and blotting

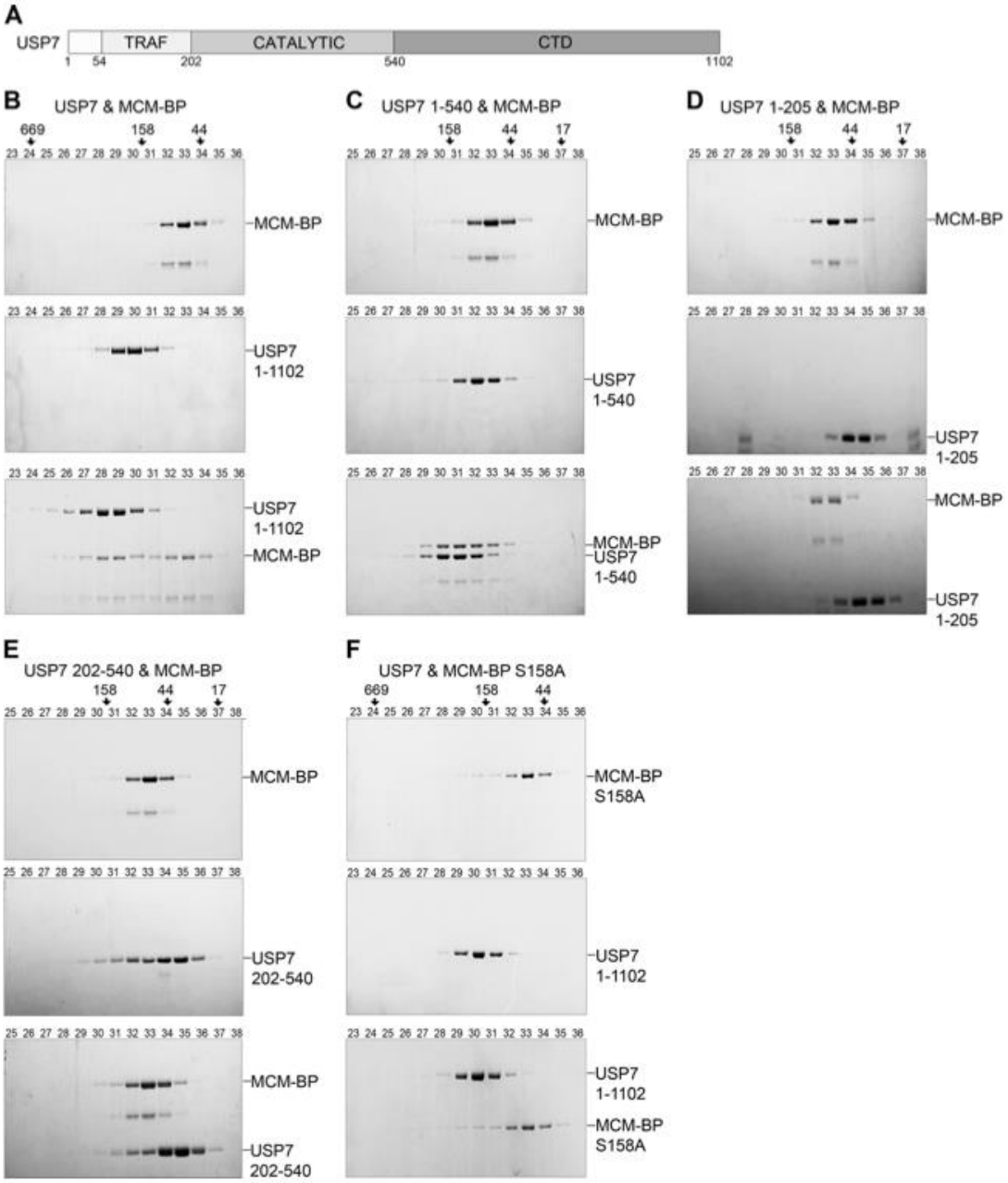

FIG 2 Gel filtration analyses of USP7–MCM-BP complexes. (A) Schematic representation of the domain organization of USP7, showing amino acid numbers. (B to E) Purified MCM-BP was incubated with equimolar quantities of purified full-length USP7 (B), USP7 1–540 (C), USP7 1–205 (D), or USP7 202–540 (E). In panel F, purified MCM-BP S158A was incubated with an equimolar quantity of purified full-length USP7. All protein mixtures were run through a Suparose gel filtration column, and equal-volume fractions were collected. Equal volumes of each of the indicated fractions were then analyzed by SDS-PAGE and Coomassie staining. The positions of the gel filtration standards myoglobin (17 kDa), ovalbumin (44 kDa), aldolase (158 kDa), and thyroglobulin (669 kDa) on the same column are indicated at the top of each panel.

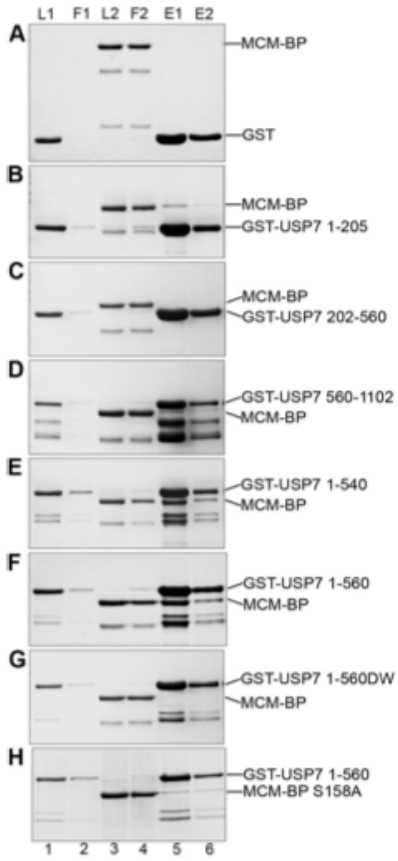

FIG 3 GST pulldown assays of USP7–MCM-BP interactions. Purified MCM-BP was incubated with equimolar quantities of purified GST (A), GST-USP7 1–205 (B), GST-USP7 202–560 (C), GST-USP7 560–1102 (D), GST-USP7 1–540 (E), GST-USP7 1–560 (F), or GST-USP7 1–560 DW (G) that was immobilized on glutathione-agarose beads. In panel H, MCM-BP S158A was incubated with an equimolar quantity of purified GST USP7 1–560. Input and 1/10 flowthrough for GST-tagged proteins are indicated by L1 and F1, respectively. Input and 1/10 flowthrough for MCM-BP/MCM-BP S158A are indicated by L2 and F2, respectively. Bound proteins were eluted with two glutathione incubations (E1 and E2) and analyzed by SDS-PAGE and Coomassie staining.

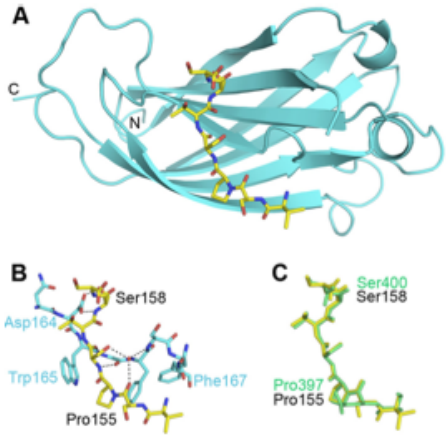

FIG 4 Crystal structure of USP7 54–205 bound to MCM-BP peptide ^{152}RVSPSTSYTP^{161}. (A) Ribbon representation of USP7 54–205 (cyan) bound to the MCM-BP peptide, shown in stick representation (yellow). PDB ID 4KG9. (B) Detailed interactions of MCM-BP (yellow), with β-strand 7 of USP7 54–205 (cyan) shown in stick representation. The hydrogen bonds are shown with black dashed lines. (C) Overlay of MCM-BP peptide (yellow) with Mdm2 ^{396}QPSTSS^{401} peptide (green) from previously determined Mdm2-USP7 structure (38).

for USP7. As shown in Fig. 1B, USP7 was recovered with the WT but not with the S158A version of MCM-BP. Importantly, both versions of MCM-BP recovered MCM3 equally, showing that the S158A mutation did not cause misfolding of MCM-BP.

Crystal structure of USP7 TRAF domain with the MCM-BP peptide. The molecular mechanism of the interaction between USP7 and MCM-BP was further examined by cocrystallizing the USP7 TRAF domain with the MCM-BP ^{152}RVSPSTSYTP^{161} peptide and determining the structure by molecular replacement (Fig. 4A). As previously reported, this USP7 domain is an eight-stranded antiparallel beta sandwich closely resembling TRAF domains in other proteins (28, 36). The MCM-BP peptide binds within a groove on the surface of the TRAF domain in proximity to strand β7. The final model of the complex was refined to an R_{work} of 0.206 and an R_{free} of 0.231 at 1.7-Å resolution with 130 water molecules. Residues 54 to 62 and 106 to 111 are disordered and were not built into the final model of the complex. The MCM-BP peptide forms several interactions with the USP7 β-strand 7 (Fig. 4B). MCM-BP S158 makes the most contacts with USP7 54–205 by forming H bonds with D164. MCM-BP residues V153, S154, and Y159 were also modeled but do not form any direct contacts with USP7 54–205. The electron density for the remainder of the peptide is disordered and cannot be modeled. Comparison of the MCM-BP peptide (^{154}VPSTSY^{159}) to the Mdm2 ^{396}QPSTSS^{401} peptide bound to the USP7 TRAF domain (38) indicated that the two peptides were superimposable over the six C_α atoms with a root mean square deviation of 0.1 Å^2 (Fig. 4C). However, unlike the Mdm2 peptide, which has water-mediated contacts with USP7 outside the PSTS sequence, contacts of the MCM-BP peptide with the USP7 TRAF domain were limited to the PSTS sequence.

A role for USP7 in the S/G_2 transition. Since MCM-BP is known to function in DNA replication, the interaction of USP7 with MCM-BP suggests that USP7 might also affect DNA replication. We examined this possibility using the HCT116 USP7 knockout cells generated previously (33). These cells are known to have a longer G_1 phase, presumably due to high p53 levels (33), but their progression through S phase has not been examined previously. We compared the S-phase progression of WT and USP7-null HCT116 cells by pulse labeling log-phase cells with BrdU and following the change in the cell cycle profile of BrdU-incorporated cells over time by fluorescence-activated cell sorting (FACS) (Fig. 5A). The two cell lines were found to progress through early and mid-S phase at similar rates, but differences

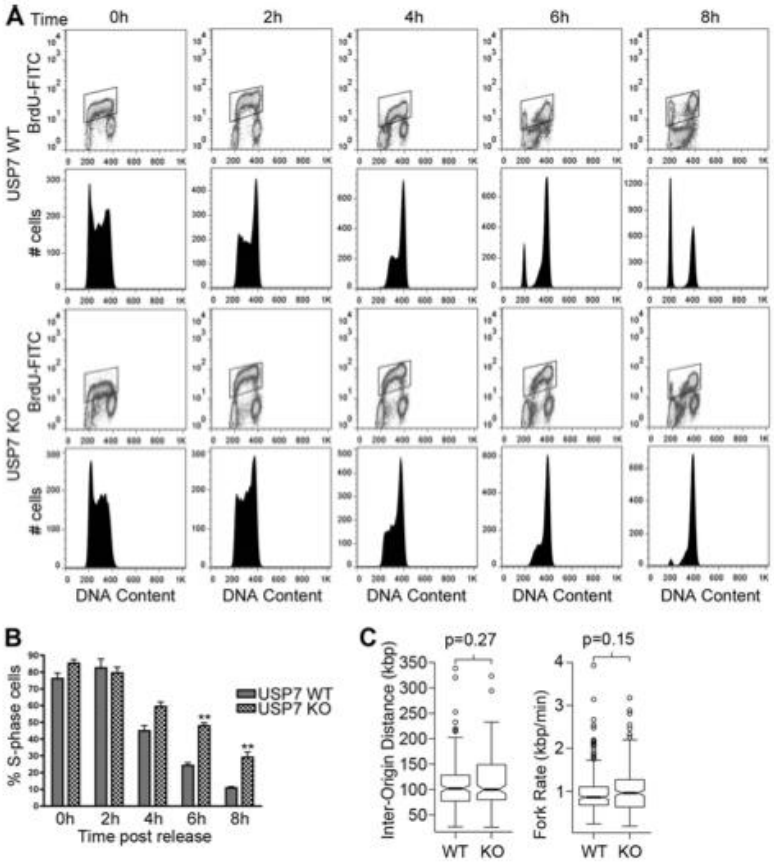

FIG 5 USP7 affects progression through late S phase. (A) WT and USP7-null cells were pulsed with BrdU and chased in the absence of BrdU for the indicated times. The DNA content of BrdU-positive cells was measured by flow cytometry at each time point. For each sample, the polygon in the top panel shows BrdU-incorporated cells, while the bottom panel shows cell phase distribution as determined by DNA content. (B) The percentages of S phase cells from three independent experiments performed as for panel A were determined using FlowJo software (Treestar Inc.) and graphed. Error bars represent standard deviations, and "**" represents $P < 0.01$. (C) Distributions of interorigin distance (IOD) and replication fork progression were obtained by DNA combing in USP7-null (KO) and WT HCT116 cells. Median values for IOD are 102 kbp (WT) and 100 kbp (KO). Median values for the fork rate are 0.86 kbp/min (WT) and 0.96 kbp/min (KO). *P* values were determined by a two-tailed Mann-Whitney U test used to compare nonnormal distributions.

became apparent at the 6- and 8-h post-BrdU pulse. At these time points, the cell cycle profile indicates that USP7-null cells have more cells in late S phase, as well as an accumulation of G_2 or M cells that have not yet transitioned back to G_1. The percentage of S-phase cells from the FACS analysis were quantified from three independent experiments (Fig. 5B), confirming that the USP7-null cells had significantly more cells in S phase at the 6- and 8-h time points than the WT cells.

We further examined possible contributions of USP7 to DNA replication using molecular combing experiments to measure the replication fork rate and origin usage by examining single DNA molecules (51–53). To this end, log-phase USP7-null or WT HCT116 cells were sequentially pulse labeled with the thymidine analogues chlorodeoxyuridine (CldU) and iododeoxyuridine (IdU). DNA fibers from these cells were then stretched uniformly on glass slides, and incorporated thymidine analogues were detected by immunofluorescence microscopy using specific antibodies. From the length of fluorescent DNA tracks and the pattern of incorporation, both the rate of replication fork progression and interorigin distance were determined in two independent experiments (a schematic diagram explaining how the fork rate and interorigin distance were obtained can be found elsewhere (50)). As shown in Fig. 5C, a lack of USP7 did not have a significant effect on the rate of replication fork movement. Lack of USP7 also did not affect interorigin distance, suggesting that it does not significantly contribute to origin activation (Fig. 5C). In addition, we found no significant change in the rate of fork movement or interorigin distance after silencing USP7 in HeLa cells (data not shown). Therefore, the contributions of USP7 to DNA replication appear to be limited to late S phase.

USP7 affects MCM protein levels on chromatin. MCM-BP depletion in human cells and in *Xenopus* egg extracts results in increased levels of MCM proteins on chromatin (16, 23). Since USP7 interacts with MCM-BP, we asked whether USP7 depletion also affected MCM protein levels on chromatin. We began by comparing MCM protein levels in whole-cell extracts and in soluble and chromatin-associated fractions from WT and USP7-null HCT116 cells (Fig. 6A). Total MCM protein levels were slightly decreased in the USP7-null cells relative to those in WT cells (left panel). However, the most striking difference was in the ratio of chromatin associated with soluble MCM proteins, where USP7-null cells had a higher fraction of each MCM protein on chromatin (relative to the soluble fraction) than wild-type cells (Fig. 6A, right panel). Blots for MEK2 (a soluble protein) and histone H3 (a chromatin-associated protein) verified that the extracts were fractionated appropriately and showed that their degree of chromatin association was unaffected by USP7. The ratio of chromatin associated with soluble proteins was determined for each MCM protein from three independent experiments, showing that each MCM protein was consistently increased on chromatin in the absence of USP7 (Fig. 6B).

To verify that the increased levels of MCMs on chromatin were a direct effect of USP7 depletion, as opposed to an indirect effect caused by G_1 accumulation or long-term growth in the absence of USP7, we repeated the above-described experiments in HeLa cells transfected with siRNA targeting USP7 or negative-control siRNA (Fig. 6C and D). Unlike the results for USP7-null cells, USP7 silencing did not significantly change the cell cycle distribution in comparison to that of control cells (Fig. 6E). USP7 silencing also did not affect the total cellular levels of MCM proteins (compare lanes 1 and 2 in Fig. 6C). However, like the USP7 knockout, it did result in an increased level of each MCM protein on chromatin (compare lanes 5 and 6 in Fig. 6C). Quantification of the total, soluble, and chromatin-associated MCM protein levels from two independent experiments is shown in Fig. 6D and confirms that USP7 depletion results in increased chromatin association of MCM proteins.

Two populations of the MCM complex are associated with chromatin during S phase. The first population comprises active CMG complexes (containing Cdc45, GINS, and the MCM complex) at the replication fork, while the second population comprises inactive MCM complexes that license dormant origins and that are not associated with GINS or Cdc45. We tested whether USP7 affected the chromatin association of CMG by blotting for the Psf2 subunit of GINS (Fig. 6F). We observed a consistent increase in the amount of chromatin-associated Psf2 in USP7-null cells (2-fold on average) compared to that in WT HCT116 cells, suggesting that USP7 can affect the chromatin association of GINS. Since MCM-BP is important for MCM complex unloading and directly binds USP7, we also tested whether MCM-BP silencing resulted in the accumulation of Psf2 on chromatin (23). To this end, HeLa cells were transfected with plasmids expressing shRNA against MCM-BP or empty plasmid, and then chromatin fractions were prepared. As shown in Fig. 6G, MCM-BP silencing resulted in increased levels of MCM proteins and Psf2 on chromatin. Together, our data indicate that at least some of the MCM complexes that are regulated by USP7 and MCM-BP are associated with GINS and therefore are likely CMG complexes.

USP7 contributes to MCM protein unloading. MCM proteins are loaded onto chromatin throughout G_1 and unloaded over the course of S phase. Therefore, the increased levels of MCM proteins on chromatin resulting from USP7 depletion could either be due to increased loading of MCM proteins (resulting in higher MCM levels on chromatin in G_1 or early S) or decreased unloading (resulting in higher MCM levels on chromatin in late S or G_2). To differentiate between these possibilities, we synchronized control and USP7-depleted HeLa cells at the G_1/S boundary using a double thymidine block and released cells into fresh medium for the indicated times. Chromatin-associated protein fractions were prepared for each time point and analyzed by Western blotting for MCM proteins (Fig. 7A). In the negative-control sample, the levels of chromatin-associated MCM proteins decreased in the 4- to 8-h samples, which corresponds to mid-S phase and late S phase, respectively (based on FACS analysis of the DNA content) (Fig. 7B). This is the expected profile for MCM protein unloading. Interestingly, USP7 levels on the chromatin slightly increased in the 4- to 8-h time points, corresponding to the unloading of the MCM proteins. In USP7-depleted cells, the levels of MCM proteins on chromatin were similar to those of the control cells at the 0- and 2-h time points, but there was no obvious decrease in MCM proteins on chromatin at 4 to 8 h. This effect was consistent in three independent experiments, and the quantification of MCM5 levels on chromatin from the 0-h (G_1/S) and 8-h (late S) time points is shown in Fig. 7C. We conclude that USP7 depletion inhibits MCM protein dissociation from chromatin in mid- to late S phase and therefore, like MCM-BP, USP7 may contribute to MCM complex unloading during S phase.

USP7 interacts with MCM-BP on chromatin and forms a ternary complex with MCM-BP and MCMs. The impaired unloading of MCM proteins from chromatin after USP7 depletion mimics the previously described effect of MCM-BP depletion (16, 23). This suggests that USP7 may be working together with MCM-BP to unload the MCM complex. If this were correct, we would expect USP7 to bind the chromatin-associated MCM-BP and to form a ternary complex with the MCM-BP and MCM proteins. To test whether USP7 interacts with chromatin-associated or soluble MCM-BP, we fractionated HeLa cells into soluble and chromatin-associated extracts, immunoprecipitated MCM-BP from each fraction, and blotted for USP7 (Fig. 8A). Although USP7 and MCM-BP were present in both the soluble and chromatin-associated extracts (see input lanes), USP7 was recovered only with MCM-BP (at levels above those of the nonspecific IgG control) from the chromatin-associated fraction. MCM6 was also recovered along with USP7 in this MCM-BP IP, which could reflect the formation of a USP7–MCM-BP–MCM6 ternary complex or individual dimeric complexes with MCM-BP.

We then investigated whether USP7 could form a ternary complex with the MCM-BP and MCM proteins by coexpressing USP7 and MCM-BP with FLAG-tagged MCM5 or MCM7 in insect cells, isolating the FLAG-MCM protein on anti-FLAG resin, and assessing recovery of MCM-BP and USP7 by Coomassie blue staining (Fig. 8B and C). Both USP7 and MCM-BP were recovered with FLAG-MCM5 or FLAG-MCM7 (lane 7 in Fig. 8B and 8C). To determine whether USP7 bound directly to the MCM protein or was tethered to it through MCM-BP, we repeated the experiment by replacing MCM-BP with the S158A MCM-BP point mutant, which is unable to bind USP7. In this case, MCM-BP was still efficiently recovered with FLAG-MCM5 or FLAG-MCM7, but

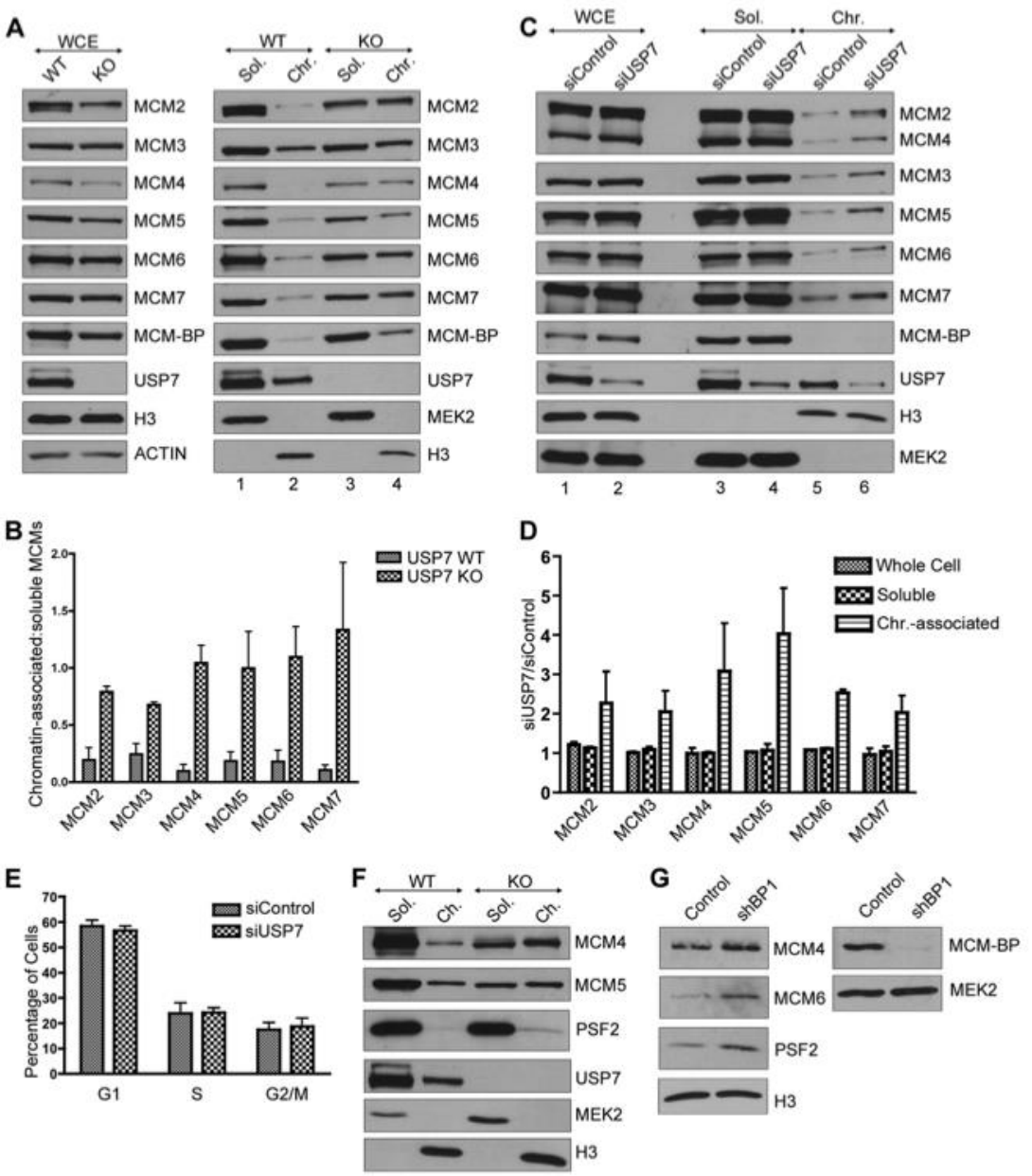

FIG 6 USP7 depletion increases the chromatin association of MCM proteins. (A) Whole-cell (WCE), soluble (Sol.), and chromatin-associated (Chr.) lysates from WT and USP7-null (KO) cells were analyzed by SDS-PAGE and Western blotting against the indicated MCM proteins and USP7. In the left panel, histone H3 and actin are used as loading controls. (B) MCM protein bands from the soluble and chromatin-associated lysate were quantified from three independent experiments by densitometry (GelEval software). The ratio of chromatin-associated to soluble protein was calculated for each MCM protein from the WT and USP7-null cells and graphed. Error bars represent standard deviations. (C) Whole-cell, soluble, and chromatin-associated lysates from HeLa cells transfected with control or USP7-targeted siRNA (siControl and siUSP7, respectively) were analyzed by SDS-PAGE and Western blotting for the indicated MCM proteins and USP7. Blots against H3 (chromatin associated) and MEK2 (soluble) are used to indicate appropriate fractionation and also serve as loading controls. Note that since only a small proportion of MCM-BP is chromatin associated, the amount of chromatin lysate loaded in this experiment is not enough to detect MCM-BP in this fraction. (D) MCM protein bands from the whole-cell, soluble, and chromatin-associated lysate were quantified from two independent

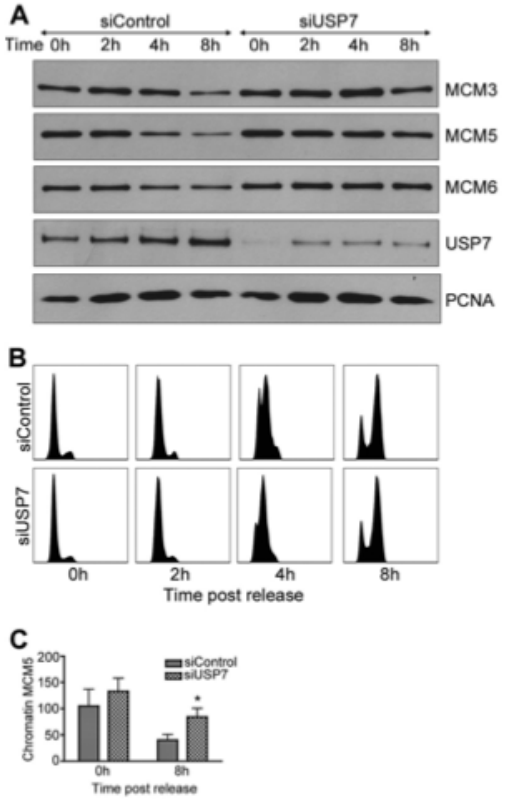

FIG 7 USP7 depletion affects unloading of the MCM complex at the end of S phase. (A) HeLa cells transfected with control or USP7-targeted siRNA were synchronized to the G_1/S boundary using a double thymidine block and released for the indicated times (0 h to 8 h). The chromatin-associated extract for each time point was analyzed by SDS-PAGE and Western blotting for the indicated MCM proteins and USP7. PCNA was used as a loading control. (B) The DNA content of the above samples was measured using flow cytometry and graphed using FlowJo software (Treestar Inc.). (C) MCM5 protein bands from the chromatin-associated fraction at 0 and 8 h after release from a double thymidine block were quantified from three independent experiments by densitometry. Average values with standard deviations are shown relative to results for 0-h siControl samples (set to 100). *, $P < 0.05$.

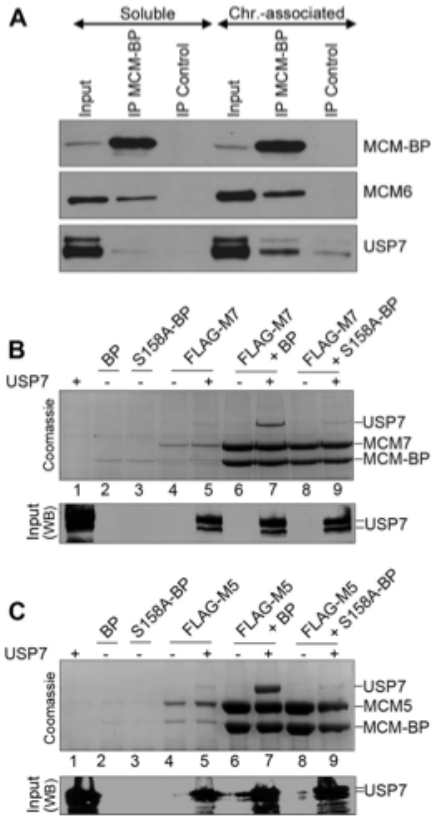

FIG 8 MCM-BP binds USP7 on chromatin and can mediate an interaction between the USP7 and MCM proteins. (A) Immunoprecipitations were performed with soluble and chromatin-associated lysates from HeLa cells using antibody against MCM-BP or negative-control IgG. Immunoprecipitants were analyzed by SDS-PAGE and Western blotting against the indicated proteins. (B and C) FLAG-tagged MCM7 (B) or FLAG-tagged MCM5 (C) was expressed individually or coexpressed with MCM-BP (BP) or MCM-BP S158A (S158A-BP) in insect cells. In each case, these proteins were expressed with and without USP7, as indicated. Insect cell lysates were then incubated with anti-FLAG resin to recover FLAG-MCM7 or FLAG-MCM5 with associated proteins. Bound proteins were eluted with protein sample buffer and analyzed by SDS-PAGE and Coomassie staining (top panel) or Western blotting for USP7 (bottom panel).

USP7 was not recovered (lane 9 in 8B and C). This indicates that USP7 is tethered to MCM proteins through MCM-BP. Note that this experiment cannot be performed in the absence of MCM-BP because MCM-BP dramatically increases the solubility and recovery of MCM proteins (compare MCM bands in lanes 4 and 5 to those in lanes 6 to 9). We conclude that USP7 binding to MCM-BP does not block MCM-BP binding to MCM proteins but rather that MCM-BP mediates the formation of a ternary complex with the USP7 and MCM proteins. Together, our results suggest

experiments by densitometry. The ratio of siUSP7 band density to siControl band density was calculated for each MCM protein in the whole-cell, soluble, and chromatin-associated lysate and graphed. Error bars represent standard deviations. (E) DNA content of HeLa cells transfected with control or USP7-targeted siRNA was measured by flow cytometry in three independent experiments and graphed using FlowJo software (Treestar Inc.). The percentages of cells in G_1, S, and G_2/M were estimated using FlowJo software and are shown in the graph. Error bars represent standard deviations. (F) Soluble (Sol.) and chromatin-associated (Ch.) lysates from WT and USP7-null cells (KO) were analyzed by SDS-PAGE and Western blotting against the indicated MCM proteins, Psf2 and USP7. Histone H3 (chromatin-associated protein) and MEK2 (soluble protein) indicate appropriate fractionation and also serve as loading controls. (G) Chromatin-associated lysates from HeLa cells transfected with control plasmid or shMCM-BP1 were analyzed by SDS-PAGE and Western blotting for the indicated MCM proteins, Psf2, and histone H3 as a loading control (left panel). Since only a small proportion of MCM-BP is chromatin associated, MCM-BP silencing was assessed by comparing equal volumes of the soluble lysate, compared to MEK2 as a loading control (right panel).

that USP7 regulates MCM complex unloading at the end of S phase in an MCM-BP-dependent manner.

DISCUSSION

The MCM complex plays critical roles in DNA replication, both in the activation of origins of replication and in enabling the progression of replication forks, by virtue of its DNA helicase activity (54–56). Although there have been many studies of the proteins and events that enable the loading of MCM complexes on DNA during G_1, their subsequent activation at the onset of S phase, and their role as a DNA helicase throughout S phase, little is known about how these complexes are unloaded from chromatin during the course of S phase and as replication forks terminate. Insight into MCM complex unloading recently came from studies of MCM-BP, a highly conserved protein that forms a variety of complexes with MCM proteins (15, 22). MCM-BP from both humans and *Xenopus* was shown to promote the dissociation of MCM complexes from chromatin in late S phase. The data presented here identify a second protein, USP7, as participating in this process and suggest that it does so through a direct interaction with MCM-BP.

An association of USP7 with MCM-BP and MCM proteins was suggested from a proteomics study of the protein interactions of deubiquitylating enzymes (24). We have verified this interaction in both primary and transformed human cells and have shown using purified proteins that USP7 binds directly to MCM-BP. Using a combination of GST pulldown assays, which can detect transient interactions, and gel filtration analysis, which detects stable complexes, we have shown that MCM-BP contacts the N-terminal TRAF domain of USP7 but requires additional contacts with the USP7 catalytic domain for stable binding. The interaction with both the TRAF and catalytic domains resembles the mechanism of interaction of the viral interferon regulatory factor 4 (vIRF4) protein of Kaposi sarcoma-associated herpesvirus (KSHV), which also contacts both of these USP7 domains (29). The contact of vIRF4 with the USP7 catalytic domain was shown to inhibit its ubiquitin cleavage activity. However, this is not the case for MCM-BP, since the addition of MCM-BP to *in vitro* assays of K48-linked diubiquitin cleavage by full-length USP7 (a substrate efficiently hydrolyzed by USP7 [57]) failed to have any effect on the ability of USP7 to cleave this substrate (Fig. 9). This suggests that unlike vIRF4, MCM-BP does not contact the catalytic site of the USP7 catalytic domain but rather contacts the catalytic domain in a way that preserves the enzymatic function of USP7.

Our data on the MCM-BP–USP7 interaction show that contacts of MCM-BP with the peptide binding pocket in the USP7 TRAF domain are critical for this interaction. Specifically, mutation of D164 and W165 in this binding pocket, which were previously shown to be critical for specific peptide recognition, abrogated the MCM-BP interaction. From our studies of other protein interactions with the USP7 TRAF domain, we previously defined an A/PxxS motif that mediates interactions with the TRAF binding pocket (28, 36, 38). Although MCM-BP contains five potential PxxS motifs, we identified one (^{155}PSTS^{158}) as being critical for the MCM-BP–USP7 interaction, since mutation of S158 to alanine greatly reduced binding of MCM-BP to USP7 both *in vitro* and *in vivo*. The crystal structure of the USP7 TRAF domain bound to the MCM-BP peptide ^{152}RVSPSTSYTP^{161} confirmed the importance of S158 from MCM-BP and D164 from USP7 for this interaction. It also showed that this interaction is very similar to those reported previously for the p53, Mdm2, and MdmX peptides with the USP7 TRAF domain (36, 38, 58).

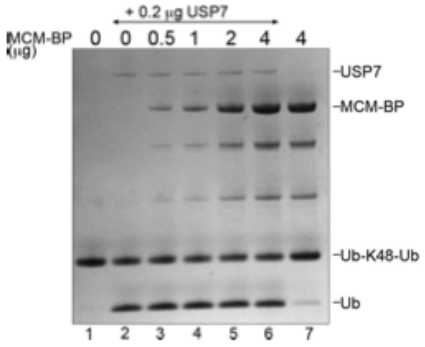

FIG 9 MCM-BP does not inhibit the catalytic activity of USP7. Purified USP7 (0.2 μg) was preincubated with increasing amounts of MCM-BP (as indicated) and then incubated with K48-linked diubiquitin (3 μg) for 10 min at 37°C. A Coomassie-stained SDS-PAGE gel is shown, where the positions of the diubiquitin substrate (Ub-K48-Ub) and monoubiquitin product (Ub) are indicated. Lanes 1 and 7 are controls lacking USP7.

The interaction of USP7 with MCM-BP prompted an investigation of the possible role of USP7 in DNA replication. Comparison of the S-phase progression of USP7-null and WT HCT116 cells indicated that progression through early to mid-S phase was unaffected by loss of USP7; however, the progression through late S phase and G_2 was noticeably affected. We also tested possible roles of USP7 in replication fork progression and replication origin activation using DNA combing experiments performed on USP7-null and WT HCT116 cells. No statistically significant differences were observed, indicating that USP7 does not globally affect replication the fork rate or origin function. This was an important possibility to consider because monoubiquitylation of histone H2B was recently shown to affect replication fork progression and replisome stability in *S. cerevisiae* (59), and USP7 is one of the enzymes that reverses this modification in higher eukaryotes (41, 42). Our data indicate that the contribution of USP7 to DNA replication is specific for late S phase/G_2 progression.

The defect in late S phase/G_2 progression caused by lack of USP7 could result from impaired replication fork termination, such as would be expected to occur if MCM complexes were not unloaded from chromatin. In keeping with this possibility, examination of the effect of USP7 on MCM proteins showed that the level of each MCM protein on chromatin increased as a result of USP7 silencing or knockout. Further analysis of MCM-chromatin interactions through S phase indicated that MCM proteins failed to dissociate from chromatin in late S phase in USP7-depleted cells. This effect on MCM-chromatin interactions mimics the effect of MCM-BP depletion, as observed in both human cells and *Xenopus* egg extracts (16, 23). The requirement for MCM-BP to dissociate MCM proteins from chromatin in late S phase, along with the ability of MCM-BP to disrupt MCM complexes, led to the conclusion that one of the functions of MCM-BP is to unload MCM complexes following DNA replication. Our data suggest that USP7 can function with MCM-BP to unload MCM complexes, although we cannot completely exclude abnormal scenarios, such as MCM reloading late in S phase in the absence of USP7.

There are two forms of MCM complexes on chromatin during S phase: (i) MCM complexes that interact with GINS and CDC45 to form the active CMG helicase at the replication fork and (ii) MCM complexes that bind dormant origins and are not associated with GINS or Cdc45 (11, 60, 61). We found that the lack of USP7 (in USP7-null cells) resulted in an increase in the Psf2 subunit of GINS on chromatin, suggesting that some of the MCM complexes that are unloaded by USP7 are part of the CMG complex or at least contain GINS. However, the MCM-chromatin association (typically increased 4- to 5-fold in USP7-null cells) was affected more than the Psf2-chromatin association (~2-fold increase in USP7-null cells), suggesting that USP7 contributes to the unloading of both "active" CMG complexes and "inactive" MCM complexes at dormant origins. We also observed that MCM-BP silencing increased Psf2 levels on chromatin, consistent with a role for MCM-BP in unloading both MCM and GINS complexes. This also fits with MCM-BP's function in MCM unloading in the *Xenopus* egg system, in which there is an ~10-fold increase in CMG complexes in comparison to findings for human cells (62–65).

Since USP7 stabilizes several of its interacting proteins by deubiquitylating them, we considered that USP7 might stabilize the MCM-BP and/or MCM protein. However, we did not find support for this possibility, since USP7 silencing did not result in lower levels of the MCM-BP or MCM protein. While USP7-null HCT116 cells did have somewhat lower levels of MCM proteins compared to WT cells, they also had lower levels of other S-phase-associated proteins, such as Sld5, Cdc45, and cyclin A (data not shown). This suggests that the lower levels of total MCM proteins in the USP7-null cells are more likely due to the slower cell cycle rather than specific stabilization by USP7.

An important feature of the MCM-BP–USP7 interaction, is that it occurs in such a way that MCM-BP retains the ability to bind MCM proteins. While the MCM-BP residues important for binding MCM proteins have not been determined, we found that the S158A mutation, which abrogates binding to USP7, had no effect on the ability of MCM-BP to bind MCM proteins (Fig. 1B). In addition, we showed that MCM-BP bridges an interaction between the USP7 and MCM proteins (Fig. 8). This bridging effect through MCM-BP may account for the recovery of some MCM proteins with USP7 previously observed in the Sowa et al. proteomic study (24). The ability of MCM-BP to bridge USP7-MCM interactions, combined with the observation that USP7 is preferentially associated with the fraction of MCM-BP that is on chromatin, suggests that MCM-BP recruits USP7 to MCM complexes on chromatin, where it could affect their function. Interestingly, the association of USP7 with chromatin was observed to increase at mid- to late S phase, a time when the MCM proteins are observed to dissociate from chromatin. This supports a scenario where the increased chromatin association of USP7 promotes the unloading of the MCM complex.

The role of USP7 in MCM unloading may or may not involve the catalytic activity of USP7, since some but not all of the cellular functions of USP7 involve its ability to cleave ubiquitin. While there is currently no evidence that MCM proteins are ever polyubiquitylated in human cells, MCM5 and MCM7 were identified as potentially monoubiquitylated proteins in a recent proteomic screen (66). Biochemical and structural studies have suggested that the MCM2-7 ring-shaped complex opens at the interface between MCM2 and MCM5, referred to as the MCM2/5 gate (67, 68). While it is not known what triggers this opening, it is possible that the opening and closing of the MCM2/5 gate is regulated by the ubiquitylation state of MCM5 or MCM7. In such a scenario, USP7 could either affect MCM unloading by cleaving ubiquitin from the MCM protein, or, since USP7 is known to interact with several E3 ubiquitin ligases (24), it might act as a scaffold to recruit the ubiquitin ligase that modifies the MCM protein.

In summary, we have shown that USP7 binds directly to MCM-BP and mirrors its function in enabling the dissociation of MCM complexes from chromatin at the end of S phase. Although USP7 has been reported to contribute to several cellular functions, this is the first time it has been shown to directly contribute to DNA replication. Our data support a model in which MCM-BP recruits USP7 to MCM complexes on chromatin to facilitate their unloading as replication terminates. Further studies will be necessary to determine how USP7 exerts this effect.

ACKNOWLEDGMENTS

We thank Dionne White for assistance with FACS analyses and Kathy Shire for excellent technical assistance. We also acknowledge Anthony La Delfa for early studies of MCM-BP peptide interactions with USP7 and Jay Yang for assistance with DNA combing experiments.

This work was supported by operating grants to L.F. from the Canadian Institutes of Health Research (CIHR) (grant number 84306) and from the Cancer Research Society. It was also supported by operating grants from the CIHR to V.S. (grant number 106583) and to G.W.B. (MOP-79368). L.F. is a tier 1 Canada Research Chair in Molecular Virology.

REFERENCES

1. **Boos D, Frigola J, Diffley JF.** 2012. Activation of the replicative DNA helicase: breaking up is hard to do. Curr. Opin. Cell Biol. **24**:423–430. http://dx.doi.org/10.1016/j.ceb.2012.01.011.
2. **Burkhart R, Schulte D, Hu D, Musahl C, Gohring F, Knippers R.** 1995. Interactions of human nuclear proteins P1Mcm3 and P1Cdc46. Eur. J. Biochem. **228**:431–438. http://dx.doi.org/10.1111/j.1432-1033.1995.tb20281.x.
3. **Lei M, Kawasaki Y, Tye BK.** 1996. Physical interactions among Mcm proteins and effects of Mcm dosage on DNA replication in Saccharomyces cerevisiae. Mol. Cell. Biol. **16**:5081–5090.
4. **Rowles A, Chong JP, Brown L, Howell M, Evan GI, Blow JJ.** 1996. Interaction between the origin recognition complex and the replication licensing system in Xenopus. Cell **87**:287–296. http://dx.doi.org/10.1016/S0092-8674(00)81346-X.
5. **Mahbubani HM, Chong JP, Chevalier S, Thommes P, Blow JJ.** 1997. Cell cycle regulation of the replication licensing system: involvement of a Cdk-dependent inhibitor. J. Cell Biol. **136**:125–135. http://dx.doi.org/10.1083/jcb.136.1.125.
6. **Donovan S, Harwood J, Drury LS, Diffley JF.** 1997. Cdc6p-dependent loading of Mcm proteins onto pre-replicative chromatin in budding yeast. Proc. Natl. Acad. Sci. U. S. A. **94**:5611–5616. http://dx.doi.org/10.1073/pnas.94.11.5611.
7. **Edwards MC, Tutter AV, Cvetic C, Gilbert CH, Prokhorova TA, Walter JC.** 2002. MCM2-7 complexes bind chromatin in a distributed pattern surrounding the origin recognition complex in Xenopus egg extracts. J. Biol. Chem. **277**:33049–33057. http://dx.doi.org/10.1074/jbc.M204438200.
8. **Ilves I, Petojevic T, Pesavento JJ, Botchan MR.** 2010. Activation of the MCM2-7 helicase by association with Cdc45 and GINS proteins. Mol. Cell **37**:247–258. http://dx.doi.org/10.1016/j.molcel.2009.12.030.
9. **Sheu YJ, Stillman B.** 2010. The Dbf4-Cdc7 kinase promotes S phase by alleviating an inhibitory activity in Mcm4. Nature **463**:113–117. http://dx.doi.org/10.1038/nature08647.
10. **Zegerman P, Diffley JF.** 2007. Phosphorylation of Sld2 and Sld3 by cyclin-dependent kinases promotes DNA replication in budding yeast. Nature **445**:281–285. http://dx.doi.org/10.1038/nature05432.
11. **Woodward AM, Gohler T, Luciani MG, Oehlmann M, Ge X, Gartner A, Jackson DA, Blow JJ.** 2006. Excess Mcm2-7 license dormant origins of replication that can be used under conditions of replicative stress. J. Cell Biol. **173**:673–683. http://dx.doi.org/10.1083/jcb.200602108.
12. **Ivessa AS, Lenzmeier BA, Bessler JB, Goudsouzian LK, Schnakenberg**

SL, Zakian VA. 2003. The Saccharomyces cerevisiae helicase Rrm3p facilitates replication past nonhistone protein-DNA complexes. Mol. Cell 12:1525–1536. http://dx.doi.org/10.1016/S1097-2765(03)00456-8.
13. Sabouri N, McDonald KR, Webb CJ, Cristea IM, Zakian VA. 2012. DNA replication through hard-to-replicate sites, including both highly transcribed RNA Pol II and Pol III genes, requires the S. pombe Pfh1 helicase. Genes Dev. 26:581–593. http://dx.doi.org/10.1101/gad.184697.111.
14. Steinacher R, Osman F, Dalgaard JZ, Lorenz A, Whitby MC. 2012. The DNA helicase Pfh1 promotes fork merging at replication termination sites to ensure genome stability. Genes Dev. 26:594–602. http://dx.doi.org/10.1101/gad.184663.111.
15. Sakwe AM, Nguyen T, Athanasopoulos V, Shire K, Frappier L. 2007. Identification and characterization of a novel component of the human minichromosome maintenance complex. Mol. Cell. Biol. 27:3044–3055. http://dx.doi.org/10.1128/MCB.02384-06.
16. Jagannathan M, Sakwe AM, Nguyen T, Frappier L. 2012. The MCM-associated protein MCM-BP is important for human nuclear morphology. J. Cell Sci. 125:133–143. http://dx.doi.org/10.1242/jcs.089938.
17. Ding L, Forsburg SL. 2011. Schizosaccharomyces pombe minichromosome maintenance-binding protein (MCM-BP) antagonizes MCM helicase. J. Biol. Chem. 286:32918–32930. http://dx.doi.org/10.1074/jbc.M111.282541.
18. Li JJ, Schnick J, Hayles J, MacNeill SA. 2011. Purification and functional inactivation of the fission yeast MCM(MCM-BP) complex. FEBS Lett. 585:3850–3855. http://dx.doi.org/10.1016/j.febslet.2011.10.033.
19. Takahashi N, Quimbaya M, Schubert V, Lammens T, Vandepoele K, Schubert I, Matsui M, Inze D, Berx G, De Veylder L. 2010. The MCM-binding protein ETG1 aids sister chromatid cohesion required for postreplicative homologous recombination repair. PLoS Genet. 6:e1000817. http://dx.doi.org/10.1371/journal.pgen.1000817.
20. Takahashi N, Lammens T, Boudolf V, Maes S, Yoshizumi T, De Jaeger G, Witters E, Inze D, De Veylder L. 2008. The DNA replication checkpoint aids survival of plants deficient in the novel replisome factor ETG1. EMBO J. 27:1840–1851. http://dx.doi.org/10.1038/emboj.2008.107.
21. Santosa V, Martha S, Hirose N, Tanaka K. 2013. The fission yeast minichromosome maintenance (MCM)-binding protein (MCM-BP), Mcb1, regulates MCM function during prereplicative complex formation in DNA replication. J. Biol. Chem. 288:6864–6880. http://dx.doi.org/10.1074/jbc.M112.432393.
22. Nguyen T, Jagannathan M, Shire K, Frappier L. 2012. Interactions of the human MCM-BP protein with MCM complex components and Dbf4. PLoS One 7:e35931. http://dx.doi.org/10.1371/journal.pone.0035931.
23. Nishiyama A, Frappier L, Mechali M. 2011. MCM-BP regulates unloading of the MCM2-7 helicase in late S phase. Genes Dev. 25:165–175. http://dx.doi.org/10.1101/gad.614411.
24. Sowa ME, Bennett EJ, Gygi SP, Harper JW. 2009. Defining the human deubiquitinating enzyme interaction landscape. Cell 138:389–403. http://dx.doi.org/10.1016/j.cell.2009.04.042.
25. Everett RD, Meredith M, Orr A, Cross A, Kathoria M, Parkinson J. 1997. A novel ubiquitin-specific protease is dynamically associated with the PML nuclear domain and binds to a herpesvirus regulatory protein. EMBO J. 16:1519–1530. http://dx.doi.org/10.1093/emboj/16.7.1519.
26. Holowaty MN, Zeghouf M, Wu H, Tellam J, Athanasopoulos V, Greenblatt J, Frappier L. 2003. Protein profiling with Epstein-Barr nuclear antigen-1 reveals an interaction with the herpesvirus-associated ubiquitin-specific protease HAUSP/USP7. J. Biol. Chem. 278:29987–29994. http://dx.doi.org/10.1074/jbc.M303977200.
27. Salsman J, Jagannathan M, Paladino P, Chan PK, Dellaire G, Raught B, Frappier L. 2012. Proteomic profiling of the human cytomegalovirus UL35 gene products reveals a role for UL35 in the DNA repair response. J. Virol. 86:806–820. http://dx.doi.org/10.1128/JVI.05442-11.
28. Saridakis V, Sheng Y, Sarkari F, Holowaty MN, Shire K, Nguyen T, Zhang RG, Liao J, Lee W, Edwards AM, Arrowsmith CH, Frappier L. 2005. Structure of the p53 binding domain of HAUSP/USP7 bound to Epstein-Barr nuclear antigen 1 implications for EBV-mediated immortalization. Mol. Cell 18:25–36. http://dx.doi.org/10.1016/j.molcel.2005.02.029.
29. Lee HR, Choi WC, Lee S, Hwang J, Hwang E, Guchhait K, Haas J, Toth Z, Jeon YH, Oh TK, Kim MH, Jung JU. 2011. Bilateral inhibition of HAUSP deubiquitinase by a viral interferon regulatory factor protein. Nat. Struct. Mol. Biol. 18:1336–1344. http://dx.doi.org/10.1038/nsmb.2142.
30. Ching W, Koyuncu E, Singh S, Arbelo-Roman C, Hartl B, Kremmer E, Speiseder T, Meier C, Dobner T. 2013. A ubiquitin-specific protease possesses a decisive role for adenovirus replication and oncogene-mediated transformation. PLoS Pathog. 9:e1003273. http://dx.doi.org/10.1371/journal.ppat.1003273.
31. Jager W, Santag S, Weidner-Glunde M, Gellermann E, Kati S, Pietrek M, Viejo-Borbolla A, Schulz TF. 2012. The ubiquitin-specific protease USP7 modulates the replication of Kaposi's sarcoma-associated herpesvirus latent episomal DNA. J. Virol. 86:6745–6757. http://dx.doi.org/10.1128/JVI.06840-11.
32. Nicholson B, Suresh Kumar KG. 2011. The multifaceted roles of USP7: new therapeutic opportunities. Cell Biochem. Biophys. 60:61–68. http://dx.doi.org/10.1007/s12013-011-9185-5.
33. Cummins JM, Rago C, Kohli M, Kinzler KW, Lengauer C, Vogelstein B. 2004. Tumour suppression: disruption of HAUSP gene stabilizes p53. Nature 428:486–487. http://dx.doi.org/10.1038/nature02501.
34. Li M, Chen D, Shiloh A, Luo J, Nikolaev AY, Qin J, Gu W. 2002. Deubiquitination of p53 by HAUSP is an important pathway for p53 stabilization. Nature 416:648–653. http://dx.doi.org/10.1038/nature737.
35. Li M, Brooks CL, Kon N, Gu W. 2004. A dynamic role of HAUSP in the p53-Mdm2 pathway. Mol. Cell 13:879–886. http://dx.doi.org/10.1016/S1097-2765(04)00157-1.
36. Sheng Y, Saridakis V, Sarkari F, Duan S, Wu T, Arrowsmith CH, Frappier L. 2006. Molecular recognition of p53 and MDM2 by USP7/HAUSP. Nat. Struct. Mol. Biol. 13:285–291. http://dx.doi.org/10.1038/nsmb1067.
37. Meulmeester E, Maurice MM, Boutell C, Teunisse AF, Ovaa H, Abraham TE, Dirks RW, Jochemsen AG. 2005. Loss of HAUSP-mediated deubiquitination contributes to DNA damage-induced destabilization of Hdmx and Hdm2. Mol. Cell 18:565–576. http://dx.doi.org/10.1016/j.molcel.2005.04.024.
38. Sarkari F, La Delfa A, Arrowsmith CH, Frappier L, Sheng Y, Saridakis V. 2010. Further insight into substrate recognition by USP7: structural and biochemical analysis of the HdmX and Hdm2 interactions with USP7. J. Mol. Biol. 402:825–837. http://dx.doi.org/10.1016/j.jmb.2010.08.017.
39. Trotman LC, Wang X, Alimonti A, Chen Z, Teruya-Feldstein J, Yang H, Pavletich NP, Carver BS, Cordon-Cardo C, Erdjument-Bromage H, Tempst P, Chi SG, Kim HJ, Misteli T, Jiang X, Pandolfi PP. 2007. Ubiquitination regulates PTEN nuclear import and tumor suppression. Cell 128:141–156. http://dx.doi.org/10.1016/j.cell.2006.11.040.
40. van der Horst A, de Vries-Smits AM, Brenkman AB, van Triest MH, van den Broek N, Colland F, Maurice MM, Burgering BM. 2006. FOXO4 transcriptional activity is regulated by monoubiquitination and USP7/HAUSP. Nat. Cell Biol. 8:1064–1073. http://dx.doi.org/10.1038/ncb1469.
41. van der Knaap JA, Kumar BR, Moshkin YM, Langenberg K, Krijgsveld J, Heck AJ, Karch F, Verrijzer CP. 2005. GMP synthetase stimulates histone H2B deubiquitylation by the epigenetic silencer USP7. Mol. Cell 17:695–707. http://dx.doi.org/10.1016/j.molcel.2005.02.013.
42. Sarkari F, Sanchez-Alcaraz T, Wang S, Holowaty MN, Sheng Y, Frappier L. 2009. EBNA1-mediated recruitment of a histone H2B deubiquitylating complex to the Epstein-Barr virus latent origin of DNA replication. PLoS Pathog. 5:e1000624. http://dx.doi.org/10.1371/journal.ppat.1000624.
43. Sarkari F, Wang X, Nguyen T, Frappier L. 2011. The herpesvirus associated ubiquitin specific protease, USP7, is a negative regulator of PML proteins and PML nuclear bodies. PLoS One 6:e16598. http://dx.doi.org/10.1371/journal.pone.0016598.
44. Tang J, Qu LK, Zhang J, Wang W, Michaelson JS, Degenhardt YY, El-Deiry WS, Yang X. 2006. Critical role for Daxx in regulating Mdm2. Nat. Cell Biol. 8:855–862. http://dx.doi.org/10.1038/ncb1442.
45. Holowaty MN, Sheng Y, Nguyen T, Arrowsmith C, Frappier L. 2003. Protein interaction domains of the ubiquitin-specific protease, USP7/HAUSP. J. Biol. Chem. 278:47753–47761. http://dx.doi.org/10.1074/jbc.M307200200.
46. Sarkari F, Wheaton K, La Delfa A, Mohamed M, Shaikh F, Khatun R, Arrowsmith CH, Frappier L, Saridakis V, Sheng Y. 2013. USP7/HAUSP is a regulator of UbE2E1/UbcH6. J. Biol. Chem.. http://dx.doi.org/10.1074/jbc.M113.469262.
47. Otwinowski Z, Minor W. 1997. Processing of X-ray diffraction data collected in oscillation mode. Methods Enzymol. 276:307–326. http://dx.doi.org/10.1016/S0076-6879(97)76066-X.
48. Brunger AT. 2007. Version 1.2 of the crystallography and NMR system. Nat. Protoc. 2:2728–2733. http://dx.doi.org/10.1038/nprot.2007.406.

49. **Jones TA, Kjeldgaard M.** 1997. Electron-density map interpretation. Methods Enzymol. **277**:173–208. http://dx.doi.org/10.1016/S0076-6879(97)77012-5.
50. **Yang J, O'Donnell L, Durocher D, Brown GW.** 2012. RMI1 promotes DNA replication fork progression and recovery from replication fork stress. Mol. Cell Biol. **32**:3054–3064. http://dx.doi.org/10.1128/MCB.00255-12.
51. **Conti C, Sacca B, Herrick J, Lalou C, Pommier Y, Bensimon A.** 2007. Replication fork velocities at adjacent replication origins are coordinately modified during DNA replication in human cells. Mol. Biol. Cell **18**:3059–3067. http://dx.doi.org/10.1091/mbc.E06-08-0689.
52. **Conti C, Herrick J, Bensimon A.** 2007. Unscheduled DNA replication origin activation at inserted HPV 18 sequences in a HPV-18/MYC amplicon. Genes Chromosomes Cancer **46**:724–734. http://dx.doi.org/10.1002/gcc.20448.
53. **Tuduri S, Tourriere H, Pasero P.** 2010. Defining replication origin efficiency using DNA fiber assays. Chromosome Res. **18**:91–102. http://dx.doi.org/10.1007/s10577-009-9098-y.
54. **Ishimi Y.** 1997. A DNA helicase activity is associated with an MCM4, -6, and -7 protein complex. J. Biol. Chem. **272**:24508–24513. http://dx.doi.org/10.1074/jbc.272.39.24508.
55. **Bochman ML, Schwacha A.** 2009. The Mcm complex: unwinding the mechanism of a replicative helicase. Microbiol. Mol. Biol. Rev. **73**:652–683. http://dx.doi.org/10.1128/MMBR.00019-09.
56. **Costa A, Onesti S.** 2008. The MCM complex: (just) a replicative helicase? Biochem. Soc. Trans. **36**:136–140. http://dx.doi.org/10.1042/BST0360136.
57. **Faesen AC, Dirac AM, Shanmugham A, Ovaa H, Perrakis A, Sixma TK.** 2011. Mechanism of USP7/HAUSP activation by its C-terminal ubiquitin-like domain and allosteric regulation by GMP-synthetase. Mol. Cell **44**:147–159. http://dx.doi.org/10.1016/j.molcel.2011.06.034.
58. **Hu M, Gu L, Li M, Jeffrey PD, Gu W, Shi Y.** 2006. Structural basis of competitive recognition of p53 and MDM2 by HAUSP/USP7: implications for the regulation of the p53-MDM2 pathway. PLoS Biol. **4**:e27. http://dx.doi.org/10.1371/journal.pbio.0040027.
59. **Trujillo KM, Osley MA.** 2012. A role for H2B ubiquitylation in DNA replication. Mol. Cell **48**:734–746. http://dx.doi.org/10.1016/j.molcel.2012.09.019.
60. **Ge XQ, Jackson DA, Blow JJ.** 2007. Dormant origins licensed by excess Mcm2-7 are required for human cells to survive replicative stress. Genes Dev. **21**:3331–3341. http://dx.doi.org/10.1101/gad.457807.
61. **Ibarra A, Schwob E, Mendez J.** 2008. Excess MCM proteins protect human cells from replicative stress by licensing backup origins of replication. Proc. Natl. Acad. Sci. U. S. A. **105**:8956–8961. http://dx.doi.org/10.1073/pnas.0803978105.
62. **Dimitrova DS, Gilbert DM.** 1998. Regulation of mammalian replication origin usage in Xenopus egg extract. J. Cell Sci. **111**(Part 19):2989–2998.
63. **Walter J, Newport JW.** 1997. Regulation of replicon size in Xenopus egg extracts. Science **275**:993–995. http://dx.doi.org/10.1126/science.275.5302.993.
64. **Arias EE, Walter JC.** 2007. Strength in numbers: preventing rereplication via multiple mechanisms in eukaryotic cells. Genes Dev. **21**:497–518. http://dx.doi.org/10.1101/gad.1508907.
65. **Blow JJ.** 2001. Control of chromosomal DNA replication in the early Xenopus embryo. EMBO J. **20**:3293–3297. http://dx.doi.org/10.1093/emboj/20.13.3293.
66. **Kim W, Bennett EJ, Huttlin EL, Guo A, Li J, Possemato A, Sowa ME, Rad R, Rush J, Comb MJ, Harper JW, Gygi SP.** 2011. Systematic and quantitative assessment of the ubiquitin-modified proteome. Mol. Cell **44**:325–340. http://dx.doi.org/10.1016/j.molcel.2011.08.025.
67. **Bochman ML, Schwacha A.** 2010. The Saccharomyces cerevisiae Mcm6/2 and Mcm5/3 ATPase active sites contribute to the function of the putative Mcm2-7 'gate.' Nucleic Acids Res. **38**:6078–6088. http://dx.doi.org/10.1093/nar/gkq422.
68. **Costa A, Ilves I, Tamberg N, Petojevic T, Nogales E, Botchan MR, Berger JM.** 2011. The structural basis for MCM2-7 helicase activation by GINS and Cdc45. Nat. Struct. Mol. Biol. **18**:471–477. http://dx.doi.org/10.1038/nsmb.2004.
69. **Antrobus R, Boutell C.** 2008. Identification of a novel higher molecular weight isoform of USP7/HAUSP that interacts with the Herpes simplex virus type-1 immediate early protein ICP0. Virus Res. **137**:64–71. http://dx.doi.org/10.1016/j.virusres.2008.05.017.